FH Aachen

Aerospace Engineering

DLR Berlin
Institute of Optical Sensor Systems

Master’s Thesis

VEM/VenSpec-M Coating Degradation Study and Thermal Performance Investigation

Joshua Weber

Berlin, 12.07.2023

Supervisor: Prof. Dr. Markus Czupalla

External: Simone del Togno M.Sc.

I. Bibliographical Information

Author: Joshua Weber
Matriculation. -Nr. 3116349
22.08.1996 | Rinteln

Title: VEM/VenSpec-M Coating Degradation Study and Thermal Performance Investigation

Extent: 92 pages, 43 tables, 63 figures, 17 equations, 44 references

Type of Work: Master’s Thesis

Course of Study: Aerospace Engineering

Cooperation: **German Aerospace Center (DLR)**
Institute of Optical Sensor Systems
Rutherfordstraße 2| 12489 Berlin

Date of Issue: 12.07.2023

Date of Submission: 11.07.2023

Key Words: Infrared Spectrometer, Degradation, Venus, TCC, Thermal, Optics, ESATAN, Coatings, Materials, ATOX, Radiation, VERITAS, EnVision

II. Scope of Work

The effects of multiple transits through the Venusian residual atmosphere on the thermal behavior of the optical payload VenSpec-M/VEM shall be investigated, within the EnVision and VERITAS missions. Based on a thorough literature research, the composition, structure, and constituents of the Venusian residual atmosphere, the effects of the constituents on different materials and coatings of the instruments, as well as the grade of degradation of these materials and coatings shall be determined.

All relevant degradations on important thermal parameters, such as thermo-optical properties, electrical resistivity, etc., shall be identified and then used in improved models in ESATAN-TMS with a preselection of materials and coatings. Based on the results of analyses of these models, suitable materials and coatings shall be selected in order to minimize negative influences on the performance of the instruments.

The procedure for the preparation of this Master's Thesis is divided into the following work packages:

- Literature research: Literature research on the instruments VEM and VenSpec-M, as well as on the composition and structure of the Venus atmosphere shall be performed. Furthermore, the effects of individual atmospheric components on different materials and coatings are to be researched. Based on this research, a pre-selection of materials and coatings shall be made.
- Familiarization with ESATAN software: Simple test models shall be created with the help of tutorials, and analyses shall be made and carried out based on these test models.
- Improvement of existing thermal models: Existing thermal models of the instruments shall be adapted and improved. These models shall be used to identify the thermal conditions on Venus and to determine thermal worst cases. The pre-selected materials and coatings shall be incorporated into the thermal models along with their expected degradations.
- Analysis and evaluation of the models: The thermal models created shall allow an analysis of the thermal behavior of the instruments over the entire mission duration. This data shall be evaluated, and conclusions shall be drawn.
- Final selection of materials and coatings: A final selection of different materials and coatings shall be made based on the findings of the previous work packages.
- Final model simulation: The thermal models developed shall be adapted, analyzed, and evaluated. Finally, a specific material/coating combination shall be recommended.
- Report writing

III. Abstract

Optical instruments on space missions are exposed to the harsh environmental conditions of space. In addition to these influences, the target planet also significantly determines these environmental influences. These environmental conditions must be considered in the design of a sensitive optical instrument by identifying possible degradations and determining negative influences on thermal and optical performance.

The goal of the present work is to determine the relevant degradation mechanisms for the near-infrared spectrometers VenSpec-M and VEM at Venus and to identify possible degradations of different materials and coatings. To ensure the best possible performance of the instruments, the materials and coatings of the baffle unit exposed to the Venusian environment are selected in such a way that they exhibit the lowest possible degradation and do not negatively affect either the thermal or the optical performance of the instruments.

Radiative analyses are performed using the ESATAN-TMS software with post-processing done by coded Python scripts to quantify the environmental impact at Venus. Furthermore, a calculation method to estimate the expected atomic oxygen flux is developed, and further degradation sources are identified by appropriate research. A degradation analysis is performed, and its results are evaluated based on thermal analysis of the instruments in ESATAN-TMS. Final trade studies compare different pre-selected coatings and justify the selection of a recommended coating combination.

Overall, it is concluded that organic coatings are particularly affected by atomic oxygen fluxes as well as solar and albedo radiation. Therefore, two ceramic and inorganic coatings were selected for the instrument’s baffle unit, Ceranovis V14 for the baffle shield made of AlMgSi10 and Acktar Fractal Black for the cone made of Ti-6Al-4V.

IV. Acknowledgement

First of all, I would like to thank my supervisors at DLR Delta and Steve.

I enjoyed working with you guys, especially because of your energetic support and exciting tasks. I was able to learn a lot and develop both professionally and personally. Thank you for letting me be part of this exciting project and I hope to see you again in future projects.

Furthermore, I would like to thank the DLR Institute for Optical Sensor Systems for this opportunity and support, as well as my friendly and helpful colleagues. I would like to take this opportunity to thank my fellow students Isabelle and Jonas, who, in addition to an entertaining and good working atmosphere in the office, have always ensured a good mood and lively exchange.

I would also like to thank Prof. Dr. Czupalla for the very uncomplicated course of this master's thesis and the effort and time spent on my behalf.

Probably the most important people to mention here are my parents Christine and Jürgen. Their support and freedom in my development have led to this study and my master's degree. They support me in every situation in life and every undertaking on my part and always stand by me with good advice. Thank you very much for that!

Finally, I would like to thank my girlfriend Sandra, who has accompanied me through my master's studies and my master's thesis and always motivates me to keep at it.

V. List of Figures

VI. List of Tables

VII. List of Abbreviations

AB	Aerobraking
AOA	Angle of Attack
AR	Anti-Reflection
ATOX	Atomic Oxygen
BBAR	Broadband Anti-Reflection
BOL	Begin of Life
D/W	Depth to Width
EOA	End of Aerobraking
EOL	End of Life
ESH	Equivalent Sun Hours
FOV	Field of View
FPA	Focal Plane Assembly
I/F	Interface
LDEF	Long Duration Exposure Facility
LEO	Low Earth Orbit
LEOP	Launch Early Operations Phase
MCRT	Monte Carlo Ray-Tracing
MISSE	Materials on International Space Station Experiment
MLI	Multi-Layer-Insulation
SNR	Signal-to-Noise Ratio
SP	Science Phase
S/C	Spacecraft
TCC	Thermal Control Coating
TRP	Thermal Reference Point
TWU	Turn Window Unit
VDG	Vapor Deposited Gold
VOI	Venus Orbit Insertion
VUV	Vacuum Ultra-Violet

VIII. List of Symbols

A	[m^2]	Surface Area
C	[J/K]	Capacity
d	[m]	Distance
ΔE	[J]	Energy Change
E	[J]	Energy
ESH	[-]	Equivalent Sun Hours
F	[-]	View Factor
GL	[W/K]	Linear Conductor
GS	[m^2]	Radiative Conductor
Q	[J]	Heat
$\dot{Q}$	[W]	Heat flow
$\dot{q}$	[W/m^2]	Heat flux density
R_{th}	[K/W]	Thermal Resistance
S	[W/m^2]	Solar Flux Density
$\frac{\partial T}{\partial x}$	[K/m]	Thermal Gradient
T	[K]	Temperature
t	[s]	Time
W	[J]	Work
α	[-]	Solar Absorptance
β	[-]	Solar Reflectance
ε	[-]	Infrared Emissivity
λ	[W/mK]	Thermal conductivity
σ	[W/m^{2}K^4]	Stefan-Boltzmann Constant
τ	[-]	Transmission

IX. Table of Contents

1. Introduction

The VERITAS mission of NASA's Jet Propulsion Laboratory (JPL) will map the surface of Venus with a high resolution. By combining near-infrared imagery with radar data, the mission aims to answer questions such as how the geology of Venus has evolved, what geologic processes currently prevail, and whether water has ever existed on the surface.

The ESA-led EnVision mission will also set its course for Venus in collaboration with this mission. EnVision aims to study Venus from its inner core to its upper atmosphere and characterize the interactions of the individual layers with each other. This will provide a holistic view of Venus' history, activities, and climate.

Onboard these two missions are the near-infrared spectrometer VEM on the VERITAS mission and VenSpec-M on the EnVision mission. These instruments will be exposed to the Venusian environment over a long period during their missions. In addition to solar, albedo, and infrared radiation from Venus, they will be exposed to atomic oxygen (ATOX), a component of Venus' atmosphere, and charged-particle radiation. For the development of these instruments, a good understanding of the degradation effects due to these degradation sources to the Thermal Control Coatings (TCC) and various space materials is required to ensure a well-functioning instrument regarding thermal aspects as well as optical performance.

An essential subunit contributing to the instrument's performance is the baffle unit, which includes a Turn Window Unit (TWU). Since the surfaces of this unit are the only ones exposed to the Venusian environment, the materials and TCCs used must be able to withstand it without suffering significant degradation. This is especially true during the aerobraking phase(s) at Venus for both missions. During aerobraking, these surfaces will be exposed to a high ATOX flux due to a low altitude of the pericenter.

The objective of this work is to select suitable TCCs to fulfill the aspects mentioned above. For this purpose, a study of Venus' environmental conditions and the degradation mechanisms due to several degradation sources are performed. Surface requirements for all baffle unit subunits are derived, as well as the environmental conditions. These conditions include an approximated ATOX flux during the aerobraking phase, the amount of solar, albedo, and infrared radiation as Equivalent Sun Hours (ESH), and specified doses of charged-particle radiation. At the same time, the orbits representing the worst case of ambient radiation fluxes during the science phase are determined and evaluated with different coating combinations on the baffle unit. In addition, common TCCs are chosen as a preselection and the expected degradation of thermo-optical properties due to the determined environment is analyzed.

In a final analysis, all pre-selected coating combinations are simulated with a detailed thermal model of the instrument in their Begin of Life (BOL) and End of Life (EOL) states regarding thermo-optical properties. In this analysis, the specified worst-case orbits are simulated to allow a proper comparison of all coating combinations in terms of their effects on the thermal performance as well as on the optical performance of the instruments. Optical performance is determined based on the thermal stability of the instrument's optical path and the temperature distribution of the optical elements.

2. Summary

ATOX fluxes, solar and albedo radiation, expressed in ESH, as well as charged-particle radiation are considered as the main degradation mechanisms for the materials and coatings of the instrument's baffle unit. The quantity of these main degradation sources for all mission phases is determined and presented in Table 2-1.

Subunit	ATOX Flux [atoms/m^2]	Aerobraking Phase ESH	Sun-Pointing ESH	Science Phase ESH	Radiation [krad]
Baffle Shield	1.581E25	12921.81	250.12	20158.71	1760
Baffle Cone	2.662E25	3119.12	146.32	2203.02	540.8
Window	1.215E25	784.79	190.17	1854.13	188.7

Table 2-1: Results Environmental Conditions for each Subunit of the Baffle-Unit

Based on these determined quantities, the expected degradation in thermo-optical properties of preselected coatings is determined. The results of the degraded thermo-optical properties at BOL, End of Aerobraking (EOA), and EOL are presented in Table 2-2 for three preselected white and three black TCCs.

Coatings	Solar Absorptance			Infrared Emittance		
	BOL	EOA	EOL	BOL	EOA	EOL
Ceranovis V14	0.0900	0.1000	0.4300	0.9200	0.9200	0.9700
Aeroglaze A276	0.2600	0.2770	0.5591	0.8800	0.8500	0.8800
AZ-93	0.1500	0.1528	0.2608	0.9100	0.9100	0.9100
Acktar Fractal Black	0.9800	0.9800	0.9800	0.9100	0.9100	0.9100
Aeroglaze Z307	0.9500	0.9300	0.9500	0.9000	0.9100	0.9500
MAP PUK	0.9700	0.9500	0.7500	0.9100	0.9200	0.9200

Table 2-2: Results BOL, EOA, EOL optical properties of preselected Coatings

Besides the applied TCCs, the expected degradation of the Anti-Reflection (AR) coating NIR-II applied on the TWU window is determined. The expected solar reflection and solar transmission values are presented in Table 2-3.

AR Coating	Reflection			Transmission		
	BOL	EOA	EOL	BOL	EOA	EOL
NIR II	0.007	0.022	0.022	0.993	0.978	0.978

Table 2-3: Results BOL, EOA, EOL optical properties of AR-Coating

In addition to the degradation of the thermo-optical properties, other effects like a glow phenomenon due to ATOX exposure are found. This glow phenomenon does not influence the instrument's optical performance. It is also concluded that TCCs with organic constituents are sensitive to ATOX, as the coatings erode due to ATOX exposure, leading to decreasing thickness and mass loss.

A final thermal analysis simulating two worst-case orbits, which are identified while determining the environmental fluxes at Venus, shows no significant differences in the instrument's thermal or optical performance between all possible coating combinations. However, two coating combinations are proved to be advantageous over all combinations. These combinations are Ceranovis V14 with Acktar Fractal Black and AZ-Technology AZ-93 with Acktar Fractal Black.

The final decision is made by trade studies on the preselected coatings. These trade studies are presented in Figure 2-1 for the white and Figure 2-2 for the black TCCs.

Requirement		Ceranovis V14	Aeroglaze A276	AZ-Technology AZ-93
Req-BS-001	Change BOL/EOL reflectivity/emissivity	0.01/0.0	0.017/-0.03	0.003/0.0
Req-BS-002	Change BOL/EOL reflectivity/emissivity	0.33/0.05	0.282/0.03	0.108/0.0
Req-BS-003	Change BOL/EOL reflectivity	0.0	0.0	0.0
Req-BS-004	Max Operating Temperature	430°C	121°C	1400°C
Req-BS-005	Alpha/Epsilon BOL	0.098	0.295	0.165
Req-BS-005	Alpha/Epsilon EOL	0.443	0.635	0.287
Req-BS-006	Electrically Conductive	Yes	Yes	Yes
Req-BS-007	Heat Flux to S/C Cavity	Low	Low	Low
Other Aspects	Other Missions	BepiColumbo	Not known	ISS
	Availability	Good	Good	Difficult
	Heritage at DLR	Used before	No	No
	Potential Improvement	Cleaning/Sealing	Not known	Not known

Figure 2-1: Results Trade Study White TCCs

Requirement		Acktar Fractal Black	Aeroglaze Z307	MAP PUK
Req-BS-001	Change BOL/EOL reflectivity/emissivity	0.0/0.0	-0.02/0.01	-0.02/0.01
Req-BS-002	Change BOL/EOL reflectivity/emissivity	0.0/0.0	0.02/0.04	-0.2/0.0
Req-BS-003	Change BOL/EOL reflectivity	0.0	0.0	0.0
Req-BS-004	Max Operating Temperature	450°C	121°C	130°C
Req-BS-005	Alpha/Epsilon BOL	1.077	1.056	1.021
Req-BS-005	Alpha/Epsilon EOL	1.077	1.000	0.815
Req-BS-006	Electrically Conductive	Yes	Yes	Yes
Req-BS-007	Heat Flux to S/C Cavity	Low	Low	Low
Other Aspects	Other Missions	Solar Orbiter	JUICE	Plato
	Availability	Good	Good	Good
	Heritage at DLR	Other Acktar	Often used	Often used
	Potential Improvement	Not known	Not known	Not known

Figure 2-2: Results Trade Study Black TCCs

Based on these trade studies the white coating Ceranovis V14 and the black coating Acktar Fractal black are chosen to be applied at the baffle shield and the baffle cone. The degradation of the NIR-II AR-coating applied on the TWU window is found to not affect the instrument's thermal or optical performance.

3. Fundamentals

3.1 Definition of Heat

The first law of thermodynamics defines the concept of heat:

$$\Delta E = W + Q + E_M \tag{1}$$

The system thus described is delimited from the environment by a system boundary and energy changes of the system can only be caused by energy transport across this boundary. As described in equation (1), this transport can occur via three forms of energy: Work W, Heat Q, and Energy E_M, which is transported with a mass over the boundary. For thermal systems, the change in energy is mostly due to heat alone. Heat can be transported across the system boundary only if there is a temperature difference between the system and its environment. This process is called "heat transfer". This heat transfer can only occur from a body with a high temperature to a body of a lower temperature. This is described by the second law of thermodynamics [1].

In the following, the basics of determining the amount of heat transferred are described, and how the heat transfer depends on the geometry of a system with different materials. Important quantities are the heat flow $\dot{Q}$ in [W]:

$$\dot{Q} = \frac{dQ}{dt} \tag{2}$$

And the heat flux $\dot{q}$ in [W/m^2], i.e., the heat flow per unit area:

$$\dot{q} = \frac{d\dot{Q}}{dA} \tag{3}$$

Heat transfer can generally occur in three ways: conduction, convection, and radiation. In the following, only conduction and radiation are described since no heat transfer by convection takes place in the system considered in this thesis. Heat transfer by convection plays a minor role in space applications and is usually only present in heat pipes, or during launch and reentry phases.

In thermal systems, the system's internal energy is described as the capacity C multiplied by its temperature T. Heat transfer across the systems boundary as well as internal heat dissipation leads to a change in the system's internal energy ΔE. Therefore equation (1) can be rewritten with external heat flows noted as $\dot{Q}_{ext}$, and internal heat flows noted as $\dot{Q}_{int}$ to:

$$C\,\frac{dT}{dt} = \dot{Q}_{ext} + \dot{Q}_{int} \tag{4}$$

3.2 Conduction

Conduction occurs through energy transport between molecules in a material where a thermal imbalance, or temperature gradient, prevails. This transport takes place through the collisions of neighboring molecules. These molecules oscillate and move around their resting position, thus possessing kinetic energy. Therefore, the temperature of a molecule is a description or quantification of the kinetic energy of the molecule under consideration. Through interactions of neighboring molecules, kinetic energy can be transferred from molecules with high kinetic energy (high temperature) to those with lower kinetic energy (lower temperature). This form of heat transfer occurs in solids, liquids, and gases [1].

The heat flux in this type of heat transfer depends only on the material's thermal conductivity λ [W/mK], provided that a temperature gradient $\frac{\partial T}{\partial x}$ prevails. Fourier's law represents this relationship:

$$\dot{q} = -\lambda \frac{\partial T}{\partial x} \tag{5}$$

Due to the preceding minus sign, a positive heat flux always flows towards a negative temperature gradient, as described by the second law of thermodynamics [1].

Gases generally have low thermal conductivities, followed by liquids and then by solids. Solids have thermal conductivities between 1 and 450 W/mK, liquids 0.1 to 0.65 W/mK, and gases between 0.015 and 0.15 W/mK [1].

To calculate a heat flow between two points with a distance d over a contact area A, another important parameter can be used, the so-called thermal resistance R_{th} [K/W]:

$$R_{th} = \frac{d}{\lambda A} \tag{6}$$

Since the heat flow behaves similarly to an electric current, complex thermal-mathematical models can be built into simplified circuit diagrams similar to those of electric circuits. This leads to the fact that contacts that depend on several parameters can be considered as series or parallel connections of several thermal resistances. For instance, this is the case for surface contacts. The thermal resistance of such contacts depends, among other things, on the materials meeting each other, their surface roughness, unevenness, and the applied pressure [2].

3.3 Radiation

Thermal radiation is a type of heat transfer in which a body emits energy in the form of electromagnetic waves, unbound to a medium, to its surroundings. The amount of heat depends on the temperature of the body. Radiation is an important type of heat transfer in space travel because it is the only way to transport heat in a vacuum. Generally, any physical body with a temperature greater than 0 K emits thermal radiation. Therefore, the emitted heat flux depends on the temperature T and the emissivity ε of the surfaces. This relationship can be described as follows:

$$\dot{q} = \varepsilon \, \sigma \, T^4 \tag{7}$$

The Stefan-Boltzmann constant σ, used in equation (7), is 5.67E-8 W/m^2K^4 and was discovered experimentally and derived theoretically. Black bodies have an emissivity of 1 and thus radiate the maximum possible heat flux, while real bodies have an emissivity of $0 < \varepsilon < 1$. The emissivity depends on the material and the surface properties of the body. Furthermore, the emissivity can depend on the temperature, the radiation direction, and the wavelength spectrum of the radiation [1].

Besides the emissivity of a body, other parameters play an important role. A body can absorb, reflect or transmit a part of radiation incident on it. The solar absorptivity is called α, the reflectivity β, and the transmissivity τ. In general, the following relationship applies:

$$\alpha + \beta + \tau = 1 \tag{8}$$

These thermo-optical properties of a body are particularly important for space travel. The amount of absorbed and reflected ambient radiation significantly determines the temperature of exposed surfaces of a spacecraft (S/C). The transmission only plays a role for transparent materials. Thus, the absorbed heat flux of an opaque surface exposed to the Sun's radiation with the solar flux density S is given by:

$$\dot{q} = \alpha\, S \tag{9}$$

In addition to radiation from the Sun, a S/C is also exposed to reflected solar radiation from the planet, referred to as albedo radiation, and thermal radiation from the planet itself [2].

To determine the radiative heat transfer between two bodies, the view factor must be determined. For this purpose, it is assumed that a body radiates diffusely into its surrounding half-space. The ratio of outgoing rays into the half-space and incident rays on the second surface, which occupies part of the half-space, determines the view factor. Figure 3-1 shows this geometric relationship [1].

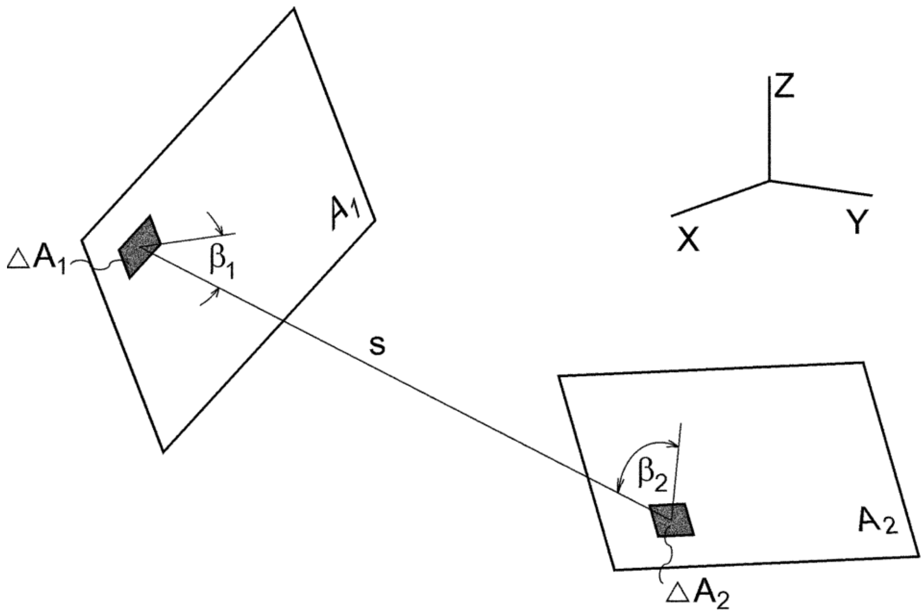

Figure 3-1: View Factor Geometric Relationship [1]

The view factor F_{12} can be derived by solving the following equation, which represents the geometrical relation shown in Figure 3-1:

$$F_{12} = \frac{1}{\pi A_1} \iint\limits_{A_2 A_1} \frac{cos\beta_1 cos\beta_2}{s^2} dA_1 dA_2 \tag{10}$$

These view factors depend on the optical properties of a surface. As soon as a specular reflection of the body is considered, an analytical determination of the view factors as described above is no longer possible. A determination of these factors is then only possible numerically, e.g., with a ray tracing method.

The task of the thermal subsystem is to establish a balance between incoming and outgoing radiation so that, with the appropriate conductive heat fluxes within the S/C, the temperatures of all components remain within their defined temperature ranges at all times during the mission duration.

3.4 ESATAN-TMS

ESATAN is a software that solves thermal models based on the lumped parameter method. These models have to be generated and specified by the user.

As mentioned, thermal models can be simply expressed as thermal networks. The first step in the development of a thermal network is the design of a geometrical model. This model includes all geometrical properties of the thermal system to be investigated, as well as material properties and thermo-optical properties of the surfaces. Employing suitable meshing, the surfaces are divided into individual faces. In the later thermal network, faces are represented by an associated simple node. This node contains all properties of the face.

A subsequent radiative analysis determines the view factors between all nodes and their environment. The analytical procedure for determining the view factors using equation (10) is only applicable for surfaces that emit purely diffusely. Since diffuse and specular reflections of the surfaces are also considered in radiative analyses, an analytical determination of the view factors is no longer possible. Therefore, ESATAN uses the Monte Carlo Ray-Tracing method (MCRT) [3].

The MCRT method is used to calculate radiative couplings and heat fluxes stochastically by making an average over a finite number of rays. These rays are emitted from radiative active surfaces of the geometric model in a random direction. The emitted rays may reach other radiative active faces of the geometry and may be reflected, transmitted, or absorbed. This interaction with other faces of the model is randomly determined, including the thermo-optical properties of the face's surface. By following the paths and including the individual history of these rays, radiative coupling between surfaces can be obtained. Accurate MCRT runs are time-consuming, especially for geometries with high reflective faces the number of emitted rays being reflected increases dramatically, leading to long simulation times [4].

The radiative exchange constant, which is called GR, between two nodes includes the emissivity ε_i, absorptivity α_j, area of the emitting node A_i, and the view factor F_{ij} between the emitting and the absorbing node. These GRs are the results derived by radiative analyses of ESATAN-TMS based on the MCRT method. The GR is defined by the following equation [3]:

$$GR = \varepsilon_i \, \alpha_j \, A_i \, F_{ij} \tag{11}$$

In addition to the radiative couplings, the conductive couplings between the faces or the nodes respectively must also be determined. The so-called GLs correspond to the reciprocal of the thermal resistance, formulated in equation (6). GLs between different parts, so-called interfaces (I/F), often have to be calculated and adjusted manually. GLs are derived based on the following equation [3]:

$$GL = \lambda \, \frac{A}{d} \tag{12}$$

Another result of a radiative analysis are the environmental heat flows as a function of time. By setting the environment properties on the radiative analysis, different environmental conditions, including whole orbits around specified bodies with a specified S/C pointing, can be identified and the associated heat flows can be determined.

The lumped parameter method uses the nodes and their determined properties, by linking them by the derived conductors. This kind of network is capable of representing even complex geometries in an easily understandable model [3].

The solution of the thermal network is obtained by solving the following equation:

$$C_i \frac{dT_i}{dt} = \sum_{j \neq i} GL_{ij}\left(T_j - T_i\right) + \sum_{j \neq i} GR_{ij}\left(T_j^4 - T_i^4\right) + \dot{Q}_{int} \tag{13}$$

The temperature of a node is T_i along with its capacity C_i [J/K] and its internal heat flows $\dot{Q}_{int}$. The linear conductance GL represents conduction, convection, or other linear processes between two nodes or between a node and the environment. The radiative exchange constant GR represents the radiation process between two nodes or between a node and the environment [3]. This equation is mainly a version of the first law of thermodynamics, described in equations (1) and (4). Energy is added to the system across the system boundary in the form of heat flows from the environment and/or internal heat dissipation as a function of time. This change in system energy then leads to a change in the temperature of the respective nodes.

Usually, the capacitances of the nodes are known, and the linear and radiative exchange constants are determined numerically using ESATAN or analytically. With the knowledge of these constants, the environmental and internal heat flows, and some boundary conditions, like initial temperatures, equation (13) can be solved for the temperatures of any node at any time representing a transient solution.

When the system is in a state of equilibrium, that is, when the system receives and releases the same amount of energy, all nodes have reached the temperature that makes this equilibrium possible. The system is then in a steady state. Prerequisites for this solution are constant heat flows of the environment and constant internal dissipation. A steady-state solution is obtained by solving the following equation [3]:

$$0 = \sum_{j \neq i} GL_{ij}(T_j - T_i) + \sum_{j \neq i} GR_{ij}(T_j^4 - T_i^4) + \dot{Q}_{int} \tag{14}$$

The conductive heat flow between two nodes or between a node and the environment can then easily be obtained by solving the following equation:

$$\dot{Q}_{ji} = GL(T_i - T_j) \tag{15}$$

And finally, the radiative heat flow between the two nodes or between a node and its environment can then be obtained by:

$$\dot{Q}_{ji} = \sigma\, GR(T_i^4 - T_j^4) \tag{16}$$

3.5 Venusian Environment

Venus has a very massive atmosphere, compared to Earth, resulting in a surface pressure that is 90 times higher than Earth's. This atmosphere consists mainly of carbon dioxide and nitrogen. The rest consists of mainly argon and other noble gases, as well as carbon monoxide, water vapor, and sulfur dioxide [5]. A summary of the species found in Venus' atmosphere compared to Earth's is given in Table 3-1.

Species	Venus	Earth
Carbon dioxide	96 %	0.03 %
Nitrogen	3.5 %	77 %
Argon	0.007 %	0.93 %
Neon	0.0005 %	0.0018 %
Water vapor	30 ppm	1 %
Heavy water	3 ppm	1 ppm
Sulfur dioxide	150 ppm	0.2 ppb
Carbonyl sulfide	4 ppm	0.5 ppb
Carbon monoxide	0.004 %	0.000012 %
Hydrogen chloride	0.5 ppm	trace
Hydrogen fluoride	0.005 ppm	trace
Atomic oxygen	trace	trace
Hydroxyl	trace	trace
Atomic hydrogen	trace	trace

Table 3-1: Composition of Venus' atmosphere compared to Earth's [5]

Venus is completely covered in clouds at altitudes around 50 km, that are optically thick at most infrared wavelengths. They can be assumed to radiate roughly the energy of a black body at a temperature of nearly 235 K. This temperature of the top of these clouds is in equilibrium with the incoming solar heat fluxes at a bond albedo coefficient of 0.76 [5].

Above the clouds dissociation of water and carbon dioxide takes place, resulting in a supply of ATOX. This process takes place on the dayside of Venus, producing oxygen atoms, which follow a general flow across the terminator to the nightside of Venus. There they descend and recombine to molecular oxygen, emitting photons, which result in a green glow [5]. This cycle of free oxygen atoms is shown in Figure 3-2.

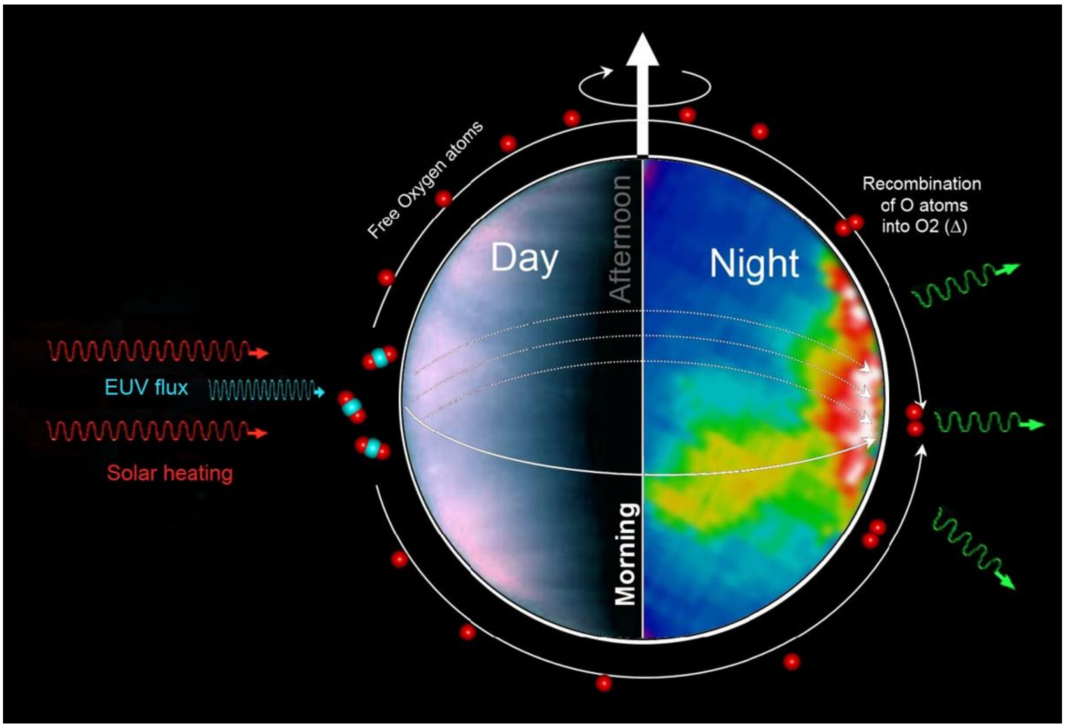

Figure 3-2: Atomic oxygen Cycle of Venus [5]

Besides the origin of ATOX, also ionization and dissociation by solar radiation of other molecular species take place at altitudes greater than 120 km. This region is called the thermosphere and extends up to altitudes of 150 km. Above this altitude, the exosphere begins, where a very low density of the atmosphere results in rare collisions between molecules [5].

At higher altitudes, the environment is defined by an induced magnetic field, which is set up by interactions between the solar wind including charged particles, and the upper atmosphere of Venus. This region is called the ionosphere. Besides this induced magnetic field there is no sign that Venus generates an internal magnetic field like Earth does. The induced magnetic field is several orders of magnitude weaker compared to Earth's magnetic field, but significant enough to limit the erosion of the upper atmosphere by the solar wind. However, the ionosphere can expand significantly, even at times of very low solar wind intensity, which allows the escape of charged particles to space, which would normally stay in the near planet environment forming radiation belts [5].

3.6 Thermal Control Coatings and the Effect of ATOX

TCCs are space-qualified coatings used on S/C surfaces to influence their thermo-optical properties. The correct TCC on a surface leads to the right amount of environmental heat fluxes absorbed and infrared fluxes emitted to establish a thermal equilibrium of the S/C to guarantee a temperature range for all components within their defined working temperature ranges. These coatings are often exposed to space and its harsh environment. Therefore, TCCs will interact with the environmental conditions and may degrade regarding their thermo-optical properties. In addition to environmental heat fluxes from the Sun and albedo fluxes in the Low Earth Orbit (LEO), ATOX in the residual atmosphere can lead to TCC degradation. Since Venus' atmosphere contains atomic oxygen as well, ATOX is a to be considered degradation source for S/C orbiting Venus at low altitudes.

The interactions of ATOX with various spacecraft materials, including polymers, TCCs, and composite materials, were well studied in the 1980s and 1990s by many orbital experiments. Especially the Long Duration Exposure Facility (LDEF) and several Space Shuttle flights (for example, STS-8) brought information on the changes in surface morphology and optical parameters of TCCs. As these experiments were performed in the LEO environment, not only the degradation due to ATOX was monitored, but also due to solar radiation, charged particle radiation, microparticle impacts, and contamination. As the interaction of different materials in LEO is well studied, the cognitions and results obtained by flight missions and several ground testing facilities will be used as a reference to determine the degradation of the TCCs of VEM/VenSpec-M in the Venusian environment. Although the mechanism of ATOX degradation at Earth is similar to that at Venus, the quantity has to be considered, not only for the ATOX flux but also for the solar radiation, charged particle radiation, microparticle impacts, etc.

ATOX is formed in the upper Earth atmosphere at altitudes typical for LEOs. The diatomic bond of oxygen molecules O_2 is broken by photodissociation by solar radiation, which has sufficient energy in short wavelengths to break the 5.12 eV diatomic bond. Due to the mean free path of the formed atoms (ca. 108 m), the probability of a reassociation or even a formation of ozone is small enough that between altitudes of 180 and 650 km, ATOX is the most abundant species [6].

Because of the erosive potential of ATOX on many spacecraft materials, an interaction between both can lead to mass loss or gain, changes in surface morphology, and in optical, mechanical, and thermal properties. This potential is increased by the orbital velocity of the spacecraft in LEO, which is typically around 8 km/s, leading to high incident fluxes, despite the low ambient density of ATOX in the LEO environment, and high collisional energies, which can lead to a degradation of the exposed surfaces. These collisional energies between the spacecraft surface and oxygen atoms typically range from 4.5 to 5 eV [7].

The reaction of atomic oxygen with spacecraft surfaces is not limited to the ram-facing surface but also to surfaces that are impacted by reflected oxygen atoms. The overall flux at Earth depends on the altitude, the orbital inclination, the solar activity, and the time of the year [8].

The collision energy can initiate numerous chemical and physical events on the surface:

- ATOX may be scattered off the surface in an altered charged or their original state. While doing so, they may react with nitrogen atoms on the spacecraft surface, forming nitrous oxide in an excited state, which can de-excite by producing a glow phenomenon
- ATOX may be captured by a potential well at or below the surface, where it forms an oxide by a chemical reaction. This oxide can then migrate from the surface into the bulk of the surface's material.

This oxidation is based on various mechanisms like abstraction, addition, elimination, replacement, and insertion, especially for polymeric materials. While abstraction is the process by which an oxygen atom abstracts an atom like hydrogen from the compound molecule, addition is the process by which an oxygen atom attaches itself to the compound molecule. This was typically seen on alkenes, producing a vibrationally excited molecule until the elimination of a hydrogen atom. If a portion of the original molecule departs after an oxygen atom has attached itself to the molecule, the process is called replacement. The oxygen then replaces a group originally present during this process and produces alkoxy and alkyl radicals. The process of insertion describes an oxygen atom lodging between two bound atoms, such as hydrogen and carbon, in an organic molecule [7].

As many TCCs comprise organic components, space shuttle missions and the LDEF experiments demonstrated the effects of ATOX exposure on organic TCC degradation. These coatings may degrade significantly during exposure to ATOX fluxes.

An additional effect of the interaction between ATOX and exposed materials was observed in LEO. So-called glow phenomena occur when the interaction between ATOX and other atmospheric species, which are also impacting the surface, cause the creation of short-lived excited state species that emit visible radiation near the surfaces of the S/C [6]. This effect is shown in Figure 3-3 during daylight on the left picture and as a time exposure at night on the right picture.

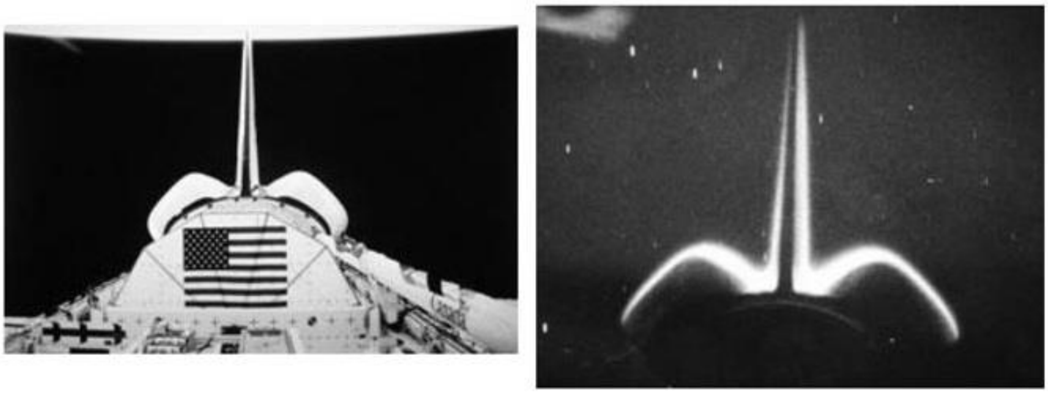

Figure 3-3: Shuttle at Day (left) and at Night (right) in LEO Environment [6]

Observations and measurements show that S/Cs in LEO produce a visible glow above surfaces oriented in the direction of motion. The glow is caused by the interaction of the S/C, traveling at approximately 8 km/s, with the high-altitude atmosphere. Based on several studies, it is apparent that various reactions between S/C surfaces and the ambient atmosphere are likely taking place, and there is not a single reaction mechanism solely responsible for glow emissions at all wavelengths. Preliminary analysis shows vibrational band structure consistent with that of NO, NO+, OH, and CO [9].

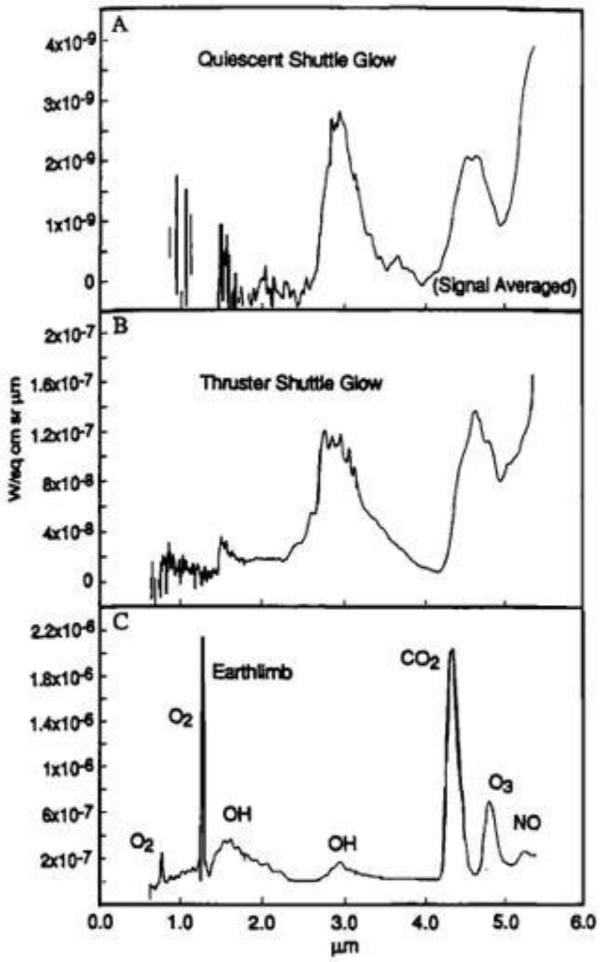

Figure 3-4: Spectrum of observed Shuttle Glow [9]

Figure 3-4 shows the signal-averaged spectrum of quiescent shuttle glow. Three peak values of this glow can be spotted, as shown in Table 3-2. Although these intensities seem to be low, this glow phenomenon may have a negative impact on the performance of optical payloads if the instrument's science wavelength band intersects with the glow phenomenon wavelengths at peak intensities.

Wavelength [nm]	**Intensity [W/cm²nm]**
3000	3.0E-12
4500	2.0E-12
5500	3.8E-12

Table 3-2: Intensities of ATOX Glow Phenomenon [9]

4. Mission and Instrument Description

4.1 Mission Overview

The launch of the EnVision S/C onboard the Ariane 62 rocket is scheduled for June 2032. A 15-month interplanetary cruise phase is followed by Venus Orbit Insertion (VOI) and a subsequent aerobraking phase which will take approximately 16 months to achieve the nominal science orbit. During the science phase, the S/C will be in a low quasi-polar Venus orbit, with an inclination between 87 to 89°, altitudes between 220 and 540 km, and an orbital period of about 92 min. This science phase will last six Venus sidereal days, which corresponds to four Earth years. The EnVision S/C will be 3 m in height and 2 m in depth with an approximately rectangular shape in stowed configuration. It will feature two deployable solar arrays for electrical power supply and a chemical propulsion system for orbit insertion. 210 Tbits of science data will be downlinked using a Ka-/X-band comms system with a 2.5 m diameter fixed high-gain antenna [10]. An overview of the payloads onboard the EnVision S/C is given in Figure 4-1.

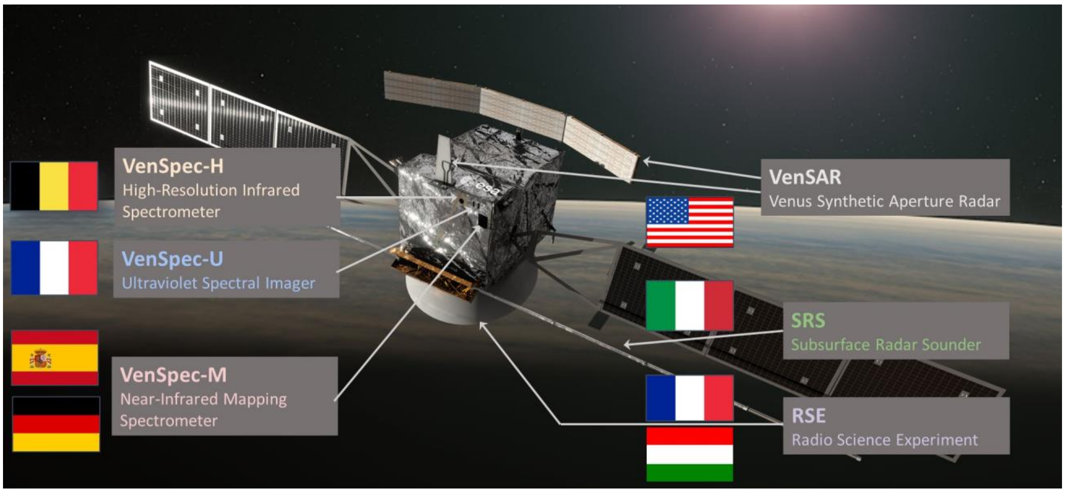

Figure 4-1: Payloads of the EnVision S/C [11]

The launch of the VERITAS S/C, with a high-performance launch vehicle that has yet to be selected, was planned to lift off in late 2027. This launch date is postponed to no earlier than 2031, due to the delay of the Psyche mission, another mission led by JPL [12].

The cruise phase will take about six months on a simple ballistic trajectory to Venus. Once arrived, VERITAS will have VOI and will switch into an aerobraking phase, which is interrupted by one of two science phases, dividing the aerobraking phase into two separate phases. The two aerobraking phases will last 5.5 and 6.1 months, while the two science phases will last 4.6 months and 2.8 years. This mission will return 224 Tbits of scientific data [13]. Figure 4-2 shows the VERITAS S/C with its payloads.

Figure 4-2: Payloads of the VERITAS S/C [13]

4.2 VEM/VenSpec-M Description

The VEM/VenSpec-M instrument is a push broom multispectral imaging system operating in a wavelength band of 850 to 1510 nm [14]. VenSpec-M, shown in Figure 4-3, will be onboard ESA's EnVision mission, while VEM will be onboard NASA's VERITAS mission. The instruments differ mainly in the geometry of the baffle shield used. VEM uses an angled baffle shield to allow inclined integration within the S/C, while VenSpec-M uses a straight baffle shield, as shown in Figure 4-3 in grey. Furthermore, VEM is covered with a Multi-Layer-Insulation (MLI) to minimize radiative interactions with the S/C. VenSpec-M controls this via a gold TCC on the outer surfaces, which are not exposed to the space environment but to the S/C cavity, to ensure low infrared emission from the instrument.

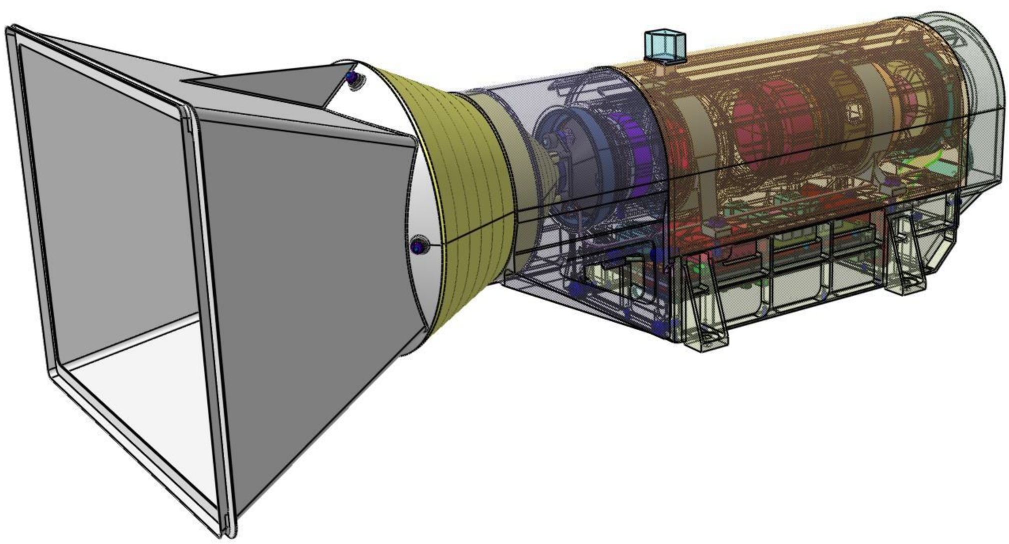

Figure 4-3: View of the VenSpec-M instrument [14]

The instrument is divided into four thermal regions mounted together in a mono-block structure. Those regions are:

- The optics
- The detector unit
- The baffle unit, including a transparent aperture cover
- The control unit

These are also the main thermal subunits of the instrument supported by spacecraft interfaces. Figure 4-4 shows all thermal areas of the instrument, as well as the conductive paths, which are strong (thick blue) or weak (thin blue) between different parts of the instrument.

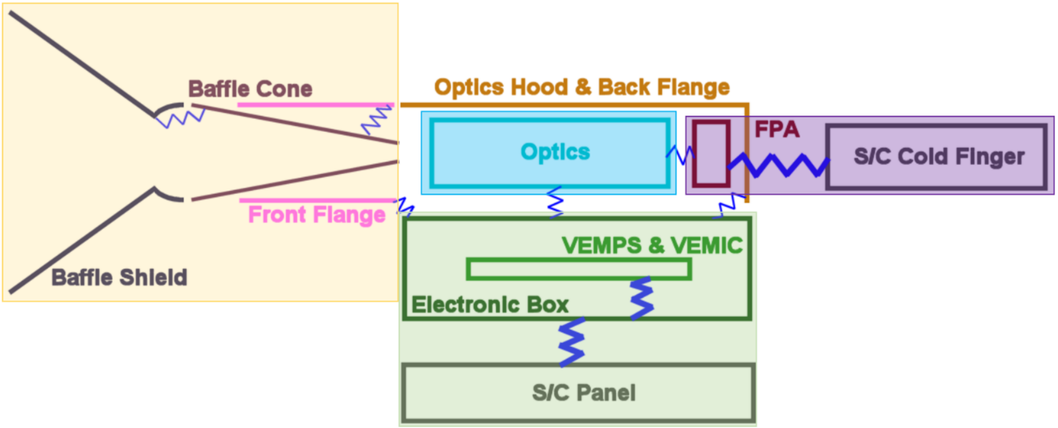

Figure 4-4: Thermal Areas of VenSpec-M [15]

Two thermal reference points (TRPs) are defined. TRP2 lies on the S/C side, representing the S/C cold finger, which is conductively attached to the focal plane assembly (FPA). TRP1 lies on the instrument itself, located at the surface of the electronic box. This electronic box is conductively attached to the S/C panel.

The FPA and the electronic box are thermally controlled via the S/C cold finger and the S/C panel so that the temperatures at the TRPs adjust to a preset temperature. This allows precise control of the FPA and electronic box to keep the installed electrical components within their operating temperature range.

The temperature of the optics will be at a level between the FPA and the electronic box. Due to the low conductivity to these two thermal regions, this temperature change takes place slowly. Thus, the temperature of the optics will follow the temperatures of the FPA and the electronic box.

A high amount of environmental heat fluxes is expected to be present for the baffle unit, as it is exposed to the space environment. Therefore, it is mostly separated from the rest of the thermal regions. This results in the temperature of the baffle unit remaining unregulated. Furthermore, the temperature of the baffle unit will probably not have a noticeable effect on the remaining thermal regions. This leads to loose temperature range requirements of the baffle unit, which is mainly dependent on the maximum operating temperature of the materials and the applied TCCs.

4.3 Cruise Phase

The Launch Early Operations Phase (LEOP) will start right after the separation of the EnVision S/C and will last no more than three days. Afterward, the S/C will be on a direct transfer orbit involving more than one complete revolution around the Sun before reaching Venus, lasting around 15 months. No gravity assist at Earth will be executed. This relatively long-lasting direct transfer orbit maximizes the mass at Venus and minimizes the aerobraking phase duration, hence the operational cost of the mission [10].

The cruise phase of VERITAS will last about six months, being on a direct transfer orbit. During the cruise phase, some trajectory correction maneuvers are planned [13].

The S/C's attitude during the cruise phase is not specified for both missions. Therefore, the S/C is assumed to be in "barbecue mode", where the S/C slowly rotates to obtain an even temperature distribution under solar radiation [16]. Due to this attitude during the cruise phase, the exposed surfaces of VEM/VenSpec-M are assumed to experience no significant degradation. Therefore, the instruments are assumed to arrive at Venus with the exposed surface's materials and coating's thermo-optical properties in a BOL state.

4.4 EnVision Aerobraking Phase

After VOI, the aerobraking phase will progressively reduce the apocenter altitude by a sequence of thousands of orbital revolutions on which the orbit dips into the upper atmosphere of Venus at the pericenter. This altitude at the pericenter is controlled to prevent the maximum heat flux, dynamic pressure, and heat load accumulated from exceeding their specified constraints. The anti-nadir panel of the S/C and the SAR reflect array will be used as the main drag surface, complemented by aerodynamic flaps, to minimize the ballistic coefficient of the S/C. Aerobraking consists of 4 different phases:

- Initial walk-in phase: The pericenter is gradually lowered with a sequence of maneuvers at a low aerodynamic regime
- Central phase: The aerodynamic regime is dominated by the peak heat flux or the peak dynamic pressure
- Final phase: The prolonged duration of the atmospheric passages makes the heat load the driving quantity for the pericenter control
- Walk-out phase: The pericenter is increased up to outside the atmosphere, achieving nominal science orbit

The central phase of the aerobraking is assumed to start 45 days after VOI. This aerobraking strategy shall allow the S/C and its payload to remain within known thermal limits of existing surface materials, with significant margins to cope with the largely unknown atmospheric density variability. An aerobraking corridor is defined as a heat flux profile as a function of the orbital period and local solar time at the pericenter and is dominated by the S/C's MLI thermal constraints until orbital periods of a few hours and then by solar array's thermal constraints towards the end of aerobraking. The aerobraking phase is assumed to last 500 days and is achieved with a total of 2000 passes through the Venus atmosphere. Figure 4-5 shows the changing altitudes of the apocenter and pericenter during the aerobraking phase [10].

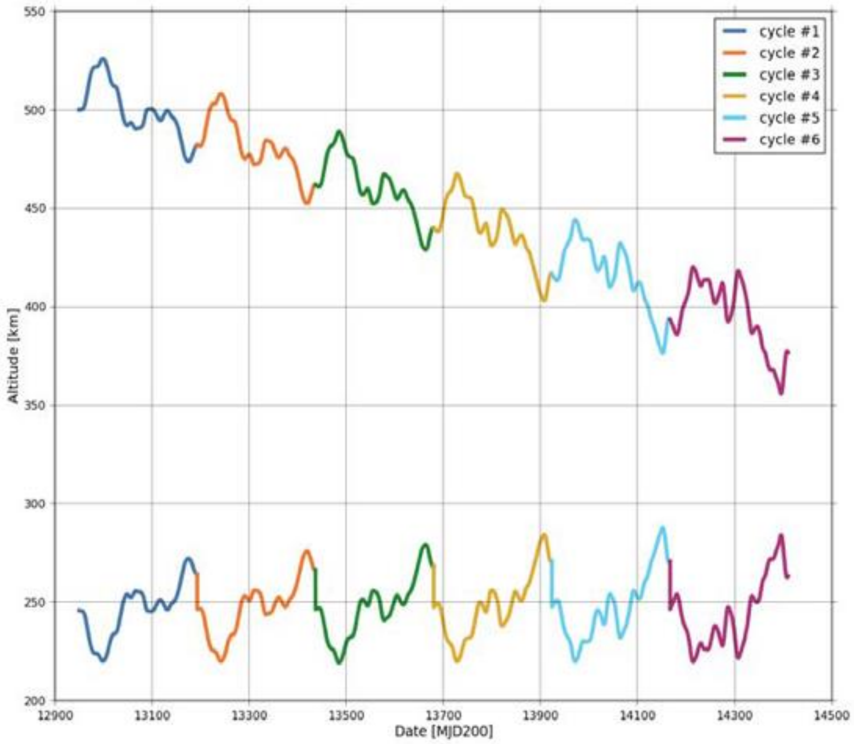

Figure 4-5: Apocenter and Pericenter altitude during Aerobraking of EnVision [10]

Figure 4-6 shows the EnVision S/C orientation during the aerobraking phase, or more precisely, the orientation during the drag passes through Venus's atmosphere near the pericenter. The anti-nadir panel (-X panel) of the S/C will be pointed toward the ram direction. Together with the backside of the SAR reflect array and the solar arrays, it will serve as the main drag surface. Therefore, the most sensitive parts of the S/C, located on the nadir panel (+X panel), are protected from the flux. This is also true for VenSpec-M as it is mounted on the nadir panel of the S/C as well. During the drag passes, the S/C may experience Angles of Attack (AOA) between -20 and 20° [10].

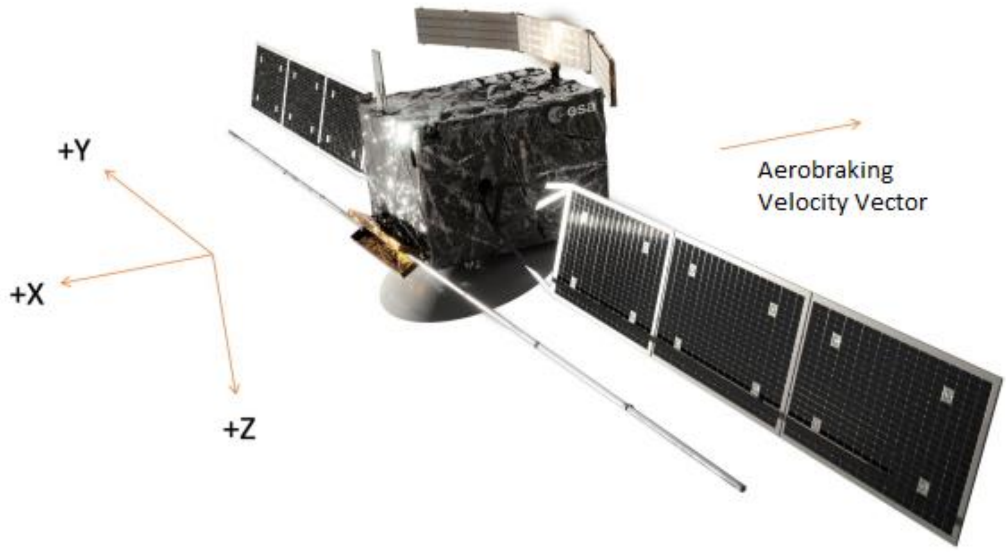

Figure 4-6: EnVision Orientation during Aerobraking [10]

Due to the pointing direction of VenSpec-M, it is assumed, that aerodynamic heating fluxes will be low. Therefore, degradation due to these heat fluxes is assumed to be neglectable. To predict the quantity of the aerodynamic heat fluxes an independent analysis on the exposed surface of the baffle unit of VenSpec-M simulating the drag passes while including the attitude of the S/C is necessary.

4.5 VERITAS Aerobraking Phase

The aerobraking phase of VERITAS is split into two roughly equal periods, AB1 and AB2, separated by 4.6 months for Science Phase 1 (SP1) as shown in Figure 4-7. The active aerobraking at Venus is expected to last 11.7 months. AB1 lasts about 5.5 months and includes the walk-in operation, one of the three periods the aerobraking phase is divided into. These periods are described as follows:

- Walk-in period: This period takes approximately ten days, on which the periapsis altitude is lowered to a target altitude of 135 km.
- Main period: This period lasts 11.6 months, in which the majority of the orbital energy is removed iteratively by hundreds of passes.
- End-game period: In this period, the pericenter is gradually raised to fine-tune orbit parameters and will last about one month, terminated with an aerobraking exit maneuver.

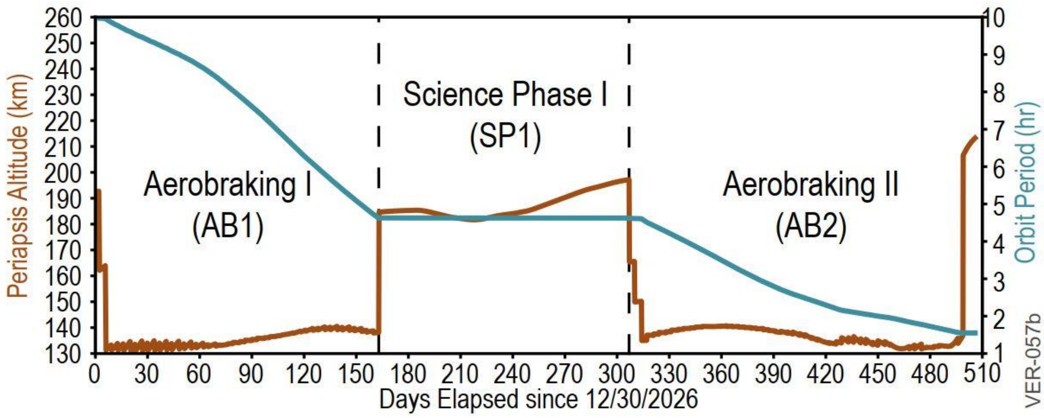

Figure 4-7: Apocenter and Pericenter altitude during Aerobraking of VERITAS [13]

Figure 4-8 shows the orientation of the VERITAS S/C during the aerobraking phase. During the drag pass near the pericenter, the -Z panel will be pointed toward the ram direction. Therefore, the solar arrays, drag flaps and the -Z panel will serve as the main drag area. The VEM instrument is located on the nadir side (-X panel) of the S/C and is located 90 degrees to the ram direction. During the drag pass no requirement states the possible AOA. The S/C is assumed to be in an aerodynamically stable attitude with loose attitude deadbands [13].

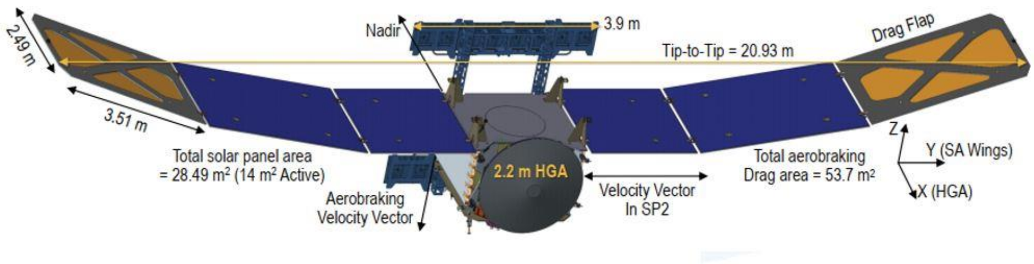

Figure 4-8: VERITAS Orientation during Aerobraking [13]

The pointing direction of VEM during the drag passes differs from that of VenSpec-M. Due to the nadir-pointing an AOA of 90° is resulting and leads to higher aerodynamic heat fluxes on the exposed surfaces of the baffle unit, compared to VenSpec-M. Therefore, the resulting heat fluxes may have a degradation effect on the applied TCCs. To specify the amount of these heat fluxes an independent analysis is necessary. However, such an analysis is out of the scope of this thesis and has to be performed in future work for both missions.

4.6 Science Phase

The transition of EnVision from the aerobraking phase to the science orbit and nominal science phase is achieved by a pericenter-raising maneuver to a height between 220 and 290 km while leaving the apocenter untouched at an altitude of 500 km. The science phase is assumed to start on 15.06.2035 and will last four years [10].

The VERITAS science phase is divided into an SP1 and SP2 phase. The SP1 phase starts after AB1 on a highly elliptical orbit with a pericenter altitude of 190 km and an apoapsis altitude of 14000 km and lasts 4.6 months. After AB2 and a six-week transition time, SP2 begins. This science phase will last almost three years [13].

5. Requirements of Surfaces and Coatings

5.1 General

In the following, the requirements for the surfaces of the baffle unit are represented. These requirements are divided into all three subunits and on their exposed and non-exposed surfaces. Furthermore, these requirements are especially important for the decision of materials and TCCs to be used on these surfaces. Most requirements deal with specifications that have not been determined yet. Parts of these values will be determined in the following chapters. In addition, bulk materials for the baffle shield and cone are selected.

5.2 Requirements Baffle Shield and Cone

The baffle unit consists of the outer baffle shield and the inner baffle cone, shown in Figure 5-1. This unit also features a TWU, protecting the optical path of the instruments of contamination, while allowing nominal operations through the protecting window. The primary goal of the baffle unit is to keep light from outside the Field of View (FOV) from shining on the instrument optics.

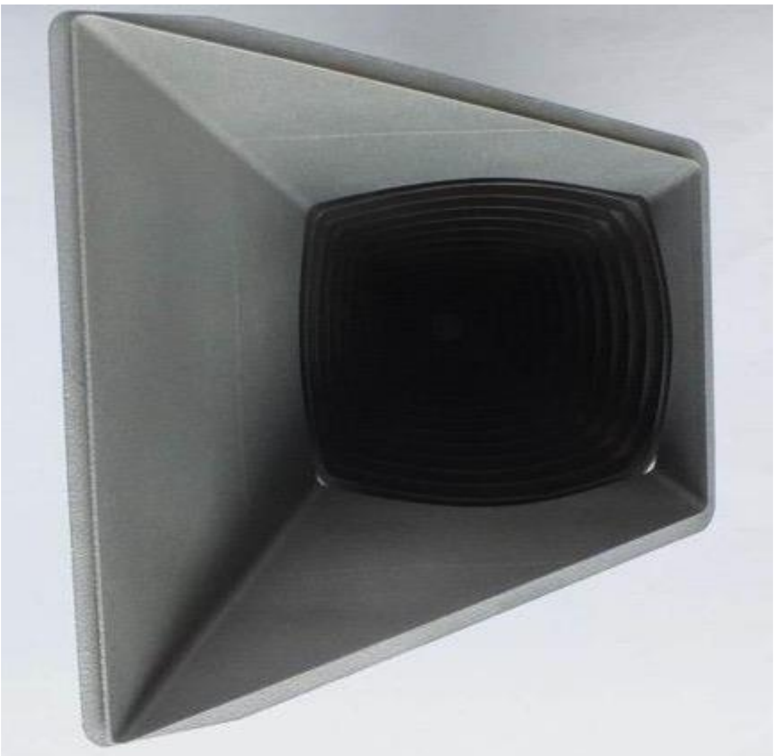

Figure 5-1: Prototype Baffle Unit of VEM without coatings [14]

As the surfaces of the baffle unit are exposed to the environment, the coatings on these surfaces are most critical to degradation effects and must comply with several requirements. The bulk material of the different subunits is protected by the applied TCCs. Therefore, the following requirements mainly relate to the applied coatings. The coatings not only have a function in thermal but also in optical aspects to reduce stray light entering the optical path of the instrument. Therefore, they shall be resistant to the conditions of the surrounding space environment over the mission duration with a minimum of degradation in thermo-optical properties. Even though the baffle unit has the least stringent temperature requirement as described in Chapter 4.2, the coatings shall stay in their specified temperature range in all operational states. Because of this loose temperature requirement, the baffle unit is mounted to the instrument with thermal isolation to mitigate the thermal interactions of this unit with the rest of the instrument. To keep the overall baffle unit low in temperature, the surfaces unexposed to the environment but with a view factor to the S/C cavity may be able to radiate heat. However, by doing so, it shall not radiate more than a specified amount of heat to the S/C. Another way to keep the temperatures at a lower level is the use of the baffle shield as a radiator. It may be beneficial to use the baffle shield like this, because of its exposure to deep space and of its relatively large surfaces.

Regarding VEM, the surfaces of the baffle unit with a view factor to the S/C cavity are covered in MLI. Therefore, they shall provide a structural connection to the used MLI around the unit. In comparison, VenSpec-M uses no MLI around the unit, therefore, this requirement is not applicable. Regarding both instruments, the baffle unit shall provide a structural connection to the outer MLI of the spacecraft.

The baffle shields' main function is straylight reduction and shielding the instrument from Sun fluxes. The baffle shield keeps light from outside the FOV from entering the instrument's optical path as a straight shot. This type of stray light can generate high noise levels on the produced image if sunlight is allowed to enter the instrument [17].

As the shield becomes sun-illuminated, a highly solar reflective and highly infrared emitting TCC is preferred to keep the unit in its desired temperature range. This also allows the usage of the baffle shield as a radiator. To assure the function of the coating, which is applied on a space-exposed surface of the instrument, the coating shall be resistant to a specified ATOX flux, irradiation flux, and charged-particle radiation dose over the mission duration with a restricted maximum degradation in the form of an increase in solar absorptivity. Also, particulate and molecular contamination shall be restrained during the science operation, which may lead to changes in the thermo-optical properties, like the reflection of the coating, due to darker particles on the surface of the coating. Table 5-1 summarizes the requirements for the TCCs and surfaces of the baffle shield with values, which are derived in the following chapters.

Req-BS-001	Exposed Surface	The applied coating shall be resistant to the approximated ATOX flux of 1.581E25 atoms/m^2 with a minimum decrease in solar reflectivity.
Req-BS-002	Exposed Surface	The applied coating shall be resistant to the expected solar flux of 20408.83 ESH with a minimum decrease in solar reflectivity.
Req-BS-003	Exposed Surface	The applied coating shall be resistant to the expected Radiation Dose of 1760 krad with a minimum decrease in solar reflectivity.
Req-BS-004	Exposed Surface	The applied coating shall be stable in the highest to be expected temperature range in all mission modes.
Req-BS-005	Exposed Surface	The applied coating shall be highly solar reflective and infrared emissive.
Req-BS-006	Exposed Surface	The applied coating shall be electrically conductive.

Req-BS-007	Un-exposed Surface	The un-exposed surfaces shall not radiate a heat flux more than (TBD) W/m^2 to the S/C.

Table 5-1: Requirements of Coatings and Surfaces of the Baffle Shield

One central aspect of the limitation of optical instruments is stray light introduced in the optical path. The primary function of the baffle cone is to remove this stray light to increase the Signal-to-Noise Ratio (SNR) on the produced image. This is done by combining a suitable geometry with a high solar absorptive TCC. Black coatings can be used on the inside of the baffle cone to absorb incoming and unwanted light. These coatings, as well as the geometrical complexity of the baffle cone, influence the factor of how much stray light is reduced. This factor typically sums up to 10^8 or more [18].

To assure a high and stable solar absorptance of the to be applied black TCC, molecular and particulate contamination shall be restrained during the science operation. If not, this may lead to a higher solar reflection caused by highly reflective contaminants present at the surface of the coating. Furthermore, the applied coating shall be resistant to a specified ATOX flux, irradiation flux, and charged-particle radiation dose over the whole mission duration with a restricted maximum decrease in solar absorptance. Also, the coating shall be stable regarding thermo-optical properties and adhesion to the bulk material in a specified temperature range. Table 5-2 summarizes the main requirements for the TCCs and the surfaces of the baffle cone with values, which are derived in the following chapters.

Req-BC-001	Exposed Surface	The applied coating shall be resistant to the approximated ATOX flux of 2.66E25 atoms/m^2 with a minimum decrease in solar absorptivity.
Req-BC-002	Exposed Surface	The applied coating shall be resistant to the expected solar flux of 2349.34 ESH with a minimum decrease in solar absorptivity.
Req-BC-003	Exposed Surface	The applied coating shall be resistant to the expected Radiation Dose of 540.8 krad with a minimum decrease in solar absorptivity.
Req-BC-004	Exposed Surface	The applied coating shall be stable in the highest to be expected temperature range in all mission modes.
Req-BC-005	Exposed Surface	The applied coating shall be highly solar absorptive.
Req-BC-006	Exposed Surface	The applied coating shall be electrically conductive.
Req-BC-007	Un-exposed Surface	The un-exposed surfaces shall not radiate a heat flux more than (TBD) W/m^2 to the S/C.

Table 5-2: Requirements of Coatings and Surfaces of the Baffle Cone

The design of the baffle cone used exploits the arrangement of a multi-vane structure as well as the number of vanes, resulting in multiple internal reflections of out-of-field light. The combination of this multi-vane structure and a highly solar absorptive TCC can provide a significant margin to a required absorption of 80%. This reduces straylight dramatically and improves the optical performance of the instruments. Figure 5-2 shows the cross-section area of the baffle unit, with the baffle shield on the left, mounted on the baffle cone. As shown, the baffle cone consists of multiple vanes with a specified mounting angle, to reduce straylight efficiently.

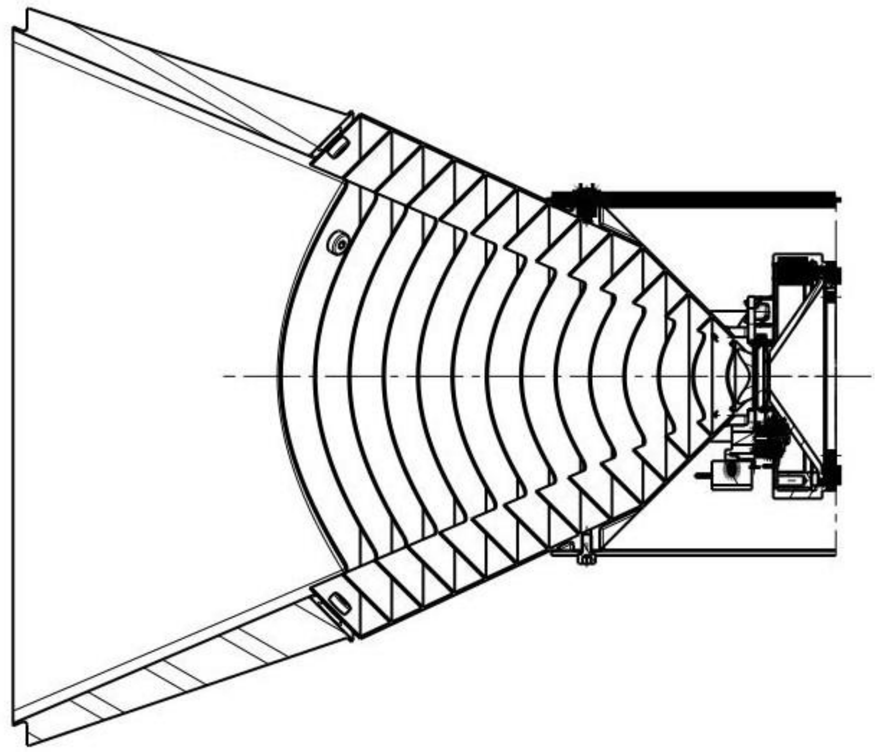

Figure 5-2: VenSpec-M Cross-section of Baffle Unit [19]

5.3 Selection Materials Baffle Shield and Cone

Common materials used in space applications are steel, aluminum, and titan. Often used alloys of these materials along with their density, thermal conductivity, and a maximum allowable operable temperature are presented in Table 5-3.

Material	**Density [kg/m³]**	**Thermal conductivity [W/mK]**	**Max. operable Temperature [°C]**	**Reference**
Steel 316	8000	15	300	[41]
Al7075	2810	130	200	[42]
AlMgSi10	2670	160	200	[43]
Ti-6Al-4V	4429	7.3	450	[44]

Table 5-3: Candidate Materials for Baffle Unit [1]

The baffle cone uses a black TCC which leads to high absorption of environmental heat fluxes, leading to high temperatures. Therefore, a material with a high maximum operable temperature is suitable, leading to steel or titan. Due to its lower density, titan is selected as the material for the baffle cone. As a common titan alloy, the use of Ti-6Al-4V on this subunit is suggested with the properties presented in Table 5-3.

Compared to the baffle cone, lower temperatures of the baffle shield are expected. This is due to the applied white TCC, leading to low absorption of environmental heat fluxes. Therefore, the maximum operable temperature plays a minor role in the selection. With its low-density aluminum may be a suitable material. Furthermore, as the baffle shield shall be used as a radiator, a high thermal conductivity is advantageous, leading to an evenly distributes temperature profile. This leads to the suggestion to use aluminum as the material for the baffle shield.

Furthermore, the complex geometry of the baffle shield offers the possibility to apply a 3D printing process. Due to the S/C MLI interface of the shield, several individual parts of the subunit would have to be milled and assembled. This can be avoided by using a 3D printing process, in which the entire subunit can be manufactured as one part. As a result, the suggested choice of aluminum alloy is AlMgSi10, an alloy that is 3D printable. The properties of the aluminum alloy are presented in Table 5-3.

5.4 Turn Window Unit

The TWU shall protect the optics in the cruise phase, especially against contamination of the optical path of the instruments. This is done via a protective window at the opening of the baffle cone, between the cone and the optical path. At the same time, it shall allow observations through the transparent window. Therefore, the window needs to be highly transmissive to reduce noise in the produced image. In case of window contamination reaching a high level, it can be opened by a one-shot mechanism, as shown in Figure 5-3.

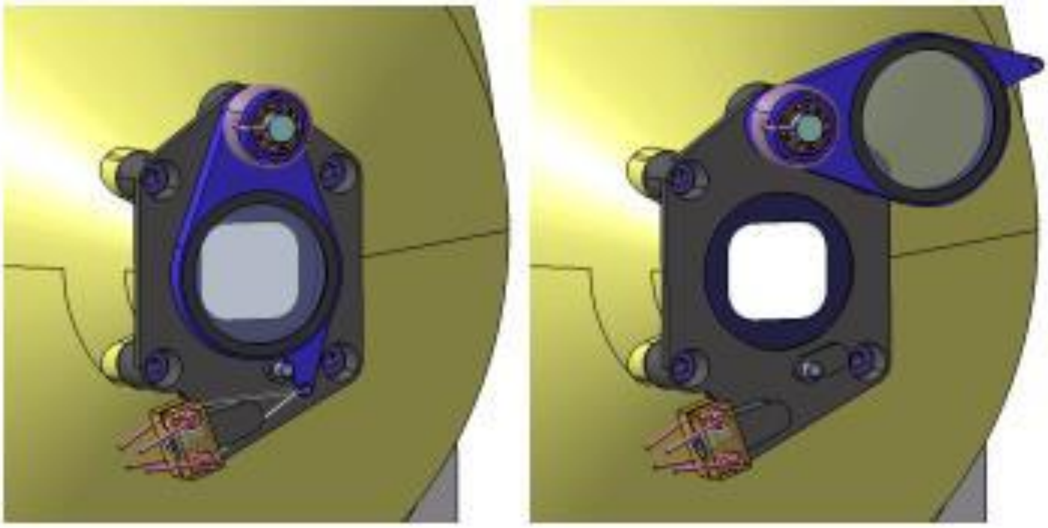

Figure 5-3: TWU closed (left) and open (right) [14]

As the window is the only part of the TWU that is directly exposed to the space environment, requirements and constraints are needed to ensure a low degradation of the thermo-optical properties of the glass. The window may be fused silica in combination with an applied AR-coating, which may be needed to be compliant with the requirements. To meet the requirements, radiation-hard glass must be used. Therefore, if an AR-coating is applied, this shall also be radiation hard. Table 5-4 summarizes the requirements of the surface and the applied AR-coating of the TWU window with values, which are derived in the following chapters.

Req-TW-001	The window of the TWU shall be resistant to the approximated ATOX flux of 1.215E25 atoms/m^2 with a minimum decrease in transmission.
Req-TW-002	The window of the TWU shall be resistant to the expected solar flux of 2044.3 ESH with a minimum decrease in transmission.
Req-TW-003	The window of the TWU shall be resistant to the expected Radiation Dose of 188.7 krad with a minimum decrease in transmission.
Req-TW-004	The window of the TWU shall not impede by design the instrument function in case of a failure of the opening mechanism.
Req-TW-005	Radiation hard glass shall be used.

Table 5-4: Requirements and Constraints of the TWU window

6. Approximation of ATOX Flux

6.1 Approach

For both missions, a cavity is formed on the S/C panel by the opening of the instrument's baffle unit, exposing this subunit directly to the environment. The surfaces are therefore exposed to an environmental ATOX flux. This is especially true during the aerobraking phase. During this phase, the ATOX flux can be described as a function of the AOA, defined between the instrument's pointing direction and the ram-direction vector during a drag pass. Therefore, the degradation of the applied coatings on these surfaces depends not on the ATOX flux in the ram direction but on the scattered amount, which is redirected inside the aperture. This scattered flux is now described as a function of the geometry as well as of the AOA of the cavity in this chapter. Impacted surfaces of the instruments are the TWU window, the baffle cone exposed surfaces, and the baffle shield exposed surfaces. The values determined here serve as the basis and justification for the requirements Req-BS-001, Req-BC-001, and Req-TW-001 from Chapters 5.2 and 5.4.

To approximate the total flux of atomic oxygen atoms hitting these relevant surfaces, a calculation method based on the paper "Atomic Oxygen Effects on Spacecraft Materials" by Bruce A. Banks [20] is developed by implementing some assumptions and simplifications.

The paper describes a Monte Carlo computational technique to determine the relative number of atomic oxygen atoms which are reactive to internal surfaces in crack openings with parallel walls, compared to atoms reacting at a reference surface outside the cavity on the S/C. The relative ATOX flux is a function of the Depth-to-Width (D/W) ratio and the AOA. To make use of this in the here described calculation method, multiple assumptions are made:

- The described technique is also valid and applicable to large openings like apertures for optical instruments.
- The number of atoms reacting at the surfaces is proportional to the number of atoms hitting the surfaces.
- The behavior of all data points produced for one specified D/W ratio is similar to all D/W ratios.
- The geometry of the aperture for both instruments is simplified to a rectangle-shaped, and therefore, parallel-walled cavity, similar to the reference cases shown in Figure 6-1.
- The approximation of the relative flow for the considered surfaces is based on the worst-case fluxes of EnVision and VERITAS for the whole mission duration.

These assumptions and simplifications must be proven conservative through a full Monte Carlo simulation of the real geometries, orbital elements, and atmospheric model. However, as a first approximation, these assumptions and simplifications are practicable.

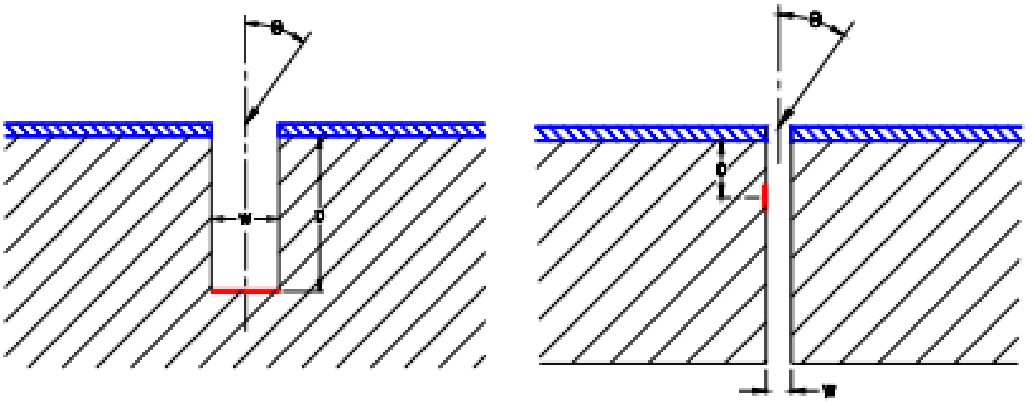

Figure 6-1: Reference cases for perpendicular (left) and parallel (right) surfaces of crack openings [20]

Figure 6-2 shows the baffle shield of VEM on the left and VenSpec-M on the right. For simplification, the shortest height of VEM is used as a worst-case to achieve a V-shaped cavity like that of VenSpec-M. However, as the orientation of the two instruments during the aerobraking phase and the specification of the worst-case ATOX fluxes for both missions are different, they will be considered separately.

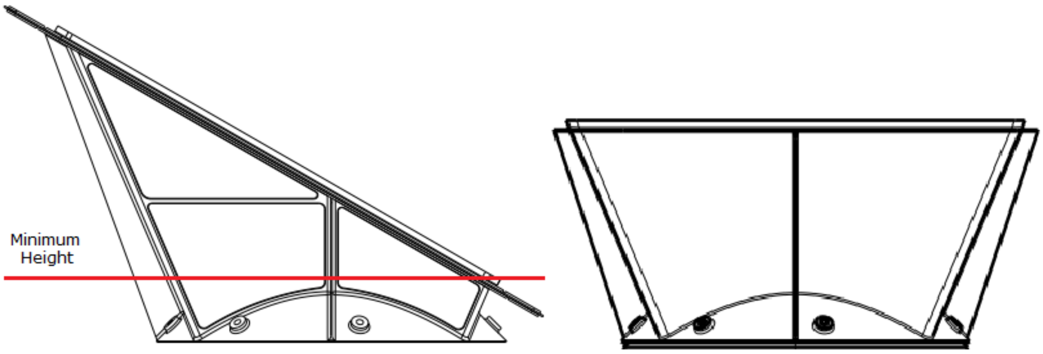

Figure 6-2: Baffle Shields of VEM (left) and VenSpec-M (right)

6.2 Simplification of the Geometries

The baffle opening of the simplified VEM instrument measures 198.82 x 165.47 mm, with the TWU window placed at a depth of 152.25 mm measured from the minimum height of the baffle shield. The width of the cavity is defined as the length which is perpendicular to the ram direction and therefore, to the S/C's velocity vector. For the instrument, this width measures 165.47 mm.

The baffle opening of the simplified VenSpec-M instrument measures 226 x 185.4 mm, with the TWU window placed at a depth of 222 mm measured from the external surface of the S/C. The width of the cavity measures 226 mm.

Perpendicular Surfaces	Parallel Surfaces
TWU Window	Upper Side Walls of Baffle Shield
Lower Fins of Baffle Cone	Side Walls at connection Baffle Shield/Cone
Upper Fins of Baffle Cone	Lower Side Walls of Baffle Cone

Table 6-1: Relevant Surfaces of VEM and VenSpec-M

Table 6-1 lists the instrument's relevant surfaces, for which the total ATOX flux is approximated. Surfaces perpendicular to the approximated flow are the TWU window, the lower fins, and the upper fins of the baffle cone. Surfaces parallel to the flow are the side walls of the baffle shield at the opening, the side walls of the baffle shield/cone at the shield's and cone's mounting point, and the side walls of the baffle cone near the TWU. Figure 6-3 shows the location of these surfaces.

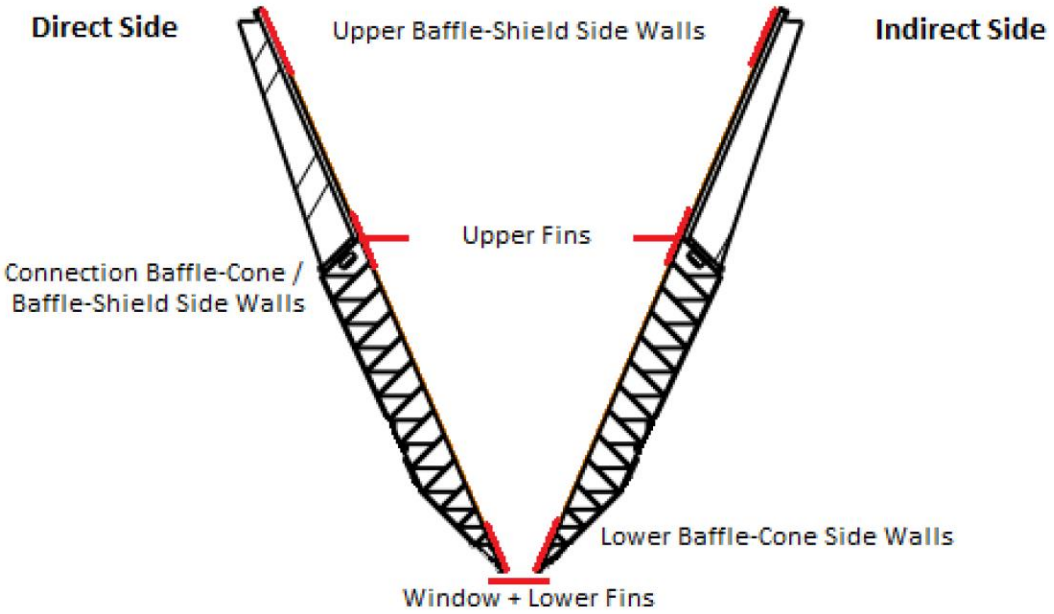

Figure 6-3: Location of relevant surfaces

For all surfaces, the D/W is calculated by using the local depth of the surface as well as the local width of the surface, which is averaged with the total width of the opening. By doing so, the real V-shape of the cavity is simplified to a parallel walled cavity, as shown in Figure 6-1. Tables 6-2 and 6-3 show the local depth, the local and averaged width, and the resulting D/W ratio for all relevant surfaces of VEM and VenSpec-M.

Surface	Local Depth [mm]	Local/Averaged Width [mm]	D/W
Upper Fins	31.09	133.91	0.23
Lower Fins	145.94	94.73	1.54
Window	152.25	92.73	1.64
Upper Side Walls of Baffle Shield	0	198.82	0
Side Walls at connection Baffle Shield/Cone	31.09	133.91	0.23
Lower Side Walls of Baffle Cone	145.94	94.73	1.54

Table 6-2: D/W ratios for relevant surfaces of VEM

Surface	Local Depth [mm]	Local/Averaged Width [mm]	D/W
Upper Fins	100.84	164.18	0.61
Lower Fins	215.69	125	1.73
Window	222	123	1.8
Upper Side Walls of Baffle-Shield	0	226	0
Side Walls at connection Baffle Shield/Cone	100.84	164.18	0.61
Lower Side Walls of Baffle-Cone	215.69	125	1.73

Table 6-3: D/W ratios for relevant surfaces of VenSpec-M

As the scattered number of atoms impacting the exposed surfaces is also a function of the AOA, three cases are considered for VEM, with case 3 as the worst-case scenario.

Compared to VEM, VenSpec-M is positioned on the S/C's anti-ram direction face, resulting in an AOA of 180°. As the calculation method is only valid for AOAs between 0° and 90°, an assumption has to be made for the anti-ram side. ESA specifies an absolute ATOX flux for the anti-ram side, which is significantly lower than the freestream in the ram direction. This reduced flux is assumed to flow into the instrument's aperture against the velocity direction of the S/C at an AOA of 0°. By making this assumption, a conservative approach is possible to calculate the flux at the S/C's anti-ram panel. Table 6-4 shows the cases which only differ in the AOA.

Instrument	Case	AOA [°]
VEM	1: Instrument perpendicular to ram-direction	90
	2: First case + 30° angled mounting inside the spacecraft	60
	3: Second Case + additional angle of attack of 20° (worst-case)	40
VenSpec-M	1: Instrument in anti-ram direction (reduced flux, worst-case)	0

Table 6-4: Relevant cases based on angles of attack

6.3 Perpendicular Flux

Figure 6-4 shows the paper's results of at least 20 runs using a 2-dimensional Monte Carlo model to approximate the relative number of atomic oxygen atoms reacting at the bottom of a cavity, compared to the number of atoms reacting at the reference surface. The results are averaged to create a single data point [20].

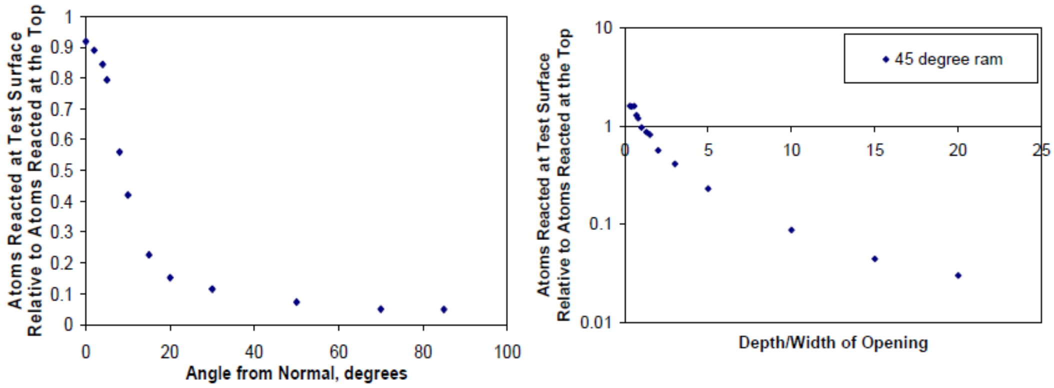

Figure 6-4: Relative number of atoms that reacted at bottom of the cavity [20]

These data points are used to make an approximation of the relative flux for all surfaces which are perpendicular to the flow. Based on the left diagram of Figure 6-4 the number of atoms that reacted at these surfaces, relative to the atoms at the reference surface, can be read as 0.06 for an AOA of 90° and 60°, 0.1 for an AOA of 40°, and 0.92 for an AOA of 0°. These values are also presented in Table 6-5.

However, these values are only valid for a D/W ratio of 10. Under the aforementioned assumption that the behavior of the data points in the left diagram of Figure 6-4 is similar to all D/W ratios, a correction factor is derived to correct for the actual D/W ratios.

As the right diagram of Figure 6-4 is also only valid for an AOA of 45°, this assumption is also applicable to these data points. The resulting error due to a possible difference in the real behavior of these data points cannot be defined unless a full Monte Carlo simulation is made. However, the expected error made by these assumptions will be lower for the defined worst-case of 40° compared to cases 1 and 2.

Looking at the right diagram of Figure 6-4 a value of 0.1 for a D/W ratio of 10 can be read. These data points are based on an AOA of 45°. Assuming that these data points behave similarly for all other AOAs, a correction factor for all D/W ratios is derived. This leads by multiplying with the before-read values to corrected values shown in Table 6-5.

Instrument Part	D/W	AOA [°]	Uncorrected Values	Correction Factor	Relative Number of Atoms
VEM	0.23	90/60	0.06	16	0.96
Upper Fins	0.23	40	0.1	16	1.6
VEM	1.54	90/60	0.06	8.2	0.49
Lower Fins	1.54	40	0.1	8.2	0.82
VEM	1.64	90/60	0.06	7.3	0.44
Window	1.64	40	0.1	7.3	0.73
VenSpec-M	0.61	0	0.92	16	14.72
Upper Fins	-	-	-	-	-
VenSpec-M	1.73	0	0.92	6.6	6.1
Lower Fins	-	-	-	-	-
VenSpec-M	1.8	0	0.92	6.4	5.89
Window	-	-	-	-	-

Table 6-5: Relative number of atoms reacting at perpendicular surfaces

For low D/W ratios and low AOAs, the factor for the relative number of atomic oxygen atoms reacting at the inner surface compared to the external reference surface can reach values significantly higher than 1 (100%). This effect is shown in the right diagram of Figure 6-4. This may be an effect of the aperture gathering and trapping a high number of atomic oxygen atoms from the incoming flow and scattering them to the upper fins, lower fins, and the window resulting in higher atomic oxygen fluxes compared to the ram direction flux, or anti-ram direction flux in the case of VenSpec-M. Also, this may be the same effect as due to a boundary layer the velocity inside a tube increases with depth. Therefore, local hot spots with high incident ATOX fluxes can occur.

The results of VEM show no difference between an AOA of 90° and 60° as the same relative number of atoms react at the surfaces for both angles. More atoms react at the upper fins, compared to the reference surface under an AOA of 40°. Especially for an AOA of 0°, the results of VenSpec-M show that significantly more atoms are expected to react at all perpendicular surfaces compared to the reference surface.

6.4 Parallel Flux

The side wall surfaces of the apertures can be split up into a direct side, facing against the incoming flux, and an indirect side, which is only impacted by scattered atoms. For both sides, three positions are considered for approximating the total ATOX flux. A surface placed directly at the top, right at the bottom, and roughly halfway down, representing the mounting point between the baffle cone and the baffle shield. A local and averaged width is calculated for all surfaces, and a rectangle-shaped cavity is assumed. This leads to three different geometries with three different D/W ratios for each instrument. As the left diagram of Figure 6-5 is only valid for a D/W ratio of 5, correction factors are made up to correct for all D/W ratios of the surfaces. The value for a D/W ratio of 5 in the right diagram of Figure 6-5 can be read to 0.04 as a reference.

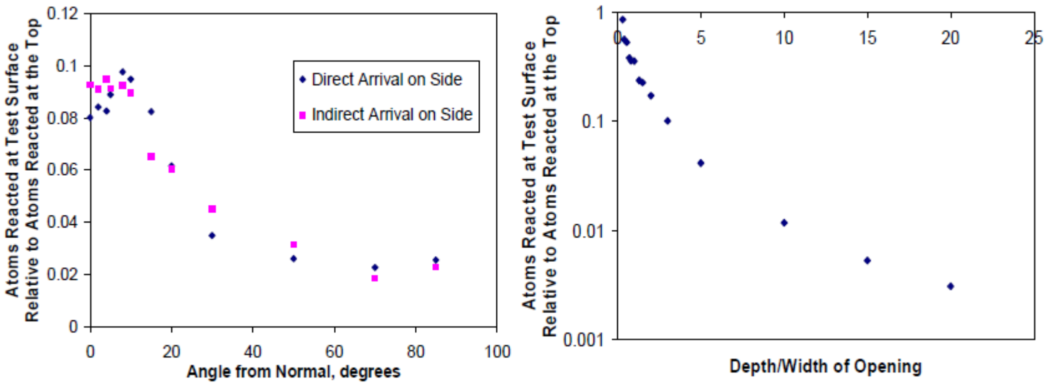

Figure 6-5: Relative number of atoms reacted at side walls of the cavity [20]

Table 6-6 summarizes all cases for the side walls approximations, as well as the corrected values of the relative number of atoms reacting on the surfaces compared to the external reference surface on the S/C. The procedure of deriving these values is similar to that used in the perpendicular flux by using the diagrams shown in Figure 6-5.

The results, presented in Table 6-6, show that the relative number of atoms reacting at the direct surface at AOAs higher than 60° is higher than those for the indirect side. However, this changes for an AOA of 40°, as more atoms are now reacting on the indirect side compared to the direct side. Also, an AOA of 90° is more critical on the indirect side than an AOA of 60°, as more atoms react at the considered surfaces. For large D/W ratios and high AOA, only as low as 13% of atomic oxygen atoms are reacting at the side walls surfaces compared to the external reference surface. This may contradict the results of the lower fins, where 44% of the atoms are reacting at the surface compared to the external reference surface. However, this contradiction can approximate the trapping, and backscatter effect of the perpendicular fins of the baffle cone. This can lead to a lower flux on the baffle cone side walls, compared to the lower fins.

Instrument Part	D/W	AOA [°]	Uncorrected Values	Correction Factor	Relative Number of Atoms
VEM	0	90	0.026	25	0.65
Upper Baffle Shield	0	60	0.025	25	0.63
Direct	0	40	0.03	25	0.75
VEM	0	90	0.024	25	0.6
Upper Baffle Shield	0	60	0.025	25	0.63
Indirect	0	40	0.038	25	0.95
VEM	0.23	90	0.026	20.75	0.54
Connection	0.23	60	0.025	20.75	0.52
Direct	0.23	40	0.03	20.75	0.62

Instrument Part	D/W	AOA [°]	Uncorrected Values	Correction Factor	Relative Number of Atoms
VEM	0.23	90	0.024	20.75	0.5
Connection	0.23	60	0.025	20.75	0.52
Indirect	0.23	40	0.038	20.75	0.79
VEM	1.54	90	0.026	5.5	0.14
Lower Baffle Cone	1.54	60	0.025	5.5	0.14
Direct	1.54	40	0.03	5.5	0.17
VEM	1.54	90	0.024	5.5	0.13
Lower Baffle Cone	1.54	60	0.025	5.5	0.14
Indirect	1.54	40	0.038	5.5	0.21
VenSpec-M	0	0	0.08	25	2
Upper Baffle Shield	-	-	-	-	-
Direct	-	-	-	-	-
VenSpec-M	0	0	0.093	25	2.33
Upper Baffle Shield	-	-	-	-	-
Indirect	-	-	-	-	-
VenSpec-M	0.61	0	0.08	13.5	1.08
Connection	-	-	-	-	-
Direct	-	-	-	-	-
VenSpec-M	0.61	0	0.093	13.5	1.26
Connection	-	-	-	-	-
Indirect	-	-	-	-	-
VenSpec-M	1.73	0	0.08	5	0.4
Lower Baffle Cone	-	-	-	-	-
Direct	-	-	-	-	-
VenSpec-M	1.73	0	0.093	5	0.47
Lower Baffle Cone	-	-	-	-	-
Indirect	-	-	-	-	-

Table 6-6: Relative number of atoms reacting at parallel surfaces

6.5 Absolute ATOX Flux

All values derived represent a relative number of atomic oxygen atoms reacting at the test surface compared to a reference surface on the external S/C. Due to this relative representation, one cannot make an absolute assumption of a total flux hitting the relevant test surfaces without knowing the total flux in the ram or anti-ram direction and the total number of atomic oxygen atoms hitting the reference surface as a function of the AOA.

For VERITAS and EnVision different total fluxes of ATOX were specified based on preliminary analyses executed by external facilities. The specified ATOX flux for VERITAS defines the total ATOX flux that VEM will be exposed to over the whole mission duration. In contrast, for EnVision the specified flux represents the amount of ATOX during the aerobraking phase for both sides in the ram and anti-ram direction. Table 6-7 shows these specified ATOX fluxes for both missions.

Mission	ATOX flux [Atoms/m^2]	Direction	Reference
VERITAS	2.6E25	Ram	[22]
EnVision	2.0E26	Ram	[21]
EnVision	1.73E24	Anti-Ram	[21]

Table 6-7: Total ATOX flux in Ram Direction

As a worst case, the total flux specified for VERITAS will be assumed to be applied entirely during the aerobraking phase of the mission. The total flux hitting the relevant test surface can be approximated by assuming that atoms hitting and atoms reacting at the surface are proportional to each other. Therefore, the already derived values can be used as a simple factor, in addition to a factor reducing the fluxes as a function of the AOA of the reference surfaces.

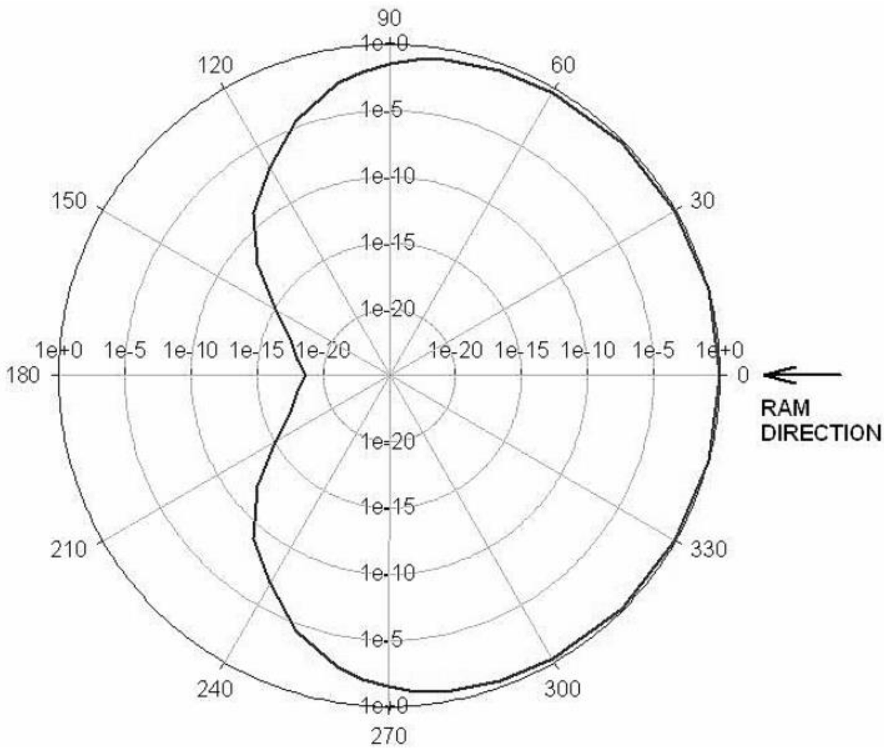

Figure 6-6: Relative ATOX flux as a function of AOA [6]

Figure 6-6 shows the relative ATOX flux as a function of the AOA, defined between the normal of the arrival surface and the ram direction for a spacecraft in a 400km LEO [6].

Based on this figure, relative factors for all relevant AOAs can be read to approximate the total number of atomic oxygen atoms hitting the reference surface of VEM. Table 6-8 summarizes these factors.

AOA [°]	Relative Factor
90	0.035
60	0.43
40	0.64

Table 6-8: Relative factors for relevant AOAs

The factors shown in Table 6-8 are not applicable for EnVision as the ATOX flux for the anti-ram direction and therefore the reference surface of VenSpec-M is already specified.

Table 6-9 summarizes the combined relative factors for all beforementioned surfaces and is therefore, a complete list with factors to be applied to a specified ATOX flux for all surfaces of both instruments whose coatings may undergo degradation in thermo-optical properties.

Surface	AOA [°]	Combined Relative Factor
VEM Perpendicular	90	0.0336
Upper Fins	60	0.4128
	40	1.024
VEM Perpendicular	90	0.0172
Lower Fins	60	0.2107
	40	0.5248
VEM Perpendicular	90	0.0154
Window	60	0.1892
	40	0.4672
VenSpec-M Perpendicular	0	14.72
Upper Fins	-	-
	-	-
VenSpec-M Perpendicular	0	6.1
Lower Fins	-	-
	-	-
VenSpec-M Perpendicular	0	5.89
Window	-	-
	-	-
VEM Parallel	90	0.0228
Upper Baffle Shield	60	0.2709
Direct	40	0.48

Surface	AOA [°]	Combined Relative Factor
VEM Parallel	90	0.021
Upper Baffle Shield	60	0.2709
Indirect	40	0.608
VEM Parallel	90	0.0189
Connection	60	0.2236
Direct	40	0.3968
VEM Parallel	90	0.0175
Connection	60	0.2236
Indirect	40	0.5056
VEM Parallel	90	0.0049
Lower Baffle Cone	60	0.0602
Direct	40	0.1088
VEM Parallel	90	0.0046
Lower Baffle Cone	60	0.0602
Indirect	40	0.1344
VenSpec-M Parallel	0	2
Upper Baffle Shield	-	-
Direct	-	-
VenSpec-M Parallel	0	2.33
Upper Baffle Shield	-	-
Indirect	-	-
VenSpec-M Parallel	0	1.08
Connection	-	-
Direct	-	-
VenSpec-M Parallel	0	1.26
Connection	-	-
Indirect	-	-
VenSpec-M Parallel	0	0.4
Lower Baffle Cone	-	-
Direct	-	-
VenSpec-M Parallel	0	0.47
Lower Baffle Cone	-	-
Indirect	-	-

Table 6-9: Combined relative factors for all test surfaces

6.6 Results of Approximated ATOX Flux

As a final result, the worst cases with the highest relative factors are identified and assigned to the subunits. Table 6-10 states these worst cases with the approximated absolute ATOX fluxes based on the specified ATOX fluxes shown in Table 6-7. For the VEM instrument, these worst cases are all under an AOA of 40°, while for VenSpec-M, they are under an AOA of 0°.

Subunits	Relative Factor	ATOX Flux based on VERITAS Ram [Atoms/m²]	ATOX Flux based on EnVision Ram [Atoms/m²]	ATOX Flux based on EnVision Anti-ram [Atoms/m²]
VEM Baffle Shield	0.608	**1.581E25**	1.216E26	-
VEM Baffle Cone	1.024	**2.662E25**	2.048E26	-
VEM TWU Window	0.4672	**1.215E25**	9.344E25	-
VenSpec-M Baffle Shield	2.33	-	-	4.031E24
VenSpec-M Baffle Cone	14.72	-	-	2.547E25
VenSpec-M TWU Window	5.86	-	-	1.019E25

Table 6-10: Total ATOX flux worst cases

Due to the conservative assumptions made on the anti-ram side of EnVision, the approximated fluxes for VenSpec-M reach values higher than 14 times the specified ATOX flux in the anti-ram direction. Thus, the ATOX flux in the anti-ram direction is almost 13% of the specified flux in the ram direction.

These final values represent a first approximation of the ATOX fluxes inside the VEM and VenSpec-M instruments and must be checked by a full Monte Carlo simulation. The boldly marked values in Table 6-10 are further used as input for a degradation analysis. These values are chosen based on a worst-case assumption. The ATOX fluxes based on the specified EnVision ram direction flux are over-conservative because they are considered with a VERITAS worst-case in the AOA, which is not equal to the orientation of the EnVision S/C during the drag passes.

7. Identification of Worst-Case Orbits

7.1 Approach

To identify the worst-case orbits during the science phase of VEM/VenSpec-M, the whole science phase (1460 days) of the VenSpec-M instrument is simulated and evaluated in terms of incident environmental heat fluxes for all subunits of the baffle unit. The VenSpec-M instrument is chosen for this simulation because of the availability of SPICE data describing the exact orbits around Venus during the whole science phase. In the following, the used ESATAN-TMS Model is described, as well as important settings, such as the orientation of the instrument. The results of the environmental heat fluxes are presented and discussed, and the worst-case orbits are determined. Furthermore, the results of this simulation are also representative of VEM, as both missions will be on similar orbits with almost the same instrument pointing. Until SPICE data is available for VEM, the determined worst-case orbits are assumed to be similar for VEM along with their environmental incident heat fluxes.

7.2 ESATAN-TMS Model Description

This simulation makes use of the MCRT method by making a radiative analysis. Therefore, the calculation time can be significantly high, due to the high reflective surfaces of the baffle shield, as described in Chapter 3.4. To reduce the calculation time a simplified model of the instrument is used as well as a selection of orbits is simulated. The results are then averaged over this selection of orbits.

As this analysis is conducted to identify the incident environmental heat fluxes for the space-exposed surfaces of VenSpec-M, a simplified model of the instrument shown in Figure 7-1 is developed. This model contains only the baffle unit with the baffle shield (grey), the baffle cone (black), and the TWU window (purple), represented by 211 thermal nodes.

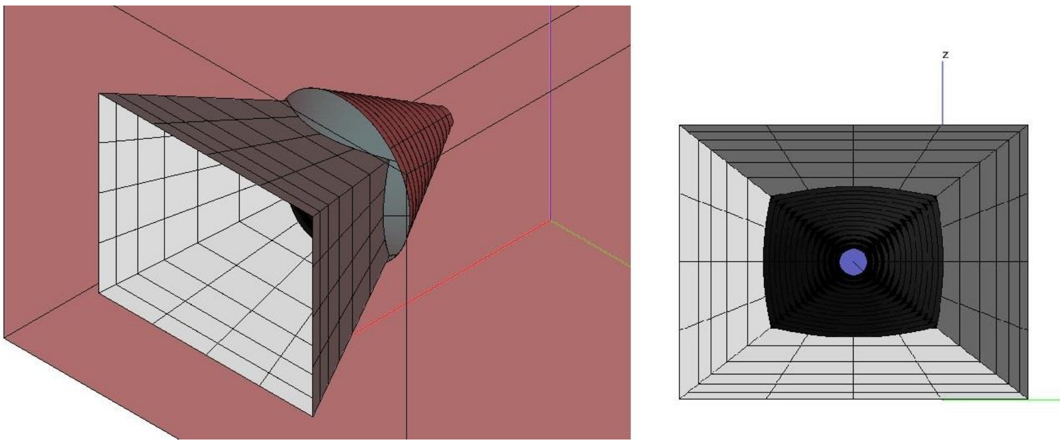

Figure 7-1: Simplified Model of VenSpec-M used for environmental heat flux determination

As shown in Figure 7-1, the internal surfaces of the baffle unit are the only ones exposed to the space environment. All other surfaces are shielded by the S/C cavity, shown in light red.

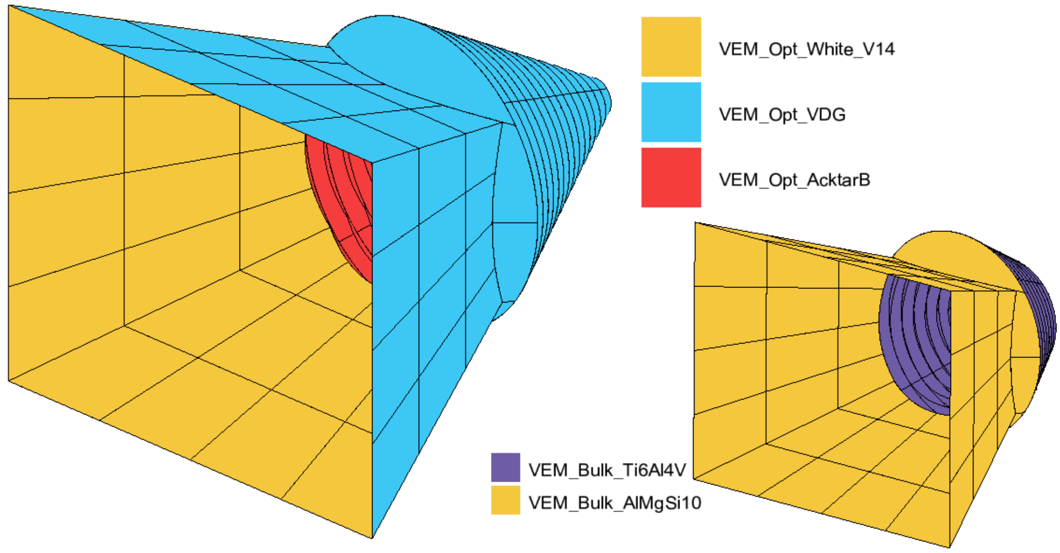

Figure 7-2: Coating and Bulk Material of Baffle Unit

Figure 7-2 shows the bulk material and the applied coating of the baffle unit. The base material of the baffle shield is made of the selected aluminum alloy AlMgSi10 and is coated with a white TCC with a reference solar absorptance of 0.2. The base material of the baffle shield is made of the selected titanium alloy Ti6Al4V and is coated with a black TCC with a reference solar absorptance of 0.9. As VenSpec-M is not wrapped in MLI, the surfaces exposed to the S/C cavity are coated with vapor-deposited gold (VDG), with an infrared emissivity of 0.03. For the TWU window not shown in Figure 7-2, quartz glass is used as the base material, simulated with a solar absorptance of 0.04, which is typical for normal uncoated glass.

Besides the use of a simplified model, which also reduces the calculation time, a timestep of 1 day is chosen to calculate the environmental fluxes. By doing so, a representative orbit, based on SPICE data, for each day is simulated. The instrument is oriented nadir-pointing for the whole simulation. Figure 7-3 shows a representative science orbit and the attitude of the whole instrument. Although Figure 7-3 shows the whole VenSpec-M instrument, this analysis uses the simplified thermal model shown in Figure 7-1.

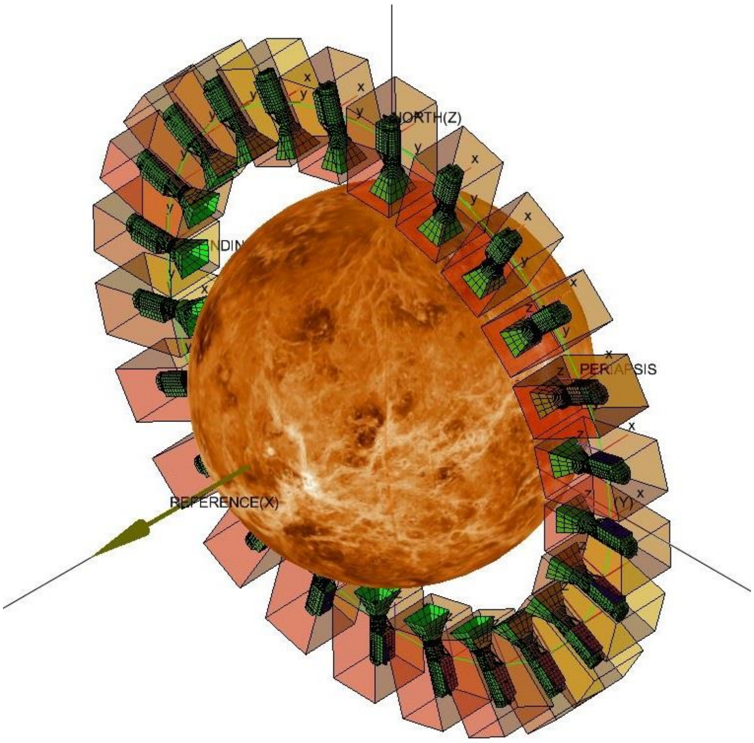

Figure 7-3: Representative Science Orbit of VenSpec-M

For this thermal model, the solar irradiance at Venus is considered to be at 2601 W/m^2 with an uncertainty of 1.5 W/m^2. The Venus bond albedo coefficient is assumed to be constant over longitude and latitude at a value of 0.76. Furthermore, Venus is considered to radiate infrared fluxes at a spectrum equivalent to a black body at a temperature of 232 K. Therefore, a value of 164 W/m^2 results for the infrared fluxes, which corresponds to the thermal radiation emitted by the clouds top [23]. This corresponds to the determined Venus environmental conditions presented in Chapter 3.5.

To evaluate the incoming environmental heat fluxes, the absorbed heat fluxes of the space-exposed surfaces are used instead of the incoming heat fluxes. This is because ESATAN-TMS includes reflective light from surfaces in the absorbed but not in the incident heat fluxes. The ESATAN-TMS processed incident heat fluxes include only solar, albedo, and planet IR radiation. Light not absorbed by a surface is reflected and can impact another surface, leading to higher irradiation of the second surface. On this second surface, the light can be reflected again or absorbed, and so on. The usage of the absorbed heat fluxes for each surface accounts for this effect and guarantees conservative values. To derive the incoming heat fluxes from the absorbed heat fluxes, they are divided by the absorptance of the surfaces' TCC. The post-processing is conducted by a post-process script written in Python, the results of which are presented in the following chapters.

7.3 Environmental Incident Heat Fluxes

The baffle shield is the part of the instrument that is predicted to see the most Sun fluxes on its surfaces, as it is intended to shield the instrument from the Sun and other light sources.

Figure 7-4 shows the resulting maximum time-averaged heat fluxes for the baffle shield over one day. The thermal node with the highest time-averaged heat flux is plotted for each timestep. This diagram is used to identify the worst-case orbit on which the environmental fluxes are maximal, making up the hot case for this part of the instrument during the science phase.

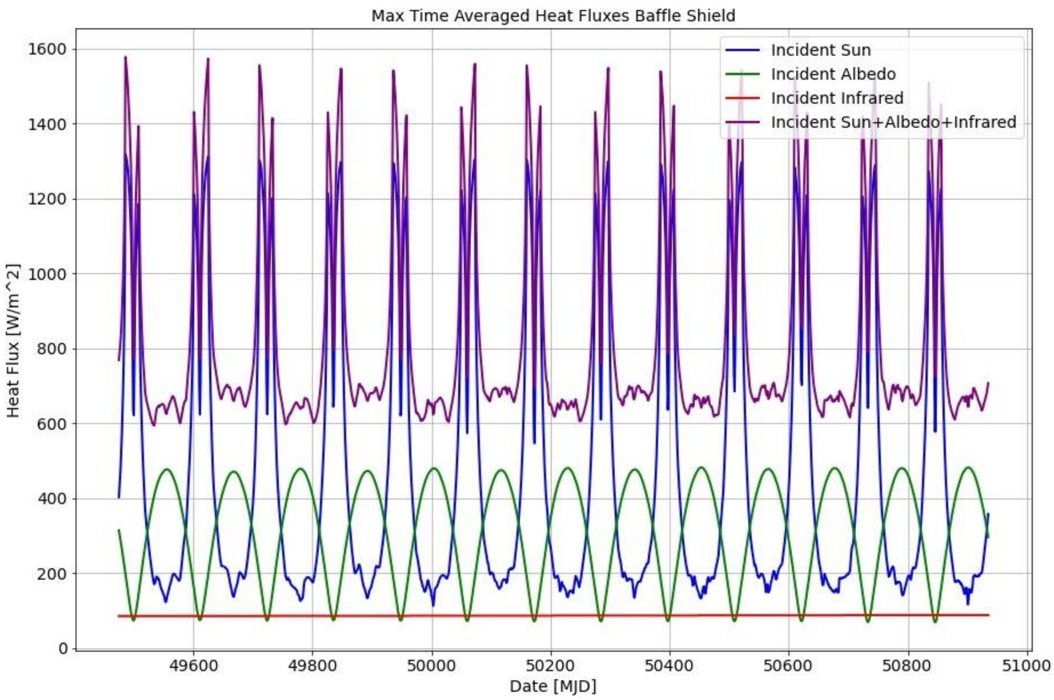

Figure 7-4: Maximum time-averaged heat fluxes for the baffle shield

The visible peaks in the time-averaged solar fluxes are present around orbits with a longitude of ascending node of 90° and respectively 270° with an offset of ca. ± 20°. During these orbits, the baffle shield gets illuminated from the Sun, while as for most of the remaining orbits, the baffle shield is covered from the Sun by Venus, due to the nadir pointing of the S/C. Since the effect of multiple reflections is permitted, the incoming solar flux is reflected from the baffle shield into the instrument, increasing the overall solar heat flux on this subunit. This effect is maximal on slightly tilted orbits with a longitude of ascending node around 70°, 110°, 250°, and 280°. The lowest time-averaged solar fluxes can be found on orbits with a longitude of ascending node of 0° and 180°, due to the orbit orbital plane being parallel to the Sun direction. These time-averaged solar fluxes are periodically stable, due to the symmetry of the geometry and the orbits. Furthermore, some minor deviations in the height of the peaks can be seen, due to a slight variation in the distance to Venus and to the Sun over the science phase.

The time-averaged albedo fluxes are minimal on orbits with a longitude of ascending node of 90° and 180° respectively, and maximal on orbits with a longitude of ascending node of 90° and 270° respectively. These fluxes are also periodically stable with minor deviations.

The incident infrared flux stays nearly constant over the simulation time and is slightly increasing over the science phase. This is due to small changes in the orbits caused by external influences over the duration of the science phase and a constant nadir-pointing orientation of the instrument. All the environmental heat fluxes sum up to a combined periodically stable incident environmental heat flux.

The highest time-averaged heat flux of the combined environmental fluxes over the whole simulation time is found in the first few days of the science phase. Table 7-1 shows the maximum time-averaged environmental heat flux on day 49486 MJD.

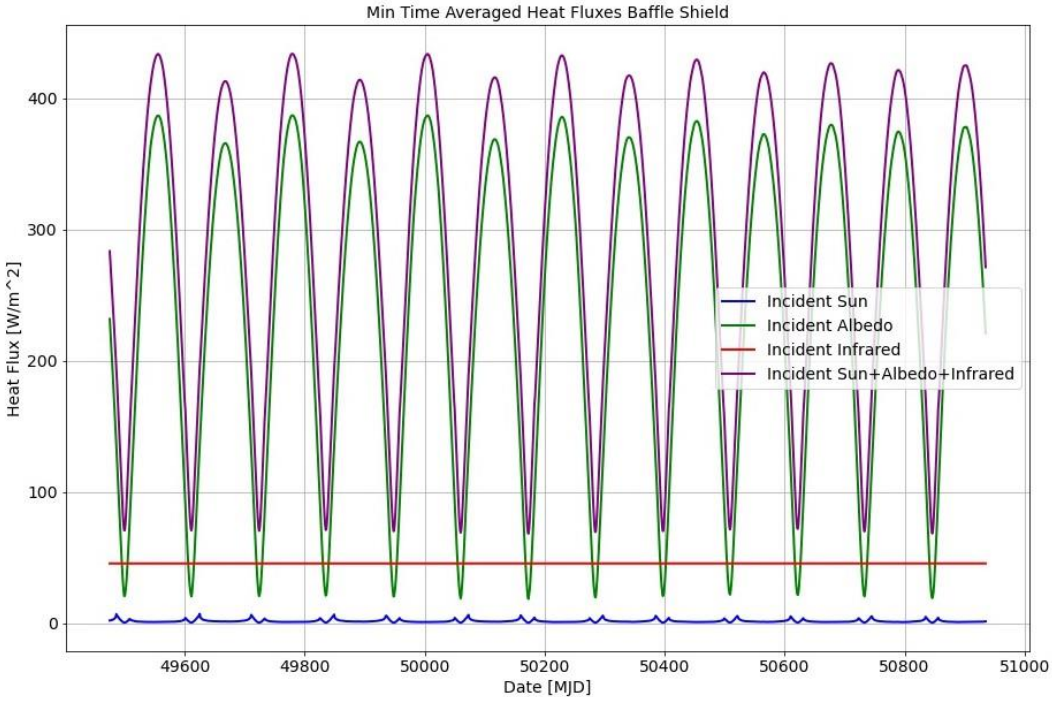

Figure 7-5: Minimum time-averaged heat fluxes for the baffle shield

Figure 7-5 shows the resulting minimum time-averaged environmental heat fluxes, which are present for the baffle shield. Here, the thermal node with the minimum time-averaged heat flux is plotted for each timestep. This diagram is used to identify the worst-case orbit on which the environmental fluxes are minimal, making up the cold case for this part of the instrument during the science phase.

The solar flux for the baffle shield is the lowest environmental heat flux regarding the minimum time-averaged heat fluxes. This is due to the baffle shield being not always fully illuminated by the Sun. Only during the orbits on which the maximum time-averaged solar fluxes are maximal, the whole baffle shield is illuminated at some point during the orbit, resulting in the low peaks shown in Figure 7-5. This is not the case for the remaining orbits, leading to a minimum time-averaged flux of almost 0 W/m^2.

Concerning the time-averaged minimum albedo flux, the same shape as for the maximum time-averaged fluxes can be identified with a maximum at orbits with a longitude of ascending node of 90° and 270°, and a minimum at orbits with a longitude of ascending node of 0° and 90° respectively. These fluxes are again periodically stable.

The minimum infrared flux stays constant over the simulation with a lower value compared to the maximum time-averaged heat fluxes. All these environmental heat fluxes sum up to a combined heat flux, whose minimum can be found in the first half of the science phase. The minimum combined time-averaged heat flux on day 50173 MJD is shown in Table 7-1.

Figure 7-6 shows the baffle shield's maximum incident peak heat fluxes. For each node, the maximum peak heat flux, which is present during one timestep of the simulation, is determined. Afterward, the thermal node with the maximum value is plotted for each timestep. This diagram is used to determine another worst-case orbit on which the peak heat fluxes are reaching their maximum, which is only applied for a short time.

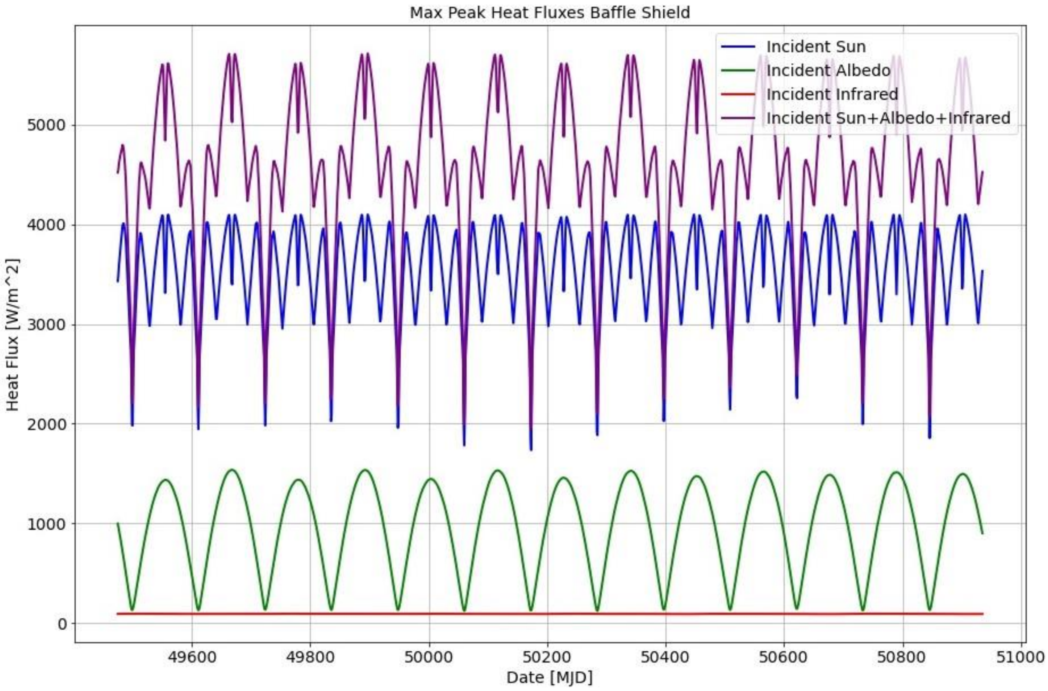

Figure 7-6: Maximum peak heat fluxes for the baffle shield

The incident solar flux reaches its maxima on the maximum peak heat fluxes on orbits which are slightly tilted around 0°, 90°, 180°, and 270°. During these orbits, the amount of direct sunlight plus multiple reflections reaches its maximum. Also, direct sun illumination peaks can be found on which mostly no reflections take place. That is the case for orbits with a longitude of ascending node of 90° and 270°. On these orbits parts of the baffle shield are illuminated by the Sun, but reflections do not redirect sunlight in the instrument and prevent the emergence of hot spots. Overall, the maximum peak Sun fluxes are periodically stable ranging between 2000 and 4000 W/m^2.

The albedo fluxes are minimal on orbits with a longitude of ascending node of 90° and 270°, and maximal on 0° and 180° as in the cases before. They are periodically stable and in a range of 200 to 1500 W/m^2.

The infrared flux of Venus stays nearly constant on a low level. The maximum peak heat flux of the combined environmental fluxes can be found in the first half of the science phase but on a different date compared to the maximum time-averaged hot case. The maximum combined peak heat flux on day 49897 MJD is shown in Table 7-1.

Baffle Shield	Date [MJD]	Heat flux [W/m²]
Hot Case (time-averaged)	49486	1577.88
Cold Case (time-averaged)	50173	68.34
Hot Case (peak)	49897	5715.59

Table 7-1: Hot and Cold Cases of the baffle shield

One may argue that the maximum incident solar peak heat flux cannot be greater than the solar constant at Venus, which is 2601 W/m² [23]. Nevertheless, the baffle shield experienced peak solar heat fluxes up to 5715.59 W/m² in this simulation. An additional simulation with only one white surface orbiting Venus in the same orbit for day 49513 is performed to exclude the possibility of an error inside the post-processing script or the simulation itself. The picked day shows a maximum peak solar flux of 3914 W/m² in the original simulation with the whole baffle unit, compared to 2533.32 W/m² in the additional simulation with only one white surface. As the additional simulation shows, the value for one white surface is being kept below the solar constant at Venus. The high solar peak fluxes on the original simulation are due to the circumstance that the incident heat fluxes are calculated based on the absorbed heat fluxes of a surface and its associated absorptance. ESATAN-TMS includes reflected heat fluxes from other surfaces having a view factor to the target surface, which can also absorb these fluxes. Due to the geometry of the baffle shield, incident environmental fluxes may be reflected with a high possibility, based on the applied white coating, and may impact other surfaces. As Figure 7-6 only depicts the nodes of the baffle shield with the highest environmental peak heat fluxes, it also depicts the nodes most affected by reflected light. Therefore, as shown in Figure 7-6, these high values are reached.

It should also be noted that these values serve as a basis for calculating the expected ESH, which in turn serves as a basis for determining the degradation of the TCCs to be applied. It may be common to determine the ESH not for a specific geometry, but for a black body with an absorptivity of 100%. If this is the case, the values determined here are to be regarded as conservative, which nevertheless lead to realistic expected degradations, as described in Chapter 9.

Based on the thermal worst-case dates, the worst-case orbits can be identified. Table 7-2 shows the associated orbits for all thermal worst cases of the baffle shield. These orbital parameters are used further as input for a thermal analysis in greater detail for the whole instrument, to derive the prevailing temperatures of the surfaces.

Orbit Parameter	Hot Case (time averaged)	Cold Case (time averaged)	Hot Case (peak)
Date [MJD]	49486	50173	49897
Longitude of Ascending Node [°]	111.91	89.49	172.40
Argument Periapsis [°]	183.28	170.23	170.95
Pericenter Altitude [km]	243.74	269.32	247.91
Apocenter Altitude [km]	502.35	438.91	480.38
Inclination [°]	86.92	87.34	86.54

Table 7-2: Worst-Case Orbits for Baffle Shield

The baffle cone is expected to see way less sun than the baffle shield, as it is less exposed. It is intended to absorb stray light from unwanted light sources, such as the Sun, and is black-coated to enable a high absorption of incoming light. The baffle cone is expected to see mostly albedo and infrared fluxes from Venus.

Figure 7-7 shows the maximum time-averaged heat fluxes, which are present for the baffle cone. The data points are derived using the same procedure as for the baffle shield.

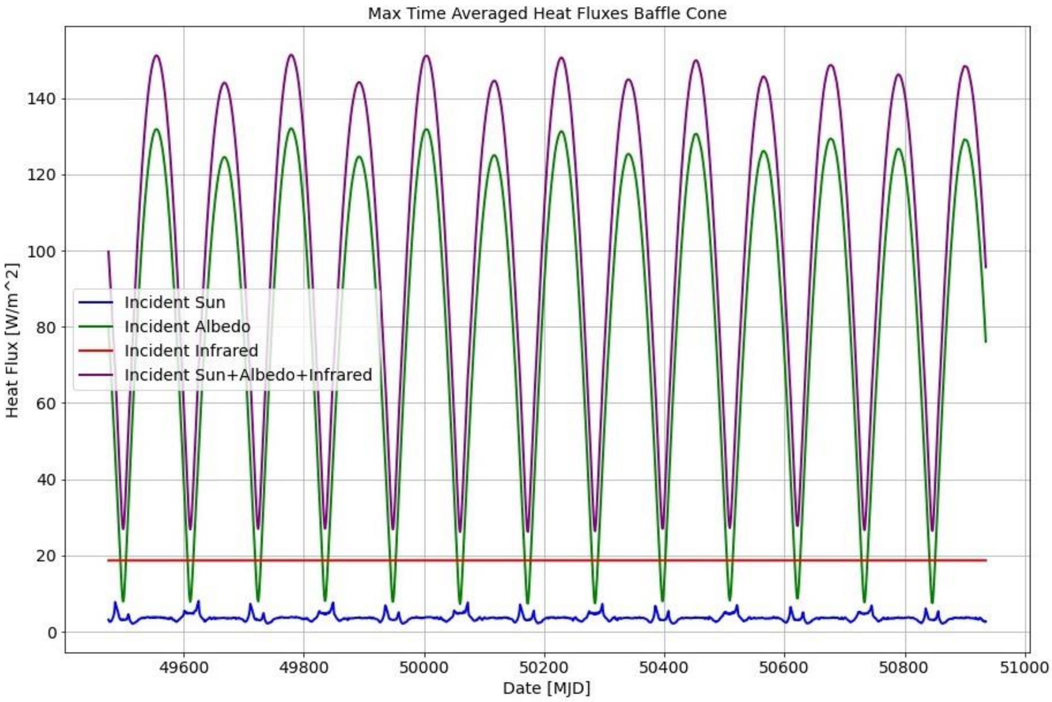

Figure 7-7: Maximum time-averaged heat fluxes for the baffle cone

As expected, the maximum time-averaged solar fluxes are much lower compared to the baffle shield fluxes. Despite small peaks on slightly tilted orbits around a longitude of ascending node with 90° and 270°, the flux stays nearly constant at a low flux of about 5 W/m^2. Due to the position of the baffle cone, Sun fluxes barely reach the surfaces of the cone. A large part of the incoming radiation is assumed to be mainly reflected solar radiation from the baffle shield.

Similar to the baffle shield the maximum time-averaged albedo heat fluxes reach their maximum at orbits with a longitude of ascending node of 0° and 180°, and their minimum at 90° and 270°. These fluxes are periodically stable in a range between 10 and 130 W/m^2 and are of a similar shape as the albedo fluxes of the baffle cone. This is expected as the geometry of the orbits is the same and only the total heat flux value can therefore be affected.

Compared to the baffle shield, the incident infrared fluxes are lower, nevertheless constant over the whole simulation time at around 20 W/m^2. The day on which the combined environmental and time-averaged heat flux reaches its maximum can be found in the first half of the science phase. This maximum value is way lower, compared to the baffle shield, due to less illumination by the Sun. The maximum time-averaged flux on day 49779 MJD, which makes up a hot case of the baffle cone during the science phase, is shown in Table 7-3.

Figure 7-8 shows the minimum time-averaged heat fluxes, which are present for the baffle cone. The data points are derived with the same procedure as for the baffle shield minimum time-averaged heat fluxes.

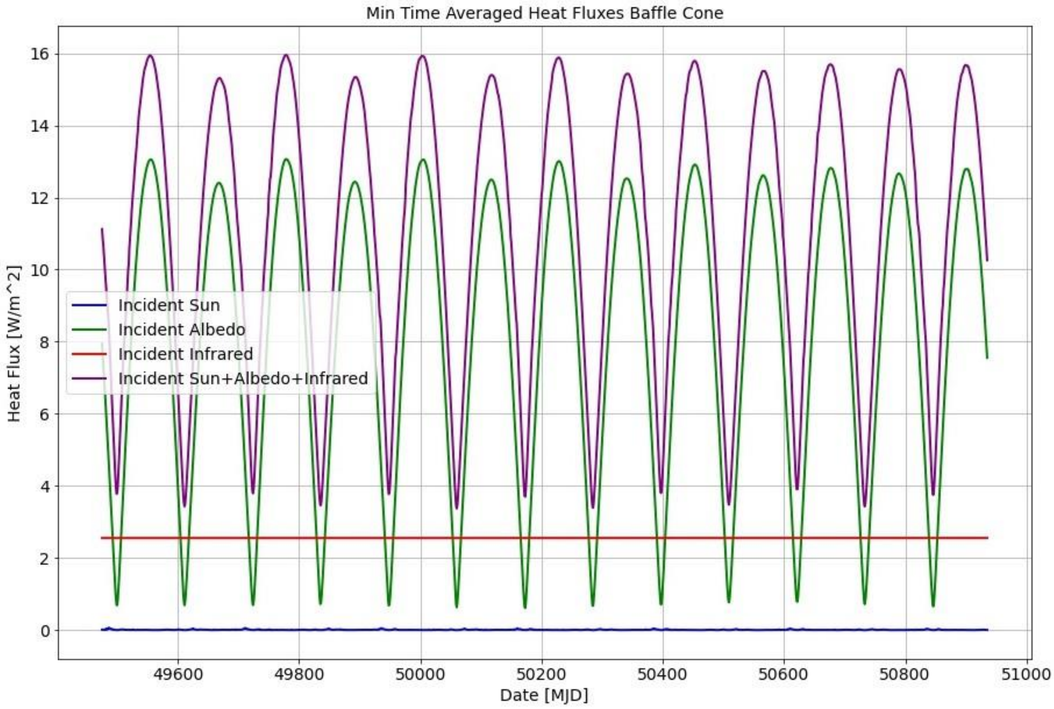

Figure 7-8: Minimum time-averaged heat fluxes for the baffle cone

Overall the fluxes have a similar shape as that of the maximum time-averaged heat fluxes, with only an offset which lowers all values. The sun fluxes are nearly constant and almost non-existent with no significant peaks. The albedo flux is similar to the maximum time-averaged fluxes but is kept in a range from 1 to 13 W/m^2. The infrared fluxes are constant at a level under 3 W/m^2 throughout the simulation.

The day on which the combined environmental and time-averaged heat flux reaches its minimum can be found in the first half of the science phase. Day 50060 MJD, which makes up the cold case of the instrument’s part, and the corresponding minimum combined, and time-averaged environmental heat flux is shown in Table 7-3.

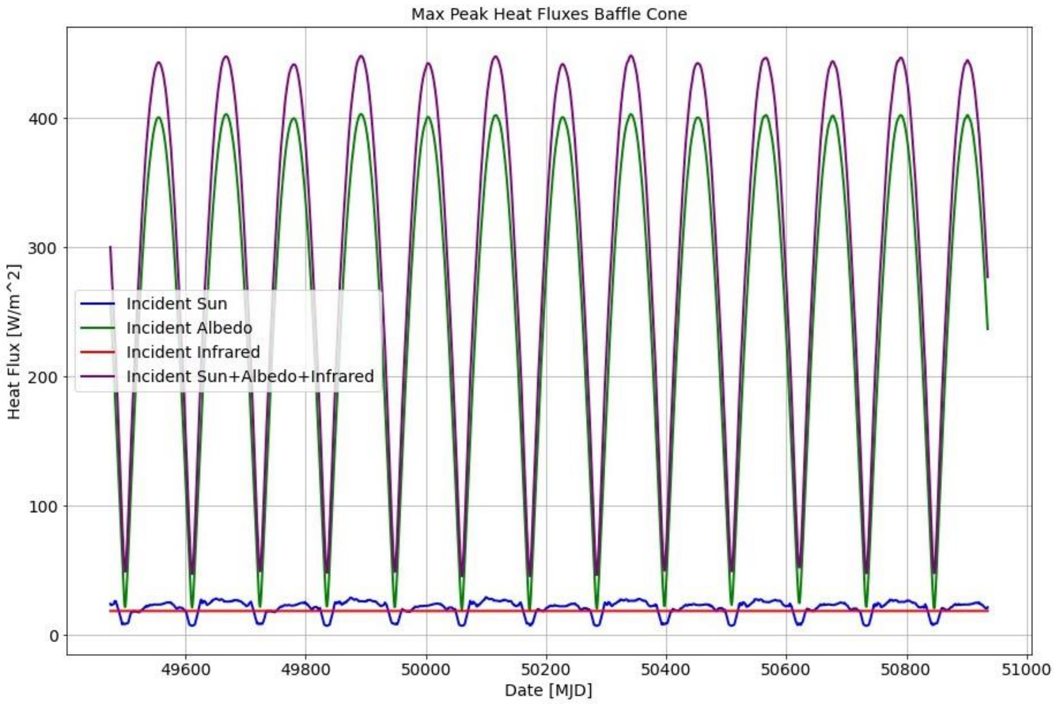

Figure 7-9: Maximum peak heat fluxes for the baffle cone

Figure 7-9 shows the maximum peak heat fluxes present for the baffle cone. The data points are derived by the same procedure as for the baffle shield.

The solar peak heat fluxes are on a low level and mainly due to reflections of sunlight from the baffle shield, staying roughly between 10 and 20 W/m^2. The fluxes reach their minimal values at orbits with a longitude of ascending node around 90° and 270°, similar to that of the albedo peak heat fluxes. The albedo peak heat fluxes have the same shape as in the cases before. This flux is periodically stable with values in the range of 20 to 400 W/m^2 and therefore lower compared to the baffle shield's albedo peak fluxes. The infrared flux stays nearly constant and at the same level as the solar flux of about 15 W/m^2. The maximum combined environmental peak heat flux present for the baffle cone is found in the middle of the second half of the science phase on day 50341 MJD and is shown in Table 7-3.

Baffle Shield	Date [MJD]	Heat flux [W/m^2]
Hot Case (time-averaged)	49779	151.33
Cold Case (time-averaged)	50060	3.37
Hot Case (peak)	50341	448.09

Table 7-3: Hot and Cold Cases of the baffle cone

Based on the dates for the presented thermal worst cases, the worst-case orbits for the baffle cone are shown in Table 7-4.

Orbit Parameter	Hot Case (time averaged)	Cold Case (time averaged)	Hot Case (peak)
Date	49779	50060	50341
Longitude of Ascending Node	0.77	269.93	180.05
Argument Periapsis	172.15	151.89	139.87
Pericenter Altitude	227.61	251.29	242.15
Apocenter Altitude	500.73	456.9	445.23
Inclination	86.65	87.22	87.04

Table 7-4: Worst-Case Orbits for Baffle Cone

The window of the TWU is expected to see only infrared radiation from Venus and almost no sun or albedo fluxes, as they will be absorbed by the baffle cone to reduce stray light. Due to the low absorption coefficient of fused silica, all values for the absorbed heat fluxes are predicted to be very low.

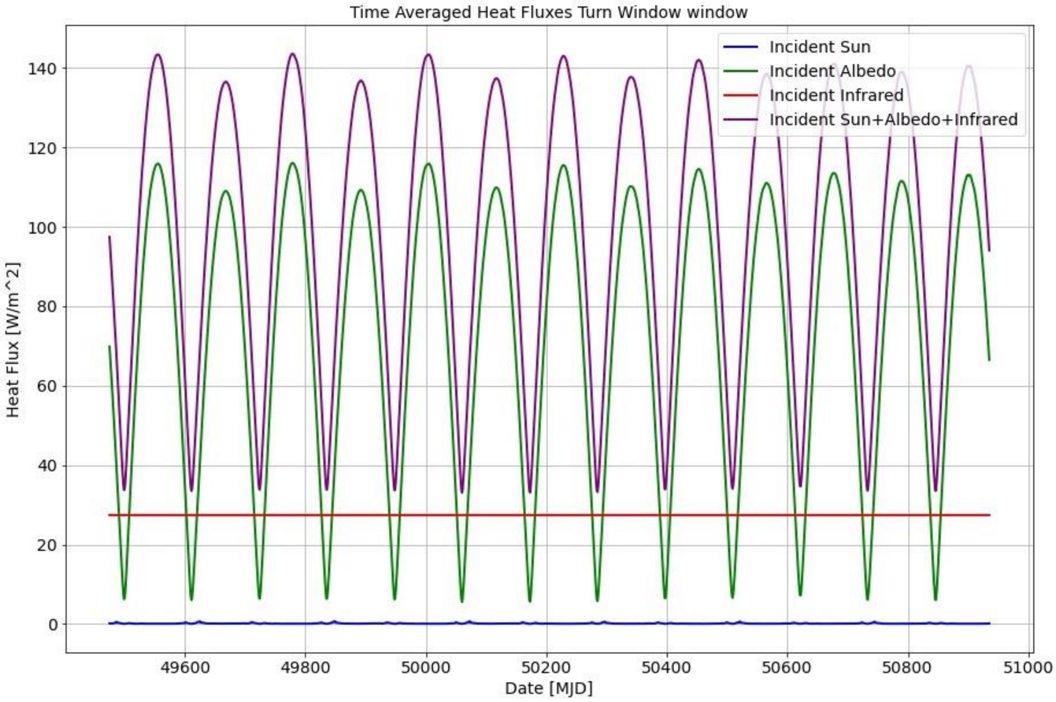

Figure 7-10: Time-averaged heat fluxes for the TWU Window

Figure 7-10 shows the time-averaged heat fluxes incident for the TWU window. As for the TWU window, only one node is modeled, and no maximum value has to be derived between all nodes of the instrument's part. Furthermore, no minimum time-averaged heat fluxes can be plotted.

The incident time-averaged Sun fluxes are almost non-existent, while the albedo fluxes are ranging between 10 and 120 W/m^2. The maximum peaks of the incident albedo fluxes can again be found on orbits with a longitude of ascending node of 0° and 180°, while the minimum fluxes are present at orbits with 90° and 270°.

The infrared fluxes are constant at a level of around 30 W/m^2. Both maximum and minimum peaks of the combined environmental fluxes can be found in the first half of the science phase at day 49778 MJD for the maximum and day 50060 MJD for the minimum peak. The values are presented in Table 7-5.

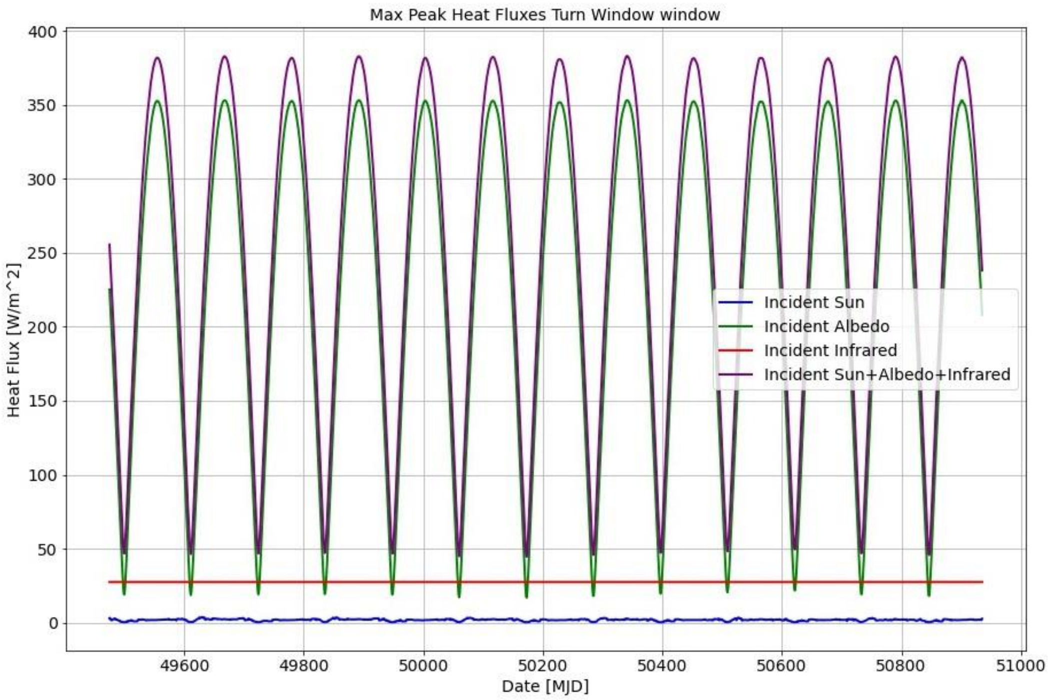

Figure 7-11: Maximum peak heat fluxes for the TWU window

Figure 7-11 shows the maximum peak heat fluxes present for the TWU window. The data points are derived by the same procedure as for the baffle shield and cone.

The incident maximum peak fluxes coming from the Sun are on a very low level and almost non-existent. The albedo maximum peak heat fluxes have their maximum and minimum peaks on similar orbits like that of the time-averaged albedo heat fluxes while ranging between 25 and 350 W/m^2. The incoming infrared fluxes are staying constant again at a level of ca. 30 W/m^2. The maximum combined peak heat flux can be found around the middle of the science phase at day 50340 MJD. Table 7-5 states the most important values.

Baffle Shield	Date [MJD]	Heat flux [W/m^2]
Hot Case (time-averaged)	49778	143.52
Cold Case (time-averaged)	50060	33.02
Hot Case (peak)	50340	383.12

Table 7-5: Hot and Cold Cases of the TWU window

Based on the dates for the presented thermal worst cases, the worst-case orbits for the TWU window are shown in Table 7-6.

Orbit Parameter	Hot Case (time averaged)	Cold Case (time averaged)	Hot Case (peak)
Date	49778	50060	50340
Longitude of Ascending Node	2.38	269.93	181.62
Argument Periapsis	172.45	151.89	140.78
Pericenter Altitude	226.33	251.29	244.11
Apocenter Altitude	501.95	456.9	443.33
Inclination	86.6	87.22	87.04

Table 7-6: Worst-Case Orbits for TWU window

7.4 Identification of Worst-Case Orbits

Based on the results obtained and presented, the worst-case orbits are determined. For each origin of the heat fluxes the corresponding day of the mission with a worst-case heat flux incident for each surface is determined. This has already been done in part by determining the days and thus the orbits on which a combined flux worst-case exists. For the remaining environmental fluxes, the respective days for which a worst-case flux is present based on the respective source must also be determined. This has to be done except for the infrared fluxes of Venus, as they are approximately constant, and therefore no specific day or worst-case can be determined. By doing so, 20 worst-case orbits are identified. These orbits are reduced to five worst-case orbits, from which three for each part of the baffle unit are identified. Table 7-7 shows these worst-case orbits with combined Sun (S) plus albedo (A) plus planet infrared fluxes (P), combined Sun plus albedo fluxes, and Sun and albedo fluxes as a separate value.

NR	Day	Part	Case	S+A+P	S+ A	S	A
1	49486	Baffle Shield	Hot Case (time averaged)	1577.88	1515.73	1318	197.73 (+284.4)
2	49779	Baffle Cone	Hot Case (time averaged)	151.33	35.92	3.89 (+4.17)	132.03
		Turn Window	Hot Case (time averaged)	143.52	116.11	0.08 (+0.65)	116.03
3	49897	Baffle Shield	Hot Case (peak)	5715.59	5623.58	4099.27 (+0.01%)	1524.31 (+0.83%)
4	50060	Baffle Shield	Cold Case (time averaged)	69.04 (-0.98%)	19.52 (-2.2%)	0.55 (-0.06)	18.97 (-1.93%)
		Baffle Cone	Cold Case (time averaged)	3.37	0.63 (+1.59%)	0.00	0.63 (+3.17%)
		Turn Window	Cold Case (time averaged)	33.02	5.61	0.05 (-0.01)	5.56
5	50340	Turn Window	Hot Case (peak)	383.12	355.71	2.70 (+1.03)	353.02 (+0.04%)
		Baffle Cone	Hot Case (peak)	447.76 (+0.07%)	429.05 (+0.08%)	26.63 (+2.82)	402.42 (+0.11%)

Table 7-7: Final Worst-Case Orbits

The red-marked fluxes, shown in Table 7-7, are not worst-case values but have a worst-case value on another day of the mission. These differences are mostly very low and allow the combination into one worst-case day. This is done if the difference is less than 5 W/m^2 in total or if the relative difference is less than 5 %. This difference is also shown in Table 7-7 in brackets.

One exception that has to be mentioned is the time-averaged hot-worst-case for the baffle shield. The albedo flux on this day is way lower than the maximum flux identified over the whole mission duration. Nevertheless, the combined fluxes of Sun plus albedo as well as Sun plus albedo plus planet infrared fluxes are higher compared to the day when the albedo flux is maximal.

These five worst-case orbits are used to evaluate the performance of the applied coatings of the baffle unit. They are simulated with coatings' optical properties being in the BOL state and the EOL state.

8. Calculation of Equivalent Sun Hours

8.1 Theoretical Basis

ESH is a measurement of the environmental fluxes in the solar spectrum which are present on a part or surface. Contributing fluxes are sun fluxes, albedo fluxes from the central body, and reflections of other surfaces. Calculating or determining the ESH of a surface, requirements, and constraints can be written, and approximations of possible degradations can be made.

To derive the ESH for each subunit of the baffle unit of VEM/VenSpec-M, the ESH for each node of the simplified thermal model, introduced in Chapter 7.2, is calculated by using the showed formula, with the time-averaged absorbed sun or the albedo flux as the absorbed heat flux $HF_{absorbed}$ for each node times the duration T the heat flux is present, divided by the solar constant (at Earth) times the absorptivity of the surface $\alpha_{coating}$. For each node, the ESH were summed up over the simulation duration resulting in the total ESH for each node of the thermal model.

$$ESH = \sum \frac{HF_{absorbed}\left[\frac{W}{m^2}\right] \cdot T[h]}{\alpha_{coating} \cdot 1366\ \frac{Wh}{m^2}} \tag{17}$$

Regarding a worst-case assumption, the nodes of the simplified model with the highest overall ESH are identified for each subunit of the baffle unit to end up with conservative values for further investigations. The ESH are divided into sun fluxes, albedo fluxes, and combined fluxes ESH. Based on these derived ESH values, the degradation effect of its own and a synergetic degradation effect with ATOX on the applied coatings of the instrument's surfaces can be determined. The values determined here serve as a basis and justification for the requirements Req-BS-002, Req-BC-002, and Req-TW-002 from Chapters 5.2 and 5.4.

8.2 Science Phase ESH

The science phase is the main phase of the EnVision mission, with a duration of 1460 days. Because of that, this phase is expected to be the main contributor to the ESH of the whole mission. Therefore, the amount of ESH in the science phase is the main factor for the degradation of the applied coatings of the baffle unit due to VUV radiation. Based on the orientation of the instrument during the science phase (nadir-pointing), it is expected that most ESH arises from the time-averaged albedo flux for the baffle cone and TWU window because the solar flux is minimal for the baffle cone and TWU window, but in case of the baffle shield higher than the albedo flux. Therefore, it is expected that the most contributing flux for the ESH of the baffle shield is the solar flux. Figure 8-1 shows the ESH for each part of the instrument's baffle unit during the science phase.

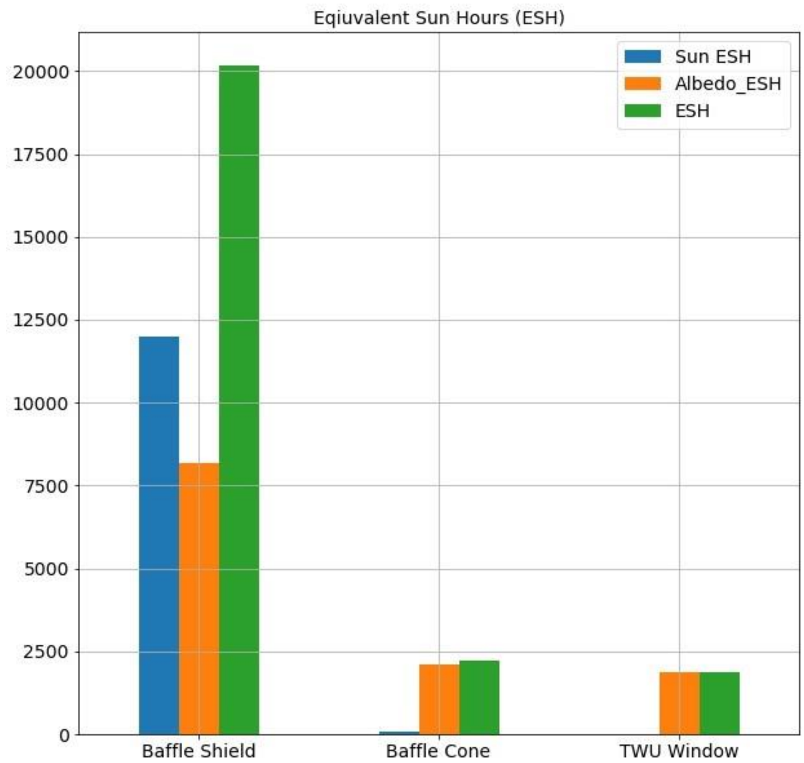

Figure 8-1: ESH Science Phase of all VenSpec-M parts

As expected for the baffle shield, most ESH arises from the sun heat fluxes compared to the albedo heat fluxes. The baffle shield is exposed to a higher number of ESH compared to the baffle cone as shown in Figure 8-1. Also, the albedo flux is the main contributor to the ESH of the baffle cone as it sees almost no sun. The ESH of the TWU window are even lower, as the window experiences almost no heat fluxes from the sun. Only albedo and infrared fluxes are present, from which only albedo fluxes contribute to the ESH. Table 8-1 shows the values displayed in Figure 8-1.

Part	Sun ESH	Albedo ESH	Sum ESH
Baffle Shield	11975.43	8183.28	20158.71
Baffle Cone	93.77	2109.24	2203.02
TWU Window	3.42	1850.7	1854.13

Table 8-1: ESH Science Phase values of VenSpec-M parts

Having a closer look at the values shown in Table 8-1, the values may seem a bit high. This is because the reflected solar and albedo fluxes are allowed inside the baffle unit. These are included in the ESH calculation in addition to the actual ambient fluxes. These additional reflections can result in local hotspots with very high irradiation. By calculating the ESH based on the nodes of the model with the highest incident fluxes, these hotspots lead to high ESH values. Nevertheless, the reflected fluxes also contribute to the degradation of the applied TCCs, so the calculated ESH can certainly be used to determine the expected degradation of these coatings.

During the science phase, the EnVision S/C will calibrate other payload instruments, located on the same S/C panel as VenSpec-M. These instruments will be calibrated by looking directly into the Sun, resulting in the VenSpec-M instrument pointing also directly into the Sun. To reduce the thermal stress on the optical sensor, the attitude control system of the EnVision S/C applies a minimum slope of 0.1°/s (TBC) during these calibration phases. There are three scenarios for a sun calibration that differ in the right ascension of the ascending node, 0°, 45°, and 90°, respectively. In total, up to twelve sun calibration phases will be performed.

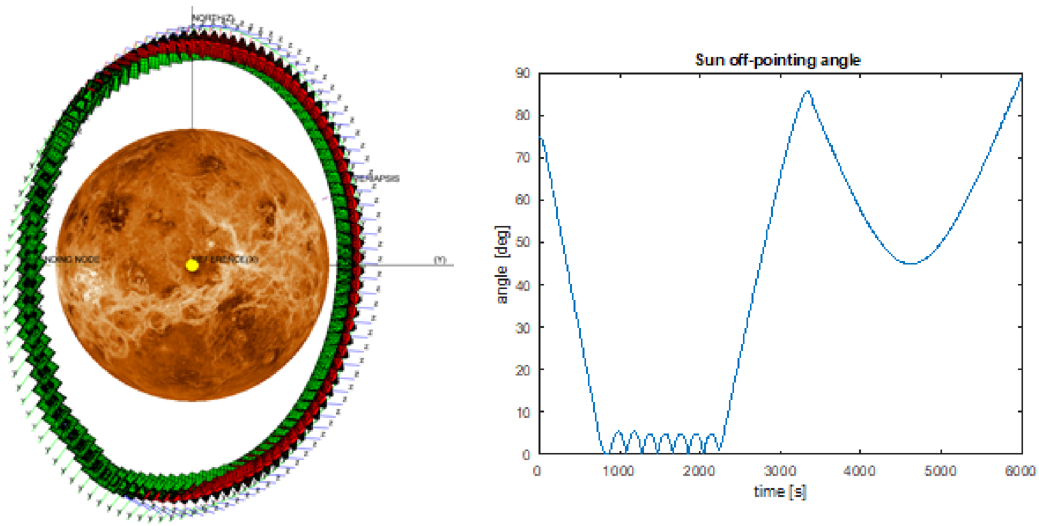

Figure 8-2: ESATAN Screenshot of Sun Calibration with RAAN 45° as seen from Sun (left), Sun off-pointing angle for RAAN 45° and 135° (right)

Figure 8-2 shows the attitude change during the science phase for Sun calibration from a Sun's viewpoint on the left and the change of the Sun off-pointing angle over the time on the right. The overall ESH of the Sun pointing orbits are very low compared with the science phase, due to their short duration, but need to be considered for the TWU. Figure 8-3 shows the total ESH of the Sun calibrations. Each scenario is evaluated separately, and the amount of ESH is multiplied by a factor of four before summing up the three scenarios, making a total of twelve sun calibration phases.

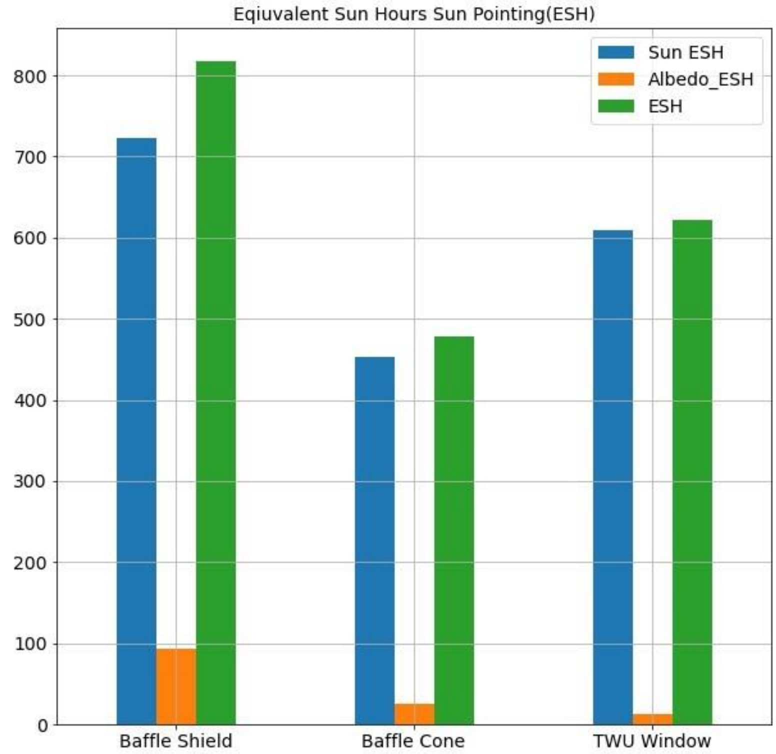

Figure 8-3: Total ESH of the Sun Calibration scenarios

As expected, the portion contributing most to the sum of the ESH comes from the Sun. It is striking that the ESH for the TWU are higher than for the baffle cone. That is due to the window being perpendicular to the incident solar radiation, while the baffle cone is angled, leading to a lower flux as compared to the window. Table 8-2 shows the exact values of the ESH for each part of the baffle unit.

Part	Sun ESH	Albedo ESH	Sum ESH
Baffle Shield	723.45	93.68	817.13
Baffle Cone	452.91	25.26	478.17
TWU Window	608.79	12.67	621.46

Table 8-2: ESH values of parts of VenSpec-M during Sun Calibration

8.3 Aerobraking Phase ESH

The Aerobraking phase is a main phase of the EnVision mission, as it will last about 657 days. So, a large part of the overall ESH for the mission will be contributed by this mission phase. To estimate the ESH during the aerobraking without simulating each orbit, which will end in a complex and time expensive simulation, a suitable selection of orbits is considered. To get a good estimation, the instrument is assumed to be pointed in an anti-velocity direction during the whole aerobraking phase, and a suitable selection of orbits that differ in the ascending node longitude is made.

A good approximation of the ESH can be made by including all orbits with a longitude of ascending node of 0°, 45°, 90°, 135°, 180°, 225°, 270°, and 315°. It is assumed that a single orbit lasts to the point the next fitting orbit is present. However, this selection of orbits leads to over-conservative ESH values as the instrument is pointed directly to the sun at orbits with a longitude of ascending node of 0° and 180°. As the assumption was made that these orbits are present until the next orbit fits, these worst-case orbits last longer than in reality. This effect can be reduced by including four additional orbits representing the beginning and end of the direct illumination of the instrument by the Sun. This is done by including the across-track FOV of the instrument. Figure 8-4 shows the across-track FOV of 46.4° for the VenSpec-M instrument.

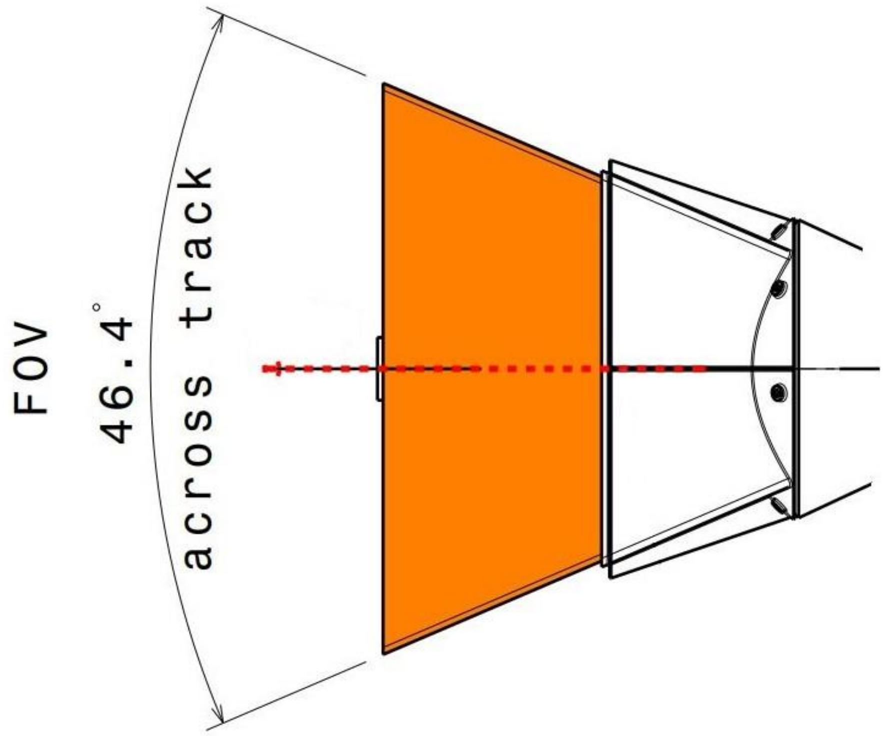

Figure 8-4: FOV of VenSpec-M [19]

Due to the instrument's across-track FOV, orbits with a longitude of ascending node of 23.2°, 156.8°, 203.2° 336.8° have been additionally selected to keep orbits, in which the instrument is pointing directly into the sun, as short as possible so they do not contribute so much to the overall ESH. Table 8-3 shows the durations and orbital elements of the selected 36 orbits.

#	Duration [d]	Pericenter altitude [km]	Apocenter altitude [km]	Inclination [deg]	Ascending node longitude [deg]
1	21.0	379.851	250289.445	98.629	88.495
2	20.5	230.210	66569.831	88.447	45.190
3	14.0	125.040	66571.884	88.930	24.078
4	15.0	132.106	66567.859	89.208	359.812
5	14.0	126.930	63255.848	88.736	335.904
6	20.5	131.145	63248.214	88.451	314.887
7	28.0	121.787	59936.524	87.584	270.080
8	21.0	124.772	56638.735	87.516	225.682
9	14.5	121.617	56646.524	88.343	203.621

#	Duration [d]	Pericenter altitude [km]	Apocenter altitude [km]	Inclination [deg]	Ascending node longitude [deg]
10	15.0	127.950	53345.764	88.488	180.023
11	14.0	132.292	53338.786	88.119	155.959
12	20.5	136.601	50024.550	87.006	135.380
13	28.0	129.011	46725.670	86.933	90.109
14	20.5	125.856	46735.926	87.820	44.886
15	14.0	126.269	43437.306	87.899	23.676
16	14.5	128.474	43434.243	87.720	359.609
17	14.0	134.398	40128.688	87.294	336.741
18	21.0	139.621	40123.131	86.983	314.372
19	28.0	134.641	36823.175	86.778	269.673
20	20.5	128.453	33530.171	87.230	225.535
21	14.5	133.784	30228.816	87.099	204.904
22	15.5	129.348	30234.339	87.517	179.472
23	14.0	130.941	26934.300	87.408	155.653
24	20.5	132.187	26932.656	87.239	134.948
25	28.0	131.782	23632.025	87.069	89.701
26	20.5	130.821	20335.511	87.174	44.385
27	13.5	129.435	20337.048	87.244	23.282
28	14.5	133.932	17035.787	87.087	0.593
29	14.0	133.600	17036.069	87.038	336.295
30	20.5	135.571	13735.190	86.986	315.447
31	28.5	134.133	10434.567	86.917	270.839
32	21.0	133.803	7139.465	86.918	224.943
33	14.0	132.284	7141.067	87.035	204.364
34	15.5	135.122	3840.365	87.099	180.601
35	14.5	133.683	2300.709	87.018	155.216
36	9.5	131.521	1102.894	86.921	134.488

Table 8-3: Aerobraking Orbits

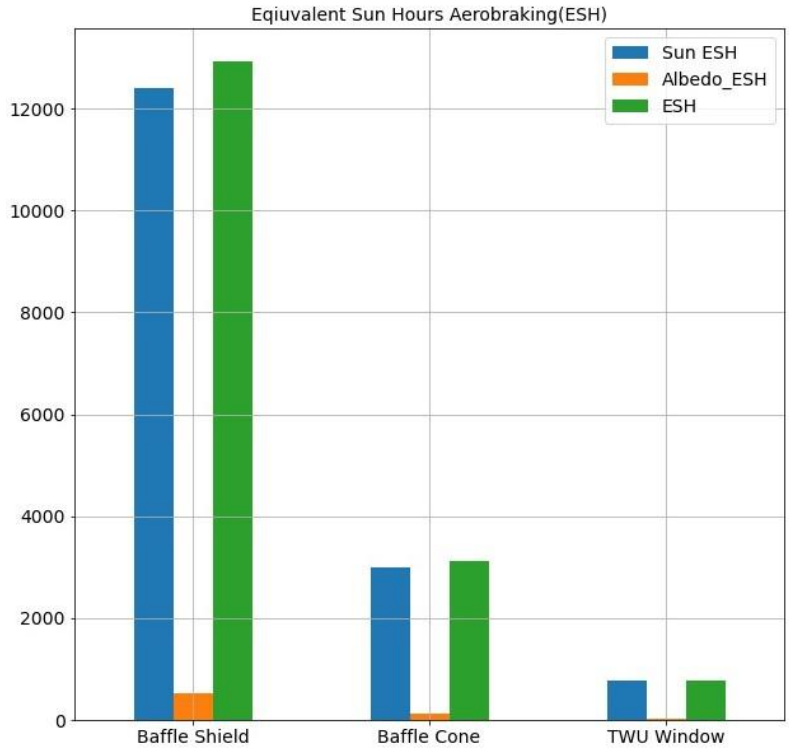

Figure 8-5: Estimated Total ESH of the Aerobraking Phase

Figure 8-5 shows the total estimated ESH for the aerobraking phase. The main contributor to the ESH is the Sun, as albedo fluxes are quite low, which can be explained by the instrument's orientation during the aerobraking. For the baffle shield, the aerobraking ESH makes up around a third of the ESH over the mission time. For the baffle cone, the aerobraking phase is the main contributor to the ESH of the mission phase as they are larger than the ESH coming from the science phase. As mentioned, these values have high uncertainty, as the amount of ESH is averaged on 36 representative orbits and with an assumed orientation, as the S/C's attitude during aerobraking is not specified. Table 8-4 shows the ESH values for each baffle unit subunit.

Part	Sun ESH	Albedo ESH	Sum ESH
Baffle Shield	12394.07	527.73	12921.81
Baffle Cone	2987.23	131.89	3119.12
TWU Window	762.97	21.82	784.79

Table 8-4: ESH values of parts of VenSpec-M during Aerobraking

As mentioned before, by assuming the pointing direction of the instrument is in the opposite of the spacecraft's velocity vector during the aerobraking phase, the instrument is pointing directly into the sun if the ascending node longitude is around 0° or 180°. At these angles, the line pointing from Venus to the Sun (Reference(X)) is in the spacecraft's orbital plane. Therefore, as shown in Figure 8-6, the Sun illuminates the TWU window. However, the sum of ESH for the TWU window is lower compared to the science phase.

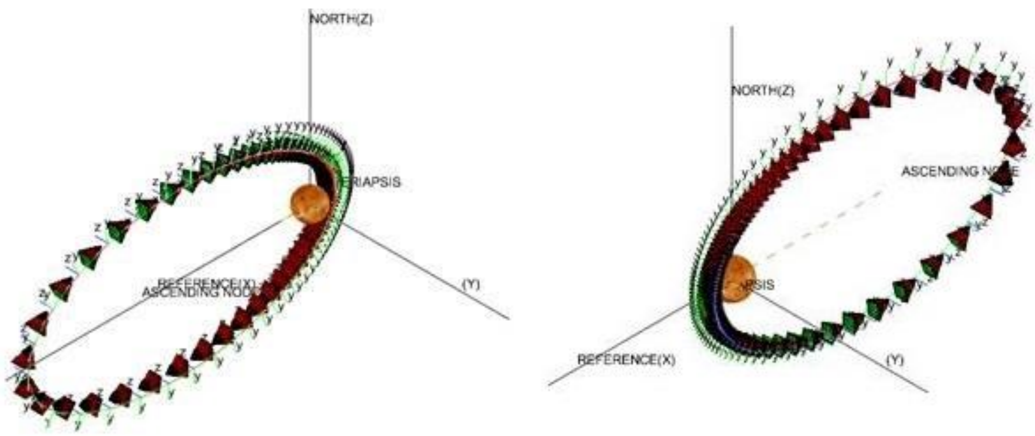

Figure 8-6: Aerobraking Orbit with Ascending node longitude 0° (left) and 180° (right)

Preceded thermal analyses to determine the temperatures of the inner parts of the instrument's optical assembly during the sun-pointing phases have derived a requirement of a minimum slope of the instrument while looking directly into the Sun. These analyses have also shown that the most sensitive part is the optical filter. The incident light is focused on this filter plate. If the slope is too low, the maximum temperature may be exceeded, resulting in a failure of this instrument's part [15].

To verify the assumption of the pointing during the aerobraking orbit, the minimum slope of the instrument, while pointing directly into the sun, as shown in Figure 8-6, has to be determined and checked to be compliant with the requirement. By doing so, this pointing attitude can be used, and the derived amount of ESH during the aerobraking phase can be used for further investigations.

Figure 8-7 shows the maximum peak heat fluxes on the TWU window during the simplified aerobraking phase simulation. In total, six spikes in the heat flux can be identified on orbits 4, 10, 16, 22, 28, and 34, corresponding to the orbit with roughly 0° or 180° on the ascending node longitude.

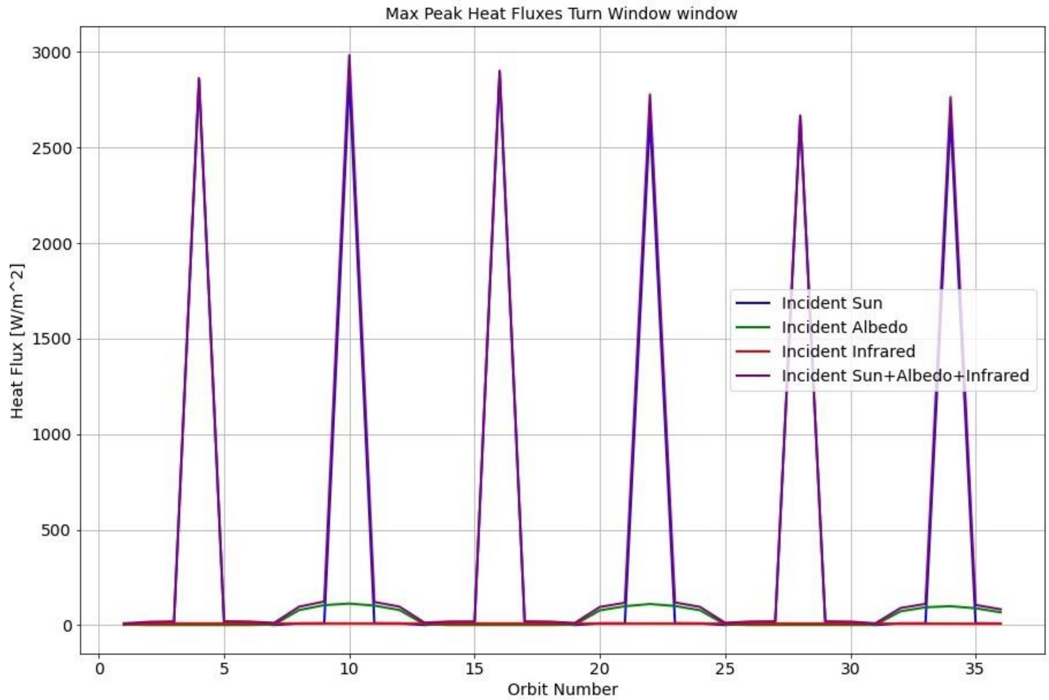

Figure 8-7: Maximum Peak Heat Fluxes of the TWU Window during Aerobraking Phase

9. Determination of EOL Optical Properties of Preselected Coatings

9.1 Procedure and Assumptions

The VERITAS/Envision mission consists of three relevant phases, which need to be considered for the degradation of the applied coatings: Cruise, Aerobraking, and the Science Phase. The quantity of the main degradation mechanism was determined for each mission phase and each relevant surface, including the ATOX fluxes and the ESH.

Another possible degradation mechanism is charged-particle radiation. The expected radiation dose has been specified for each subunit of the baffle unit and is presented belong the other degradation source quantities in Table 9-1. These values of charged-particle radiation serve as a basis and justification for the requirements Req-BS-003, Req-BC-003, and Req-TW-003 from Chapters 5.2 and 5.4. A degradation analysis based on these doses is not performed. That is due to the low doses of charged-particle radiation which are not necessarily negligible but uncritical for the exposed surfaces' thermo-optical properties.

Subunit	ATOX Flux [atoms/m²]	Aerobraking Phase ESH	Sun-Pointing ESH	Science Phase ESH	Radiation [krad]
Baffle Shield	1.581E25	12921.81	250.12	20158.71	1760
Baffle Cone	2.662E25	3119.12	146.32	2203.02	540.8
Window	1.215E25	784.79	190.17	1854.13	188.7

Table 9-1: Environmental Conditions for each Subunit of the Baffle-Unit

During the cruise phase, it is assumed that the overall ESH of the subunits are low due to the S/C attitude being in "barbecue mode". As no ATOX is present in interplanetary space, no relevant degradation of the TCCs is expected.

As mentioned in the ATOX flux approximation, the whole ATOX flux is assumed to be applied during the aerobraking phase. The overall ESH of this phase are lower compared to the ESH over the mission duration, making the degradation based on the interaction with oxygen atoms the driving degradation mechanism. Therefore, high ATOX fluxes in combination with low ESH are assumed over this mission phase.

The science phase is mainly driven by solar radiation as the pericenter altitude is raised outside Venus's atmosphere, making ATOX a lower concern. So, the assumption is made that the ESH are the main driving degradation mechanism, while the ATOX flux is very low compared to the aerobraking phase.

By applying this assumption, the optical parameters of the applied coatings are in a BOL status after the cruising phase, at an EOA status after the aerobraking phase, caused by degradation due to ATOX fluxes, and finally in an EOL status after the science phase, caused by degradation due to solar radiation.

9.2 White Thermal Control Coatings

Based on the requirements and constraints of the surfaces of the baffle shield, a TCC with a low solar absorptance, high solar reflection, and high infrared emittance shall be used on the baffle shield. Consequently, three white coatings are preselected:

- Ceranovis V14 (White, ceramic coating) from Nanovation
- A276 (White, organic coating) from Aeroglaze
- AZ-93 (White, ceramic coating) from AZ Technology

All these coatings have been used in space applications before, especially AZ-93 is used on many surfaces on the ISS [24]. The A276 coating is a well-known TCC, and the degradation in the LEO environment is well-studied on STS missions and in the LDEF experiment [7]. The V14 is a relatively new coating, which has been used on the ESA mission BepiColombo and was specially developed to withstand the environmental conditions at Mercury with its high environmental solar irradiance [25]. Therefore, all three coatings are good candidates for usage on the VEM/VenSpec-M baffle shield. The preselected white coatings are presented in Table 9-2.

Coating	Absorptance BOL	Emittance BOL	Binder	Max. operable Temperature [°C]
Ceranovis V14	0.09	0.92	Potassium Silicate	430
Aeroglaze A276	0.26	0.88	Polyurethane	121
AZ-Technology AZ-93	0.15	0.91	Silicate	1400

Table 9-2: Preselected white TCCs

The V14 coating is a white ceramic coating comprising a sintered mixture of oxides/nitrides like aluminum oxide (Al_2O_3) and boron nitride (h-BN) bonded by a potassium silicate binder. Therefore, no organic carbon is present in the coating [25]. The BOL optical properties are presented in Table 9-3.

Preliminary tests carried out in the ESTEC TEC-QEE LEOX facility on the ATOX sensitivity of this ceramic coating showed that it has a high stability against ATOX fluxes. The change in mass, solar absorptance, and reflectance was measured to be very low. The most representative sample with an ATOX flux of 1.77E25 atoms/m^2 showed an increase in the solar absorptance of 0.01 and no detectable change in the solar emittance of the coating. Furthermore, the test sample did not show any visual degradation nor a sign of erosion after irradiation to the ATOX flux [26].

Several different ceramic and inorganic TCCs were tested during the Materials on International Space Station Experiment (MISSE) for degradation in optical parameters due to the LEO environment. In the MISSE-3, the samples on the leading edge were exposed to an ATOX flux of 1.3E25 atoms/m^2 and roughly 1750 ESH of solar radiation. The tested ceramic TCCs were three versions of Z-93 and two of YB-71. On average, they experienced a total increase in solar absorption of 0.006, while there was no measurable change in the emittance [27].

Both results show the same behavior in the degradation of the coating. Regarding worst-case assumptions, an increase of 0.01 of the solar absorptance and no change of the emittance is being considered for the EOA status of the coating, as shown in Table 9-3.

For the qualification of V14 for ESA’s BepiColombo mission, the coating was tested on high ESH of solar radiation in combination with contamination. Samples were exposed to a simulated space environment, including exposure to solar UV/VUV radiation and outgassing products. The pristine samples showed an increase in the solar absorptance of 0.32 and an increase in the emittance of 0.05. In contrast, the samples cleaned with a special ozone treatment showed an increase of 0.13 in solar absorptance and a decrease in the emittance of 0.01 [25].

The results of the pristine samples are used for the EOL status determination of the optical parameters, because contamination must be considered, based on the requirements presented in Chapter 5.2. The EOL optical parameters are presented in Table 9-3. These results show that the Ceranovis coating is resistant to ATOX fluxes but sensitive to solar radiation.

The A276 is a glossy white paint containing titanium dioxide (TiO_2) as pigment and a polyurethane binder. The polyurethane binder makes this paint an organic coating [7]. The BOL optical parameters are presented in Table 9-3.

The degradation of this coating due to the LEO environment was tested on several space shuttle flights as well as in the LDEF. The results showed a degradation of the polyurethane binder resulting in a porous and powdery surface, which may be due to ATOX reactions with the organic binder. These results were also observed in ground-simulation tests. Especially samples on the leading edge of LDEF showed that the polyurethane binder of the paint was broken down, leaving a white chalky pigment on the surface. At the same time, there was no observable change in optical properties. These samples have received a total UV radiation of 11000 ESH and a total ATOX flux of 8.99E25 atoms/m^2. After exposure, the coating samples had a total increase in absorptance of 0.016 and a total decrease of 0.03 in the emittance [7].

Other organic paints on the MISSE showed, after being exposed to solar radiation of 1750 ESH and an ATOX flux of 1.25E25 atoms/m^2, an increase in absorptance of 0.017 and a decrease in emittance of 0.03, which is comparable to the results of the LDEF mission [27]. As these quantities are in the same range as the determined values for the aerobraking phase of the VERITAS/EnVision mission, these degradation values are used to estimate the EOA optical properties of the coatings as shown in Table 9-3.

The samples on the LDEF mission were positioned on different AOAs to the ram flux, resulting in different ATOX and solar radiation exposure. Samples on the trailing edge were exposed to low ATOX fluxes but relatively high ESH of solar radiation. These samples had discoloration after they were recovered and disintegrated to brown color and a change in absorptivity as well [28]. Figure 9-1 shows the relation between the absorptance and the ESH of solar radiation for the specimens on the LDEF mission.

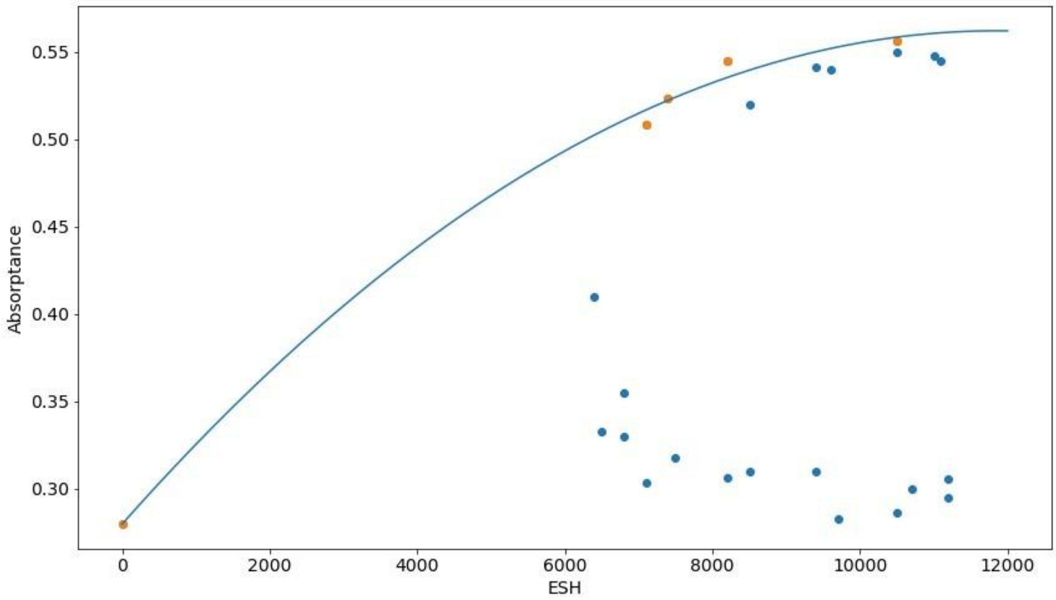

Figure 9-1: LDEF results: Absorptance over ESH for A276 coating

The data points in the lower half of Figure 9-1 represent specimens located near the leading edge exposed to high ATOX fluxes. As in the science phase, the ATOX flux is quite low compared to the overall ESH of solar radiation, the data points on the upper half of Figure 9-1, colored in orange, are representative of the mission phase. Consequently, excluding the lower data points, the plot shows a quadratic function reaching a plateau at 10000 ESH.

Assuming that the coating reached its EOL conditions after 10000 ESH a quadratic regression was performed, and the maximum of this quadratic function was determined to identify the EOL solar absorptance of the A276 coating. This solar absorptance level was found to be 0.56, resulting in a total change of 0.28 compared to the reference sample with a solar absorptance of 0.28.

The highest change in infrared emission was found to be 0.03 [28]. In terms of a worst-case assumption, this change in emission is used to determine the EOL optical properties of this coating, as presented in Table 9-3.

AZ-93 is an inorganic, ceramic white TCC with a silicate binder. It was designed especially for spacecraft surfaces exposed to the space environment that have a working temperature range from -180 to 1400 °C. With its low solar absorptance of 0.15 and high infrared emission of 0.91, it is suitable for thermal control of thermal sensitive parts. It has been exposed to ATOX, charged particle radiation, and vacuum ultraviolet (VUV) radiation with low changes in absorption and emittance. The coating is used on several surfaces of the International Space Station and was tested on many flight experiments like LDEF and MISSE [29]. The optical properties and the heritage of this coating make it a good choice for the to be applied coating of the VEM/VenSpec-M baffle shield. The BOL optical properties are shown in Table 9-3.

In the MISSE-3, several AZ-93 coatings in different versions were exposed to an ATOX flux of 1.25E25 atoms/m^2 and 1750 ESH of solar radiation [27]. These quantities are comparable to the expected environmental conditions during the aerobraking phase of VERITAS/EnVision. The results showed an average increase of the solar absorptance of 0.003 and no change in the infrared emittance. These values are used to determine the EOA optical parameters of the coating.

In laboratory testing, samples from AZ Technology were exposed to UV radiation in a vacuum. This test's goal was to compare the optical properties of AZ-93 samples with a fluoropolymer overcoat with pristine AZ-93 samples after exposure to UV radiation. This overcoat can be used to protect the coating from contamination during ground handling and is eroded down by ATOX in the LEO. If this overcoat is not eroded down completely, it will darken due to solar irradiation [30].

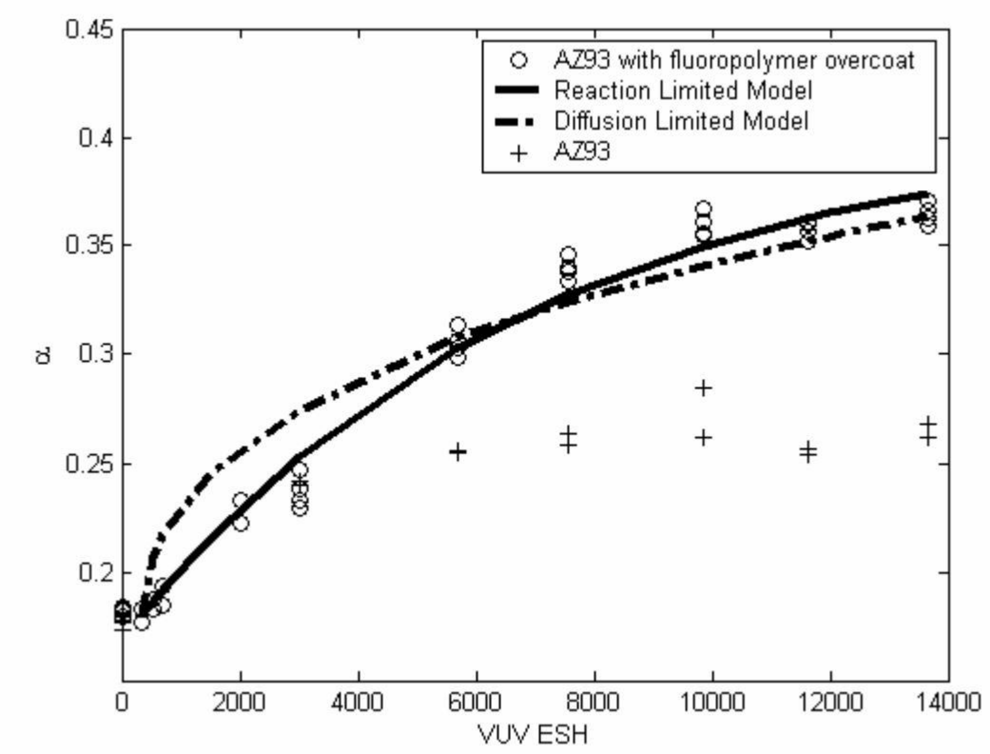

Figure 9-2: Test Results Absorptance change due to UV Radiation [30]

Figure 9-2 shows the optical properties of the pristine sample and the sample with an overcoat for VUV irradiations up to 14000 ESH. The degradation of the pristine sample reaches a plateau starting at 8000 ESH with a solar absorptance of around 0.27. The maximum degradation shown in this diagram is a total increase of 0.108 in absorptance. The infrared emittance did not change due to UV radiation [30]. These values are used to estimate the EOL properties of the AZ-93 coating and are shown in Table 9-3.

Table 9-3 shows the BOL and the estimated EOA and EOL optical properties of all preselected white TCCs for the baffle shield of VEM/VenSpec-M. The degradation of the optical parameters due to ATOX environmental fluxes seems uncritical compared to the degradation based on solar irradiation. Nevertheless, degradation due to ATOX environmental fluxes can alter the surface of the coatings by eroding the binder, which will not drastically influence the optical properties but the mechanical properties of the coating. Solar irradiation leads to a darkening of the white TCCs, especially of organic coatings like Aeroglaze A276. The ceramic coatings are less sensitive to solar irradiation, but in combination with contamination, high increases in the solar absorptance and a darkening of the surface is the consequence.

White Coating	Absorptance			Emittance		
	BOL	EOA	EOL	BOL	EOA	EOL
Ceranovis V14	0.0900	0.1000	0.4300	0.9200	0.9200	0.9700
Aeroglaze A276	0.2600	0.2770	0.5591	0.8800	0.8500	0.8800
AZ-93	0.1500	0.1528	0.2608	0.9100	0.9100	0.9100

Table 9-3: BOL, EOA, EOL optical properties of preselected white thermal control coatings

Based on this comparison, the AZ-93 coating performs best over the mission duration. This is mainly due to the good EOL condition of the coating, whose predicted degradation is based on a laboratory experiment with controlled contamination of the sample. Therefore, this sample's contamination was very low compared to the V14 sample, which was intentionally exposed to a 23g CFRP contamination source within the test chamber [25]. Consequently, the EOL optical properties of AZ-93 might be more degraded if contamination is apparent.

To decrease the amount of contamination on the V14 coating, a coating process was developed by sealing the surface with an overcoating second layer of boehmite that closes the pores of the pristine coating, making it less prone to adsorb organic contamination. Using this technique, the increase of solar absorptance can be as low as 0.07, resulting in an EOL absorptance of 0.26 instead of 0.52 [25]. With this improvement of V14, the degradation due to ESH is now comparable with AZ-93, making the V14 coating a good choice for the baffle shield based on its thermo-optical properties.

9.3 Black Thermal Control Coatings

Based on the requirements and constraints of the exposed surfaces of the baffle cone, a TCC with a high solar absorptance, low solar reflection, and high infrared emissivity shall be used on the baffle cone. Consequently, three black coatings are preselected:

- Fractal Black from Acktar
- Z307 (black, organic coating) from Aeroglaze
- PUK from MAP Space Coatings

All these coatings have a great heritage at DLR, as Z307 and PUK are often used on other space missions. Also, different coatings from Acktar were used before. The preselected black TCCs are presented in Table 9-4.

Coating	Absorptance BOL	Emittance BOL	Binder	Max. operable Temperature [°C]
Acktar Fractal Black	0.98	0.91	Inorganic	450
Aeroglaze Z307	0.95	0.90	Polyurethane	121
MAP PUK	0.97	0.91	Polyurethane	130

Table 9-4: Preselected black TCCs

Fractal Black is a black TCC with a solar reflectivity lower than 3% and is therefore among the blackest coatings known. As shown in Figure 9-3, these reflection values can be lower than 2% in the science wavelength band of the instruments making it suitable for near-infrared spectrometers [31].

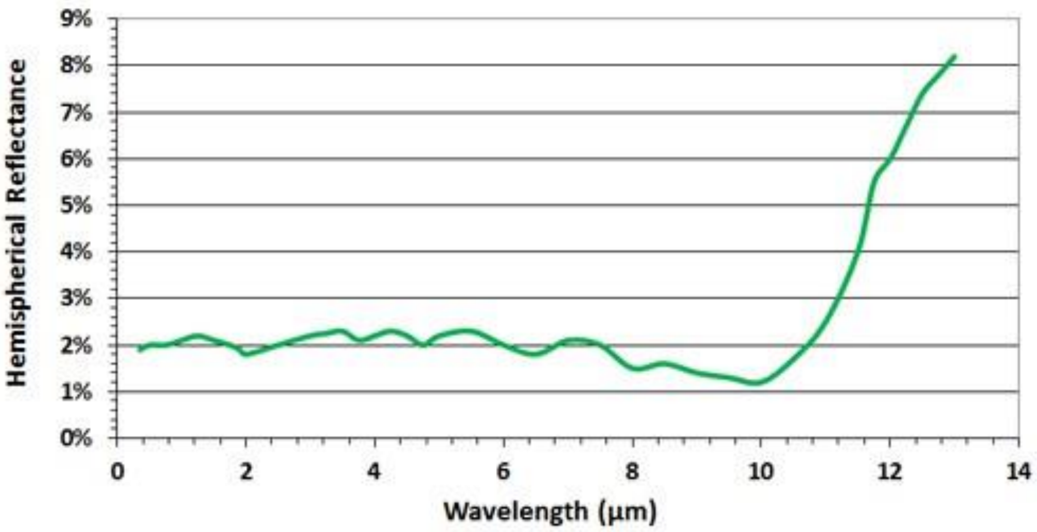

Figure 9-3: Acktar Fractal Black Reflectance over Wavelength [31]

During the qualification of Acktar black coatings for space applications, Fractal Black was exposed to an ATOX flux of 3E24 atoms/m^2. The results of the optical parameter determination after exposure showed that the total reflectance did not change and was kept below 2%, that the emittance did not change, and that there was no change in the visual appearance [32]. Furthermore, other inorganic coatings in the MISSE-3 experiment showed no change in absorptance after exposing the black TCC samples to an ATOX flux of 1.3E25 atoms/m^2 [27]. Based on these results it is assumed that no change in optical parameters occurs during the aerobraking phase of the mission, as shown in Table 9-5.

Fractal Black was qualified for space applications with high exposure to solar radiation as part of the ESA's Solar Orbiter mission. It is used among two other coatings on the mission. After testing them to a total solar radiation flux of 26000 ESH, they all have been found to stay at their original absorptance and emission values [33]. Therefore, no degradation of the optical parameters of Fractal Black is expected during the mission phase. These EOL optical properties are shown in Table 9-5.

Z307 is a black organic paint with carbon as pigment and a polyurethane binder. Experiments have shown that this paint degrades significantly due to UV radiation and that the polyurethane binder gets broken down by ATOX exposure. Like the A276 coating, the Z307 coating was part of the LDEF mission, where it was almost completely eroded by binder degradation upon UV exposure and binder, as well as pigment degradation by ATOX. After the exposure, only a little powder was left on the surface. Samples exposed to a high ATOX flux of 8.99E25 atoms/m^2 showed a decrease in the solar absorptance of 0.02 and an increase in the infrared emittance of 0.01 [7].

In the MISSE-3, other organic paints have been tested, like the MH12. After exposure to 1.25E25 atoms/m^2 and solar radiation of 1750 ESH, the painting experienced no measurable change in solar absorptance. Based on worst-case assumptions, the results of the LDEF mission are used to determine the optical properties of the coating after completing the aerobraking phase of the mission because of the high expected ATOX flux. The optical parameters for the predicted EOA status are presented in Table 9-5.

Samples with high solar exposure of more than 10000 ESH on the LDEF mission were occasionally eroded down to the red primer after exposure to this solar radiation. A decrease in solar absorptance of 0.02 and an increase of 0.04 in the infrared emittance was observed in these samples [28]. These results are used to determine the EOL conditions of the black TCC and are shown in Table 9-5.

PUK is an organic black conductive coating with polyurethane as a binder. As few experiments on the degradation based on an ATOX flux or solar radiation were made, it is assumed that the degradation during the aerobraking phase of the mission will be equal to the degradation of Z307, as they are using the same organic binder. Based on this a decrease in the solar absorptance of 0.02 and an increase in the infrared emittance of 0.01 are expected. These values are shown in Table 9-5.

Several samples, including PUK-coated ones, were tested to a combined flux of protons with energy levels of 50 keV, electrons with energy levels of 50 keV, and UV radiation with 8760 ESH to simulate the environmental condition on GEO. The obtained results showed a decrease in the solar absorptance of 0.17, while the emissivity remains unaffected [34]. Assuming the EOL properties of the coating are already reached after 8760 ESH, these results will be used to determine the EOL conditions of the coating, as presented in Table 9-5.

Table 9-5 shows the optical properties of all preselected black coatings at BOL, EOA, and EOL. For the Aeroglaze coating, the degradation due to ATOX interaction with the coating's material and due to solar radiation is comparable, while ATOX exposure has a slight bleaching effect, and UV exposure darkens the coating. Because of the usage of the degradation levels after combined testing, the degradation of the MAP PUK coating due to UV radiation is high and performs worse than the Aeroglaze coating. The Fractal Black TCC is expected to be stable to ATOX and UV radiation interactions with its materials.

Black Coating	Absorptance			Emittance		
	BOL	EOA	EOL	BOL	EOA	EOL
Acktar Fractal Black	0.98	0.98	0.98	0.91	0.91	0.91
Aeroglaze Z307	0.95	0.93	0.95	0.9	0.91	0.95
MAP PUK	0.97	0.95	0.75	0.91	0.92	0.92

Table 9-5: BOL, EOA, EOL optical properties of preselected black thermal control coatings

These results are used further in a thermal analysis to evaluate the thermal performance of the overall instrument during the worst-case orbits, which were determined in Chapter 7.4.

9.4 Anti-Reflection Coatings

AR coatings are used to improve the efficiency of an optical element by increasing its transmission. This is especially important for optical instruments with multiple optical parts, as reflections on these surfaces can create ghost images on the detector. Around 4% of the incoming light will be reflected at each interface of an uncoated glass substrate due to Fresnel reflection. This sums up to a total reflection of 8% of the incoming light, which can lead to performance issues. By using an AR coating, the reflections of optical elements can be as low as 0.7% [35].

Typically, these coatings consist of different metallic layers from which most of them are susceptible to ATOX erosion. Double-layer and triple-layer coatings often include MgF_2 layers which can experience transmission losses up to 51% after exposure to ATOX fluxes as high as 6.93E25 atoms/m^2 experienced on the LDEF mission [7].

The NIR-II Coating is a Broadband Anti-Reflection (BBAR) coating option consisting of multiple layers to improve the transmission of an optical element in the near-infrared wavelengths (750nm to 1550nm). This coating can reduce the total reflection over the specified wavelength to less than 0.7%. Sample #5 of MgF_2 layers has been exposed to a fluence of 2.5E25 atoms/m^2 at a sample temperature of 100°C. This sample experienced a transmission change, as shown in Figure 9-4 [36].

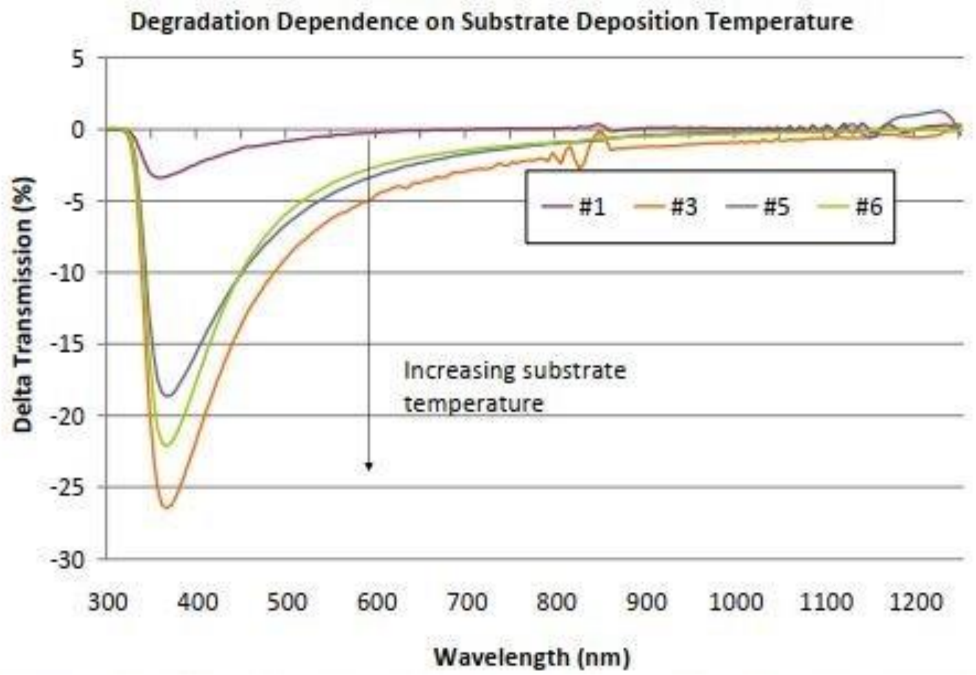

Figure 9-4: Sample degradation of MgF_2 layer used as AR coatings [36]

In the range of ca. 350 nm, the transmission change was leading up to 18%. As VenSpec-M/VEM operates in a wavelength range of 790 to 1510 nm, an approximate decrease in transmission of ca. 1.5% can be approximated after the aerobraking phase.

Also, an ATOX test of optical materials for EnVision was conducted at ESTEC testing various samples of TWU windows with and without coating, including NIR-II-coated samples. The NIR-II sample was exposed to a total ATOX fluence of 2.7E24 atoms/m^2, a lower flux than expected during the aerobraking phase. Also, due to predicted heat fluxes during the aerobraking phase and a resulting temperature increase of the window, the sample was held at a constant temperature of 100 °C. Some preliminary test results showed a very low smoothing and smearing at 315 – 320 nm of the NIR-II coated windows, comparable to the wavelength mentioned above of ca. 350 nm being outside the operable spectrum of VEM/VenSpec-M. The final results showed no significant changes in any spectra within the regions the instrument operates due to ATOX exposure. A small change in the form of a shift in the transmission spectra was found, outside the region of interest. These shifts could be caused by ATOX exposure due to minor chemical modifications of the outer layer of the AR-coating [37].

Regarding a conservative approach, a degradation of 1.5% in transmission is considered during the aerobraking phase, as derived from the MgF_2 layer experiments. As all other effects, including UV illumination, as this will mainly be the case for the science phase, are statistically negligible compared to the degradation based on ATOX erosion, no degradation is expected during the science phase. Table 9-6 shows the optical parameters for the NIR-II coating.

AR Coating	**Reflection**			**Transmission**		
	BOL	**EOA**	**EOL**	**BOL**	**EOA**	**EOL**
NIR II	0.007	0.022	0.022	0.993	0.978	0.978

Table 9-6: BOL, EOA, EOL optical properties of preselected AR-Coating

10. Final Thermal Analysis

10.1 Approach

To find a suitable coating combination of the preselected white and black TCCs for the baffle unit, the determined worst-case orbits of Chapter 7.4 are simulated with ESATAN-TMS using a detailed geometry model of VenSpec-M. Due to the otherwise long calculation times, two representative worst-case thermal orbits are selected. These are worst-case orbit 4 at day 50060 MJD as a cold case and worst-case orbit 5 at day 50340 MJD as a hot case. To evaluate the thermal performance of the instrument, the maximum, minimum, and average temperatures of essential components as well as the conductive heat fluxes over the instrument's interfaces and the radiative heat fluxes to the S/C cavity, are determined. The results of this analysis enable a comparison of all coating combinations in terms of the thermal and optical performance of the instrument.

10.2 Model Description

The analysis is performed using a detailed geometry model of VenSpec-M. Compared to the analysis described in Chapter 7, the complete instrument with all its components is used to make statements about the thermal and optical performance. Figure 10-1 shows the used geometrical model containing the instrument inside the S/C cavity (shown in red/gray). In total this model includes 1366 thermal nodes, 3072 GL conductors, and 517622 GR conductors. The subunits of most interest are the baffle shield, baffle cone, TWU window, detector, optical elements, and optical barrel.

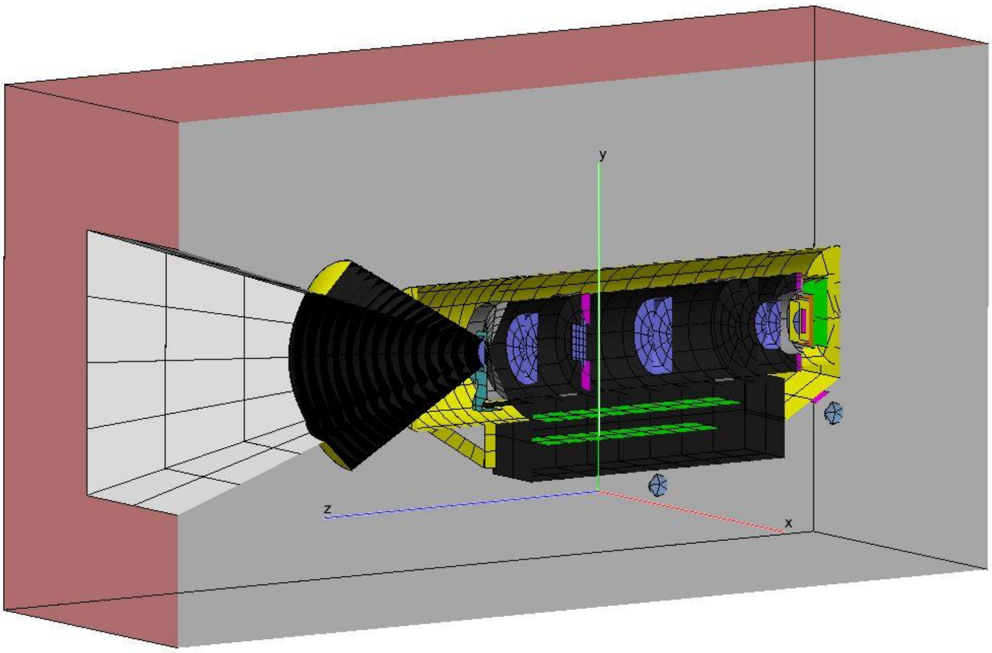

Figure 10-1: Cross Section of detailed VenSpec-M Geometry Model

The analysis is performed in multiple cases divided between a worst hot-case and a worst cold-case orbit. Figure 10-2 shows the worst hot-case orbit (left) and the worst cold-case orbit (right). As shown, the instrument is pointed in the nadir direction, looking directly at Venus during the whole orbit.

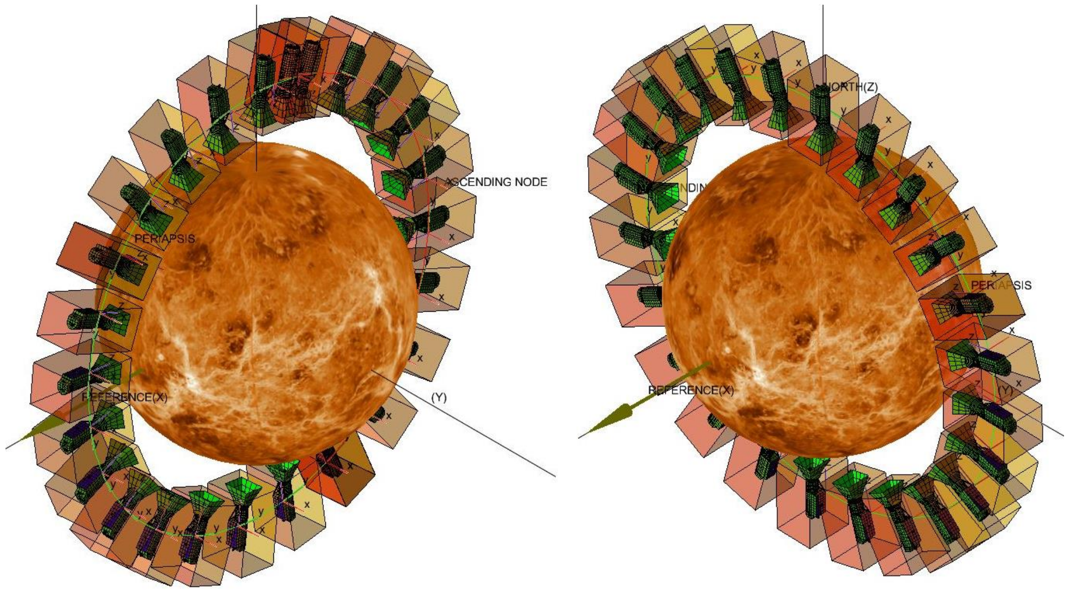

Figure 10-2: Worst Hot-Case (left) and Worst Cold-Case (right) Orbits

Figure 10-3 shows the materials used for the subunits of the detailed geometry model. The materials of the baffle unit are identical to those of the simplified thermal model described in Chapter 7.2. The optics hood is made of steel, while the electronics box and FPA cover are made of Al7075. The flange connecting the baffle unit with the electronics box is made of Ti6Al4V, the same material as the baffle cone. This results in good thermal isolation of the baffle unit from the rest of the instrument, due to the low thermal conductivity of titanium.

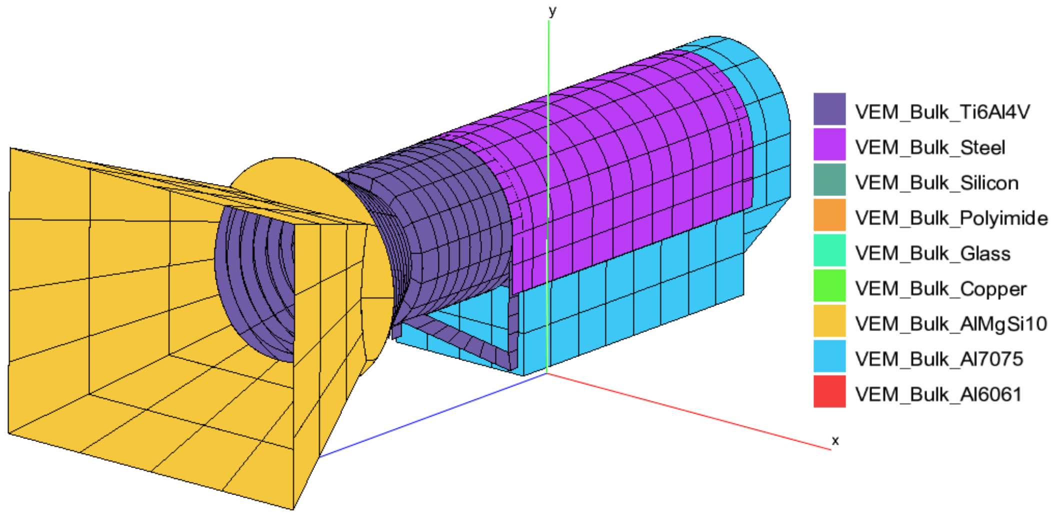

Figure 10-3: Detailed VenSpec-M Geometry Model Bulk Materials

In addition to the baffle shield and the cone, the TWU window is of great interest for this particular analysis because of the expected degradation of the applied AR-coating. As shown in Figure 10-4, the material of the window is glass, while the window frame is made of Ti6Al4V. The optical barrel is made of Al7075, which is held by two connectors made of Ti6Al4V to reduce the thermal effects of the electronics box on the optics. The material of the optical elements, namely glass, has the same properties as the TWU window.

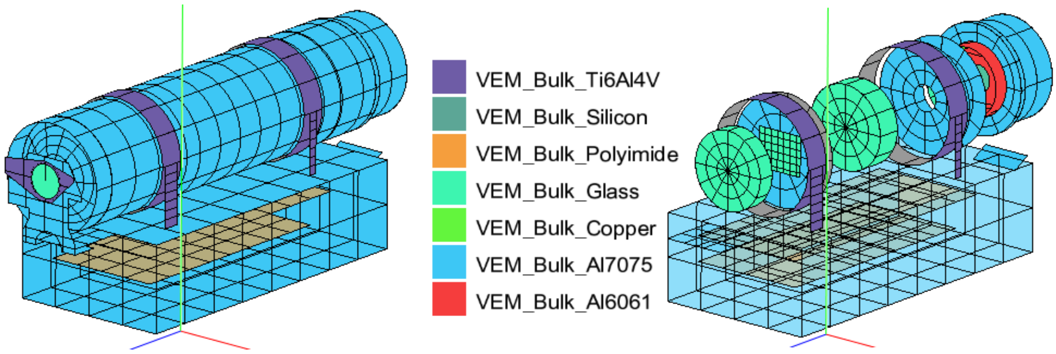

Figure 10-4: VenSpec-M Optics Bulk Materials

The materials used for the FPA are shown in Figure 10-5. The housing of the detector is made of two different aluminum alloys that house the detector and an electronic circuit board.

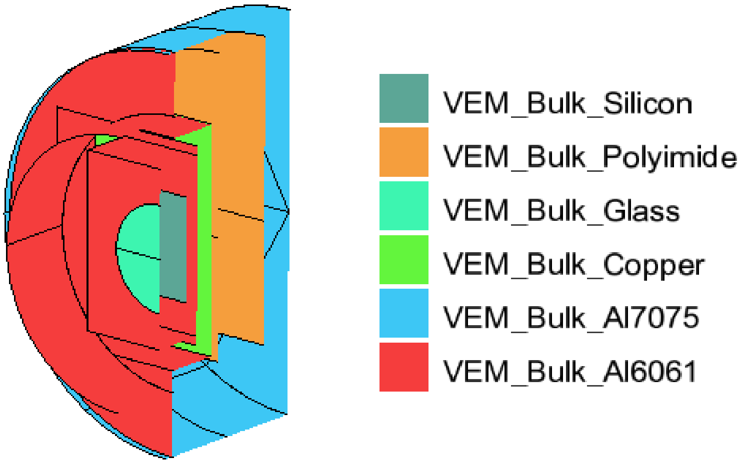

Figure 10-5: VenSpec-M FPA Bulk Materials

For each worst-case orbit, all possible coating combinations are simulated by changing the optical properties of the coated baffle shield, baffle cone, and TWU window surfaces in the detailed geometry model based on the thermo-optical properties for each coating, determined in Chapter 9. These cases are subdivided into coating combinations in BOL and EOL conditions, summing up to thirty-six thermal cases.

The coatings applied to the detailed geometry model are shown in Figure 10-6. As mentioned earlier, a white TCC is used for the baffle shield, and a black TCC is used for the baffle cone. The optical properties of these TCCs are processed for all coating combinations. In addition, they are also matched to the optical properties in BOL and EOL status. This is also true for the AR coating of the TWU window. A black TCC, Aeroglaze Z307, is used for the electronics box, while a low infrared emissivity VDG coating is used for the baffle and optics surfaces exposed to the S/C cavity.

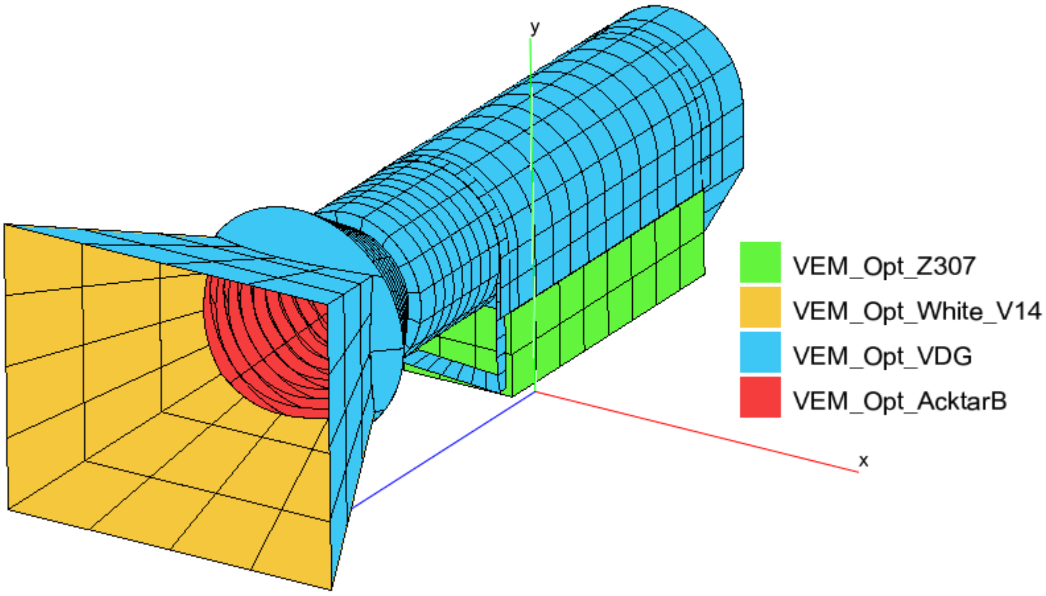

Figure 10-6: Detailed VenSpec-M Geometry applied TCCs

Figure 10-7 shows the thermo-optical properties used for the optical barrel (left), which corresponds to an aluminum surface, while the surfaces of the connectors holding the cylinder have the optical properties of polished titanium. The TWU window (right) uses the optical properties of the NIR-II coating, which is referred to as glass in Figure 10-7. These properties are changed when the coating is in a BOL or EOL state.

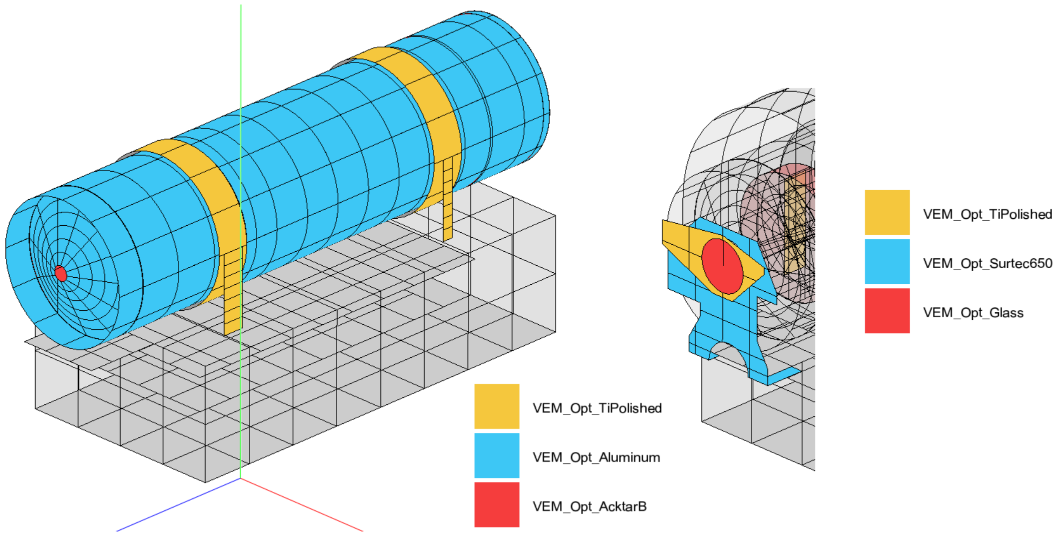

Figure 10-7: VenSpec-M Optical Barrel (left) and TWU (right) applied TCCs

The thermo-optical properties of the FPA correspond to the material used for the FPA parts, as shown in Figure 10-8. The outer surfaces of the housing are coated with a VDG TCC, as are the other surfaces of the device exposed to the S/C cavity.

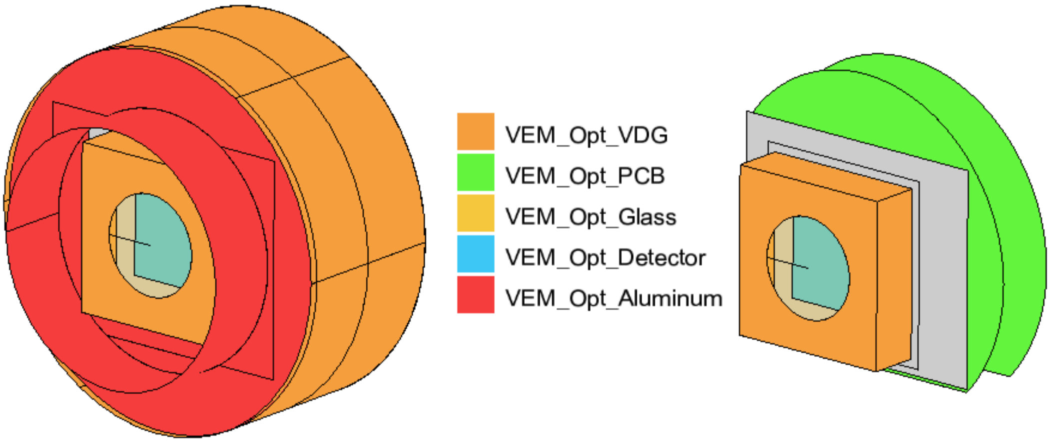

Figure 10-8: VenSpec-M FPA applied TCCs

The radiative fluxes of the environment have already been obtained by the radiative analysis described in Chapter 7. These are used as environmental input fluxes for their corresponding case, including solar radiation, albedo radiation, and infrared radiation from Venus. The GL conductors are equal over all coating combinations, but the GR conductors are derived based on an MCRT method for each coating combination.

During the simulation, TRP2 (S/C Cold Finger) is at its constant specified temperature of 12°C for science mode. The temperature of the S/C panel, which is conductively connected to the electronic box, is held at a constant temperature of 15.49°C. Under this temperature, the TRP1, placed on the electronic box, reaches a starting temperature of 35°C, which is also its specified temperature during the science mode.

This analysis is a thermal analysis using the lumped parameter method as described in Chapter 3.4. Therefore, the calculation times are shorter compared to a radiative analysis using the MCRT method. Nevertheless, due to the thirty-six different cases, the calculation time is increased significantly, which justifies the selection of only two representative worst-case orbits. In the following, the results of the temperatures and heat flows of and between the considered nodes are presented.

10.3 Temperatures of Subunits

To evaluate the thermal performance of VenSpec-M, the maximum, minimum, and average temperatures of a variety of components are determined for all coating combinations. Besides the baffle shield, cone, and TWU window of the baffle unit, which are mostly affected by using different coating combinations, the temperatures of the main components of the instrument have to stay in their specified temperature range during the mission. Essential components are the detector, the optical elements, and the optical barrel. These components have to be thermally stable meaning to stay at a nearly constant temperature during science. If the temperature increases or decreases drastically during the science mode, the instrument's optical performance can be influenced negatively by a possible wavelength shift. Furthermore, the optics shall have an equally distributed temperature profile with low thermal gradients to guarantee the instrument's optical performance. If high thermal gradients are present, an out-of-focus effect may occur, which deteriorates the instrument's optical performance.

As mentioned, a cold-case and a hot-case orbit with BOL and EOL conditions of the applied coating combinations are simulated. Based on the obtained results, the maximum temperatures shown in Table 10-1 are determined. These temperatures represent the maximum temperature reached over all simulated cases of one coating combination and are mostly present in the hot-case orbit with EOL conditions.

Coating Combination	Baffle Shield	Baffle Cone	TWU Window	Detector	Optical Elements	Optical Barrel
V14_Acktar	99.71	106.35	39.55	30.61	32.12	32.17
V14_Z307	99.73	105.78	39.47	30.61	32.10	32.14
V14_PUK	99.79	104.73	39.39	30.60	32.06	32.10
A276_Acktar	115.96	112.68	39.66	30.61	32.18	32.23
A276_Z307	115.98	112.70	39.64	30.61	32.17	32.22
A276_PUK	116.13	112.83	39.57	30.61	32.13	32.17
AZ93_Acktar	79.17	101.99	39.42	30.60	32.06	32.11
AZ93_Z307	79.31	101.38	39.36	30.60	32.04	32.08
AZ93_PUK	79.15	99.74	39.36	30.60	32.00	32.04

Table 10-1: Maximum Temperatures of selected instrument parts [°C]

The maximum temperatures indicate no significant differences in the maximum temperatures of the TWU window, detector, optical elements, and optical barrel when a different coating combination is selected. This shows that these instrument parts are almost unaffected by the coating combination on the baffle unit. Furthermore, the change in the maximum temperatures by varying the black coating on the baffle cone for one specific white coating on the baffle shield is almost negligible. All black coatings are performing almost similarly, concerning the maximum reached temperatures.

On the other hand, the selection of the white coating has a more significant effect on the maximum temperatures. This selection primarily affects the maximum temperature of the baffle shield and has a minor impact on the baffle cone. As expected, the white coatings with the lowest solar absorptance are causing the baffle shield to reach lower temperature levels than those with higher solar absorptance. As all of these values are representative of the EOL conditions of the coatings, the solar absorptance of the coatings is on a higher level, due to degradation, compared to the BOL conditions.

Overall, AZ-93 shows the lowest temperatures, with roughly 79°C on the baffle shield and around 100°C on the baffle cone, followed by V14 with 100°C on the baffle shield and around 105°C on the baffle cone. A276 reaches 116°C on the baffle shield and roughly 113°C on the baffle cone, being the only coating where the shield reaches higher temperature levels than those of the baffle cone. These results are a direct consequence of the degradation levels and the EOL solar absorptances of the coatings as presented in Chapter 9.

Table 10-2 shows the minimum temperatures of the baffle unit components as well as the minimum temperatures of some selected instrument parts. These values indicate the same behavior as those of the maximum values. The minimum temperatures of the TWU window, detector, optical elements, and optical barrel are almost identical over the different coating combinations with no significant best-performing coating combination.

Coating Combination	Baffle Shield	Baffle Cone	TWU Window	Detector	Optical Elements	Optical Barrel
V14_Acktar	-29.06	-24.39	30.96	30.42	29.33	29.31
V14_Z307	-29.08	-24.44	30.99	30.42	29.34	29.31
V14_PUK	-29.03	-24.34	30.99	30.42	29.33	29.31
A276_Acktar	-24.19	-19.93	31.05	30.42	29.35	29.33
A276_Z307	-24.23	-20.01	31.05	30.42	29.36	29.33
A276_PUK	-24.21	-19.95	31.06	30.42	29.36	29.33
AZ93_Acktar	-27.19	-22.64	30.98	30.42	29.33	29.30
AZ93_Z307	-27.18	-22.64	31.00	30.42	29.34	29.31
AZ93_PUK	-27.44	-22.60	30.99	30.42	29.34	29.31

Table 10-2: Minimum Temperatures of selected instrument parts [°C]

As before, no significant temperature change results from choosing different black coatings for one specific white coating. However, the results comparing the different coating combinations differ from those of the maximum temperatures. Here, V14 has the lowest temperatures with -29°C on the baffle shield and -24°C on the baffle cone, followed by AZ-93, with -27°C on the shield and -23°C on the cone. As before, A276 reaches the highest temperatures with -24°C on the shield and -20°C on the baffle cone.

The results show that all instrument parts stay in comparable temperature ranges, concerning maximum and minimum temperatures during the science phase. These values serve as a basis for the requirements Req-BS-004, and Req-BC-004 from Chapter 5.2. Also, no significant improvement in the temperature range on the parts critical for the instrument’s optical performance can be seen by using one specific coating combination.

Coating Combination	Baffle Shield	Baffle Cone	TWU Window	Detector	Optical Elements	Optical Barrel
V14_Acktar	8.32	1.83	0.14	0.003	0.04	0.04
V14_Z307	8.37	1.62	0.11	0.002	0.04	0.04
V14_PUK	8.24	1.57	0.11	0.003	0.04	0.04
A276_Acktar	6.27	1.45	0.12	0.003	0.05	0.05
A276_Z307	6.34	1.34	0.19	0.002	0.04	0.04
A276_PUK	6.28	1.30	0.08	0.003	0.04	0.04
AZ93_Acktar	3.14	0.74	0.08	0.002	0.02	0.02
AZ93_Z307	3.17	0.36	0.04	0.001	0.01	0.01
AZ93_PUK	3.09	0.42	0.06	0.001	0.02	0.01

Table 10-3: Absolute Change of average BOL and EOL Temperatures during Cold Case [K]

Table 10-3 shows the absolute temperature changes during the cold-case orbit of the average temperatures from the BOL to the EOL condition. The baffle shield temperature increase is mainly a function of the white coating, with the lowest increase of 6 K, followed by V14, with an increase of 8 K. The baffle cones temperature increase is low on all coating combinations, being below 2 K. The rest of the instrument is unaffected by these temperature increases and stays on the same level with the BOL and EOL conditions of the coatings on the baffle unit.

Table 10-4 shows the absolute temperature changes of the average temperatures with BOL and EOL conditions during the hot-case orbit. The baffle shield is mainly affected by temperature increases up to 29K using V14, up to 18K using A276, and up to 11K using AZ-93. The baffle cone is less affected with a temperature increase lower than 5 K. The remaining parts of the instrument stay at the same temperature levels at EOL compared to BOL conditions.

Coating Combination	Baffle Shield	Baffle Cone	TWU Window	Detector	Optical Elements	Optical Barrel
V14_Acktar	29.30	4.35	0.35	0.009	0.14	0.14
V14_Z307	29.43	4.14	0.33	0.008	0.13	0.13
V14_PUK	29.20	3.27	0.24	0.006	0.09	0.08
A276_Acktar	18.15	2.98	0.25	0.007	0.11	0.11
A276_Z307	18.21	2.78	0.24	0.007	0.11	0.10
A276_PUK	17.15	2.08	0.18	0.004	0.06	0.06
AZ93_Acktar	11.04	1.61	0.10	0.003	0.05	0.05
AZ93_Z307	11.14	1.34	0.08	0.003	0.04	0.04
AZ93_PUK	10.92	0.51	-0.01	0	-0.002	-0.002

Table 10-4: Absolute Change of average BOL and EOL Temperatures during Hot Case [K]

These results indicate good thermal insulation between the baffle unit and the remaining parts of the instrument. Therefore, the temperature-critical parts are decoupled from the baffle unit and unaffected by any degradation.

Figures 10-9 and 10-10 show the temperatures of the baffle cone, shield, detector package, the TWU window, and the TRPs during the hot-case orbit with BOL and EOL conditions of an example coating combination of V14 and Fractal Black. While the baffle cone just experienced a temperature offset, the baffle shield is more affected due to degradation. With this coating combination, the baffle shield reaches temperatures in the range of the baffle cone temperatures and produces some spike temperatures with fast increasing and afterward decreasing maximum temperatures at about 40 and 80 minutes into orbit.

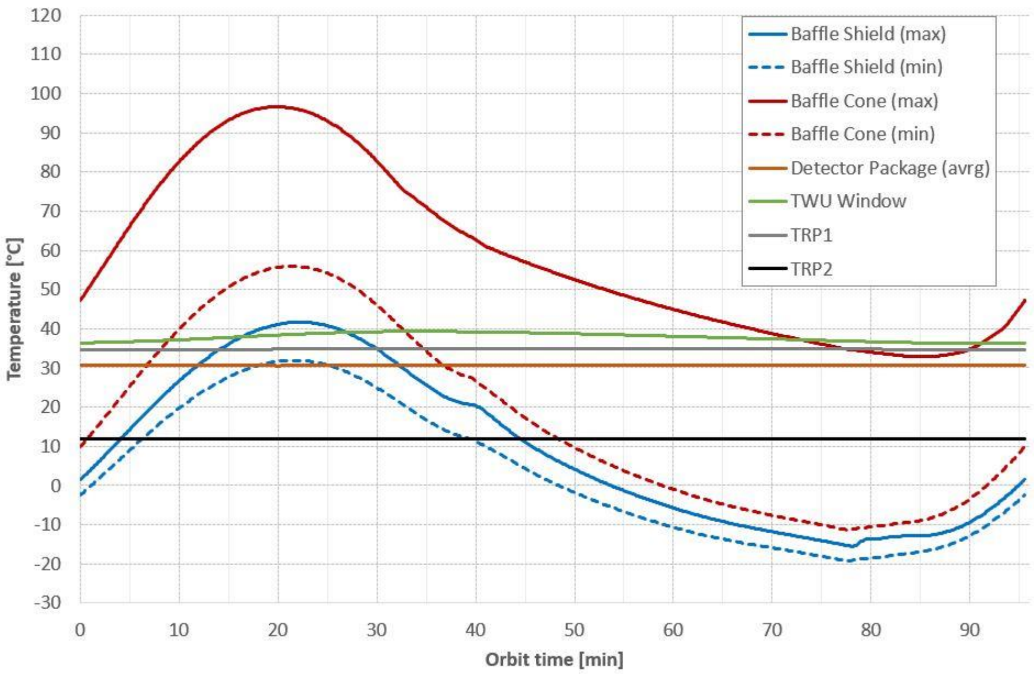

Figure 10-9: Temperatures during Hot Case Orbit of Example Combination Ceranovis V14 and Acktar Fractal Black BOL

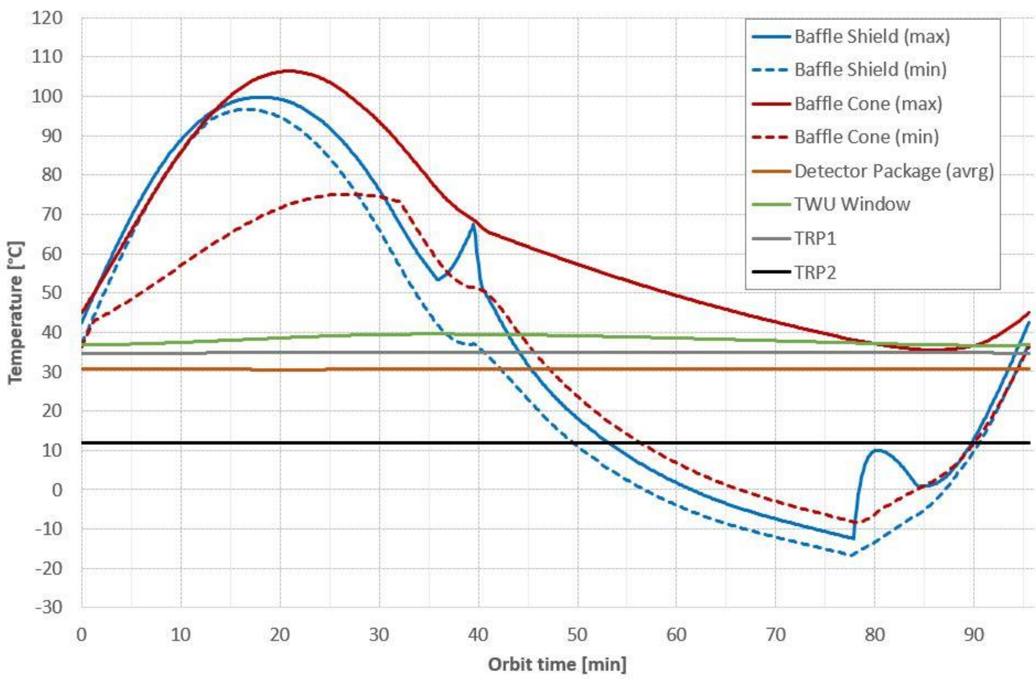

Figure 10-10: Temperatures during Hot Case Orbit of Example Combination Ceranovis V14 and Acktar Fractal Black EOL

This effect can be explained by sudden solar irradiation. The baffle shield is in the shade for a long time until the angle of the sun allows the shield to be irradiated. As a result, the outer edge is suddenly irradiated, which causes the temperature to rise locally to a greater or lesser extent, depending on the value of the solar absorptance of the applied TCC. This effect subsides again through more extensive irradiation of the baffle shield until the point at which only the outer edge is locally irradiated again, and a second temperature peak occurs.

10.4 Stability of Optical Path

A main criterion to evaluate the optical performance of the instrument is a uniform temperature profile of the optical elements used in the optical path. These are mostly optical lenses that are held in place by the optical barrel. Temperature differences in the barrel and the lenses can cause the thermal expansion of materials affecting the optical performance, resulting in out-of-focus effects. To reduce these effects, the heat coming from other parts of the instruments as well as from the environment shall be spread along the length of the optical barrel, resulting in an evenly distributed temperature profile. Table 10-5 shows the temperature differences between the optical elements and the optical barrel during the cold-case orbit in BOL and EOL conditions. The values are derived by calculating the difference between the maximum and minimum temperatures reached during the orbit. Therefore, these values are considered conservative, as the minimum and maximum temperatures are not reached at the same time. Consequently, the actual temperature difference will always be lower than the values shown.

Coating Combination	Optical Elements (BOL)	Optical Elements (EOL)	Optical Barrel (BOL)	Optical Barrel (EOL)
V14_Acktar	0.09	0.09	0.12	0.13
V14_Z307	0.09	0.09	0.12	0.13
V14_PUK	0.09	0.09	0.12	0.13
A276_Acktar	0.09	0.10	0.13	0.13
A276_Z307	0.09	0.10	0.13	0.13
A276_PUK	0.09	0.10	0.13	0.12
AZ93_Acktar	0.09	0.09	0.13	0.13
AZ93_Z307	0.09	0.09	0.13	0.13
AZ93_PUK	0.09	0.09	0.13	0.13

Table 10-5: Temperature Differences of optical elements and optical barrel for Cold Case [K]

Table 10-5 shows that the differences between the maximum and minimum temperatures for the optical elements and the barrel during the cold-case orbit are almost negligible. No significant improvements can be achieved by using a particular coating combination since the temperature differences are identical for all coating combinations. These low values suggest that the optical performance of the instrument is not negatively affected.

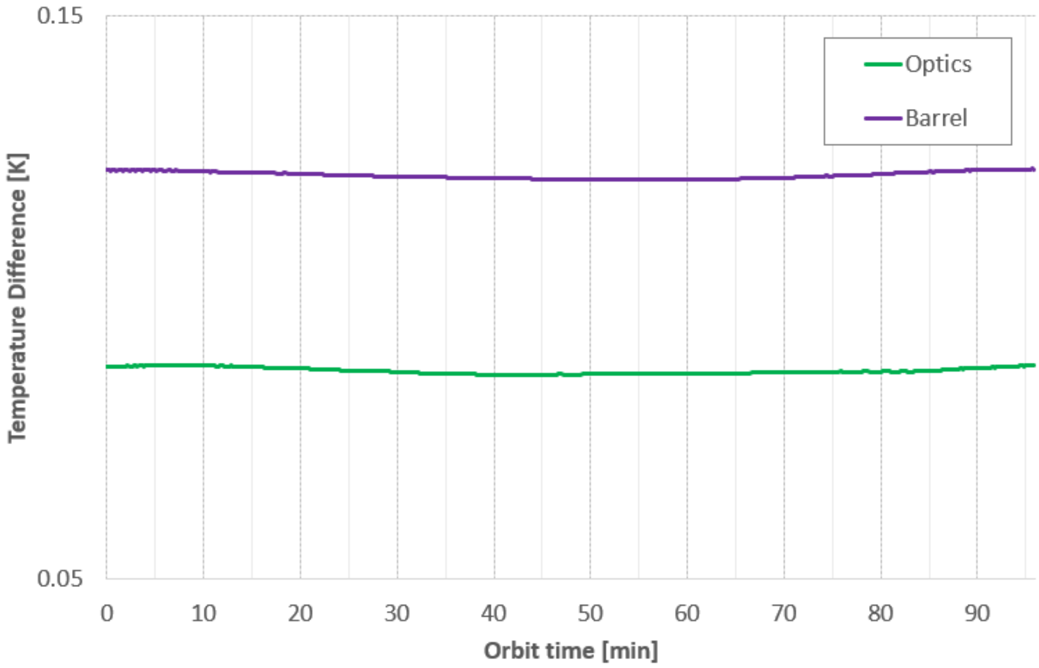

Figure 10-11: Temperature Differences of Optics and Optical Barrel during Cold Case Orbit of Example Combination V14 and Fractal Black EOL

Figure 10-11 shows the change in temperature differences for an example coating combination of Ceranovis V14 and Acktar Fractal Black in the EOL state during the cold-case orbit over time. For both the optical elements and the barrel, the temperature differences are at a constant and very low level with no significant change. This confirms a consistent temperature profile of the subunits, which also have no negative impact on the optical performance of the instrument.

Coating Combination	Optical Elements (BOL)	Optical Elements (EOL)	Optical Barrel (BOL)	Optical Barrel (EOL)
V14_Acktar	0.42	0.43	0.51	0.53
V14_Z307	0.42	0.43	0.51	0.52
V14_PUK	0.42	0.43	0.51	0.52
A276_Acktar	0.43	0.44	0.52	0.53
A276_Z307	0.43	0.44	0.52	0.53
A276_PUK	0.43	0.43	0.52	0.52
AZ93_Acktar	0.42	0.43	0.52	0.52
AZ93_Z307	0.42	0.43	0.51	0.52
AZ93_PUK	0.42	0.42	0.51	0.51

Table 10-6: Temperature differences of optical elements and optical barrel for Hot Case [K]

The same holds for the optical path during the hot-case orbit. The totality of the temperature differences is higher compared to the cold-case values but kept way below 1 K. No improvements can be found by using a specific coating combination also, the increase in the temperature differences due to degradation of the applied coatings are almost identical over the different coating combinations, as shown in Table 10-6.

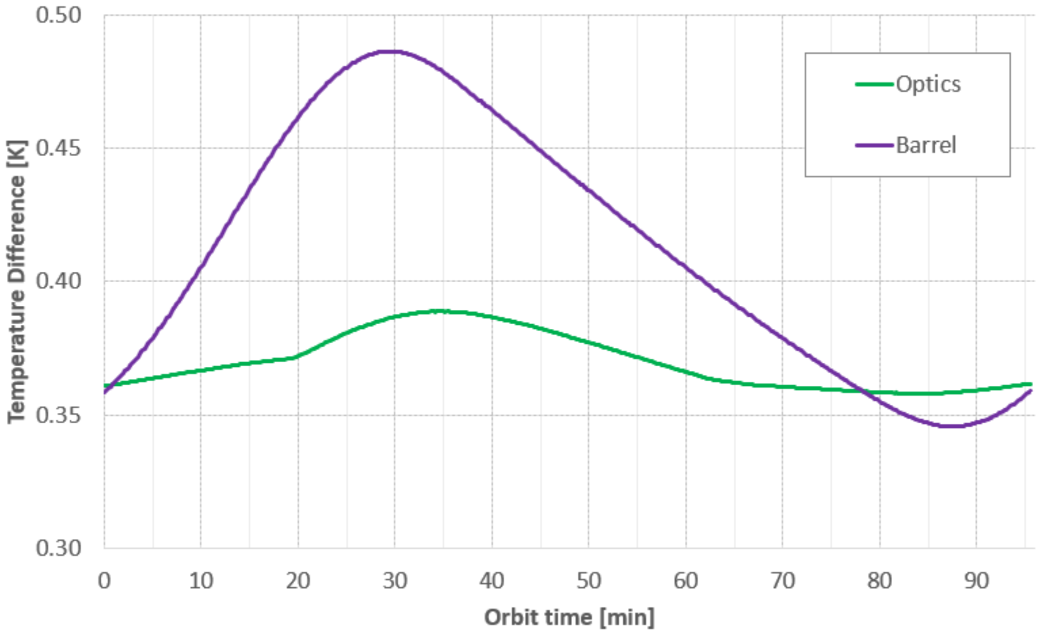

Figure 10-12: Temperature Differences of Optics and Optical Barrel during Hot Case Orbit of Example Combination V14 and Fractal Black EOL

Figure 10-12 shows the change in temperature differences for an example coating combination of Ceranovis V14 and Acktar Fractal Black in the EOL state during the hot-case orbit over time. The temperature differences in the optical barrel range between 0.35 and 0.48 K while the differences in the optical elements range between 0.36 and 0.39 K. These small changes in temperature differences also do not affect the optical performance of the instruments.

The maximum and minimum temperatures of the optical elements and the optical barrel over time are shown in Figure 10-13 during the cold-case orbit and in Figure 10-14 during the hot-case orbit at the example coating combination of V14 and Fractal Black at EOL conditions. The graphs of the other coating combinations appear almost identical by showing the same behavior of temperature deviations over time, besides a small offset in the overall temperature.

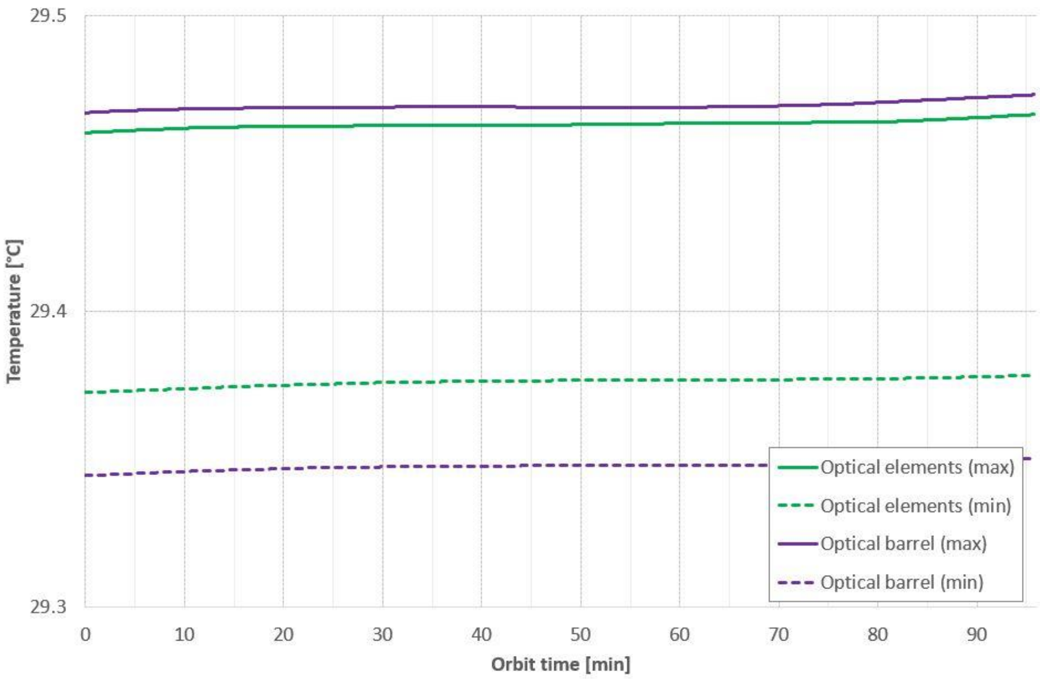

Figure 10-13: Maximum and Minimum Temperatures of Optics during Cold Case of Example Combination V14 and Fractal Black EOL

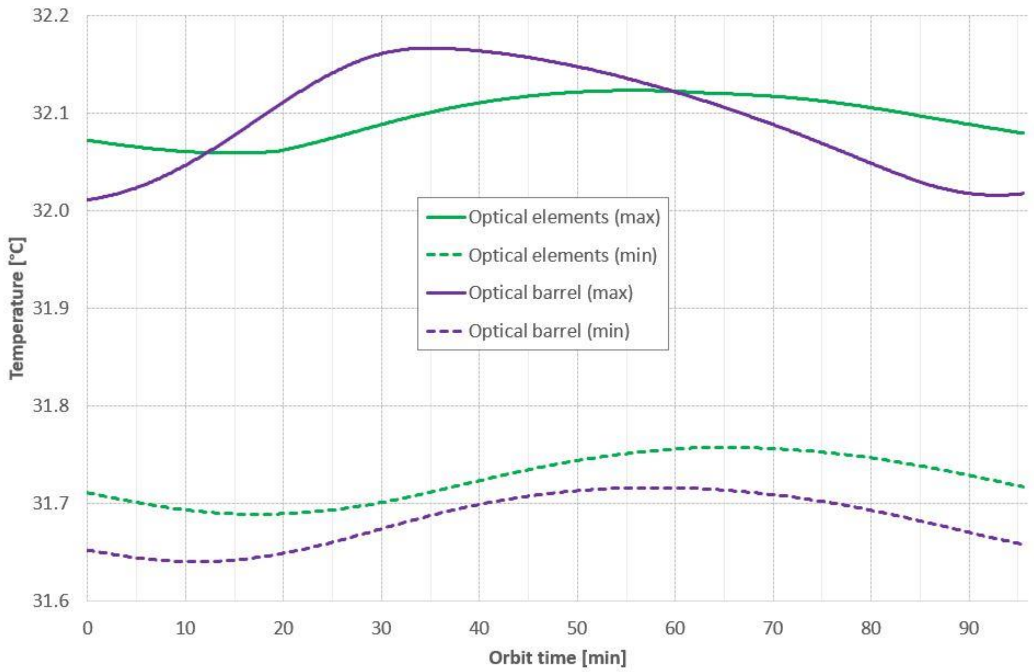

Figure 10-14: Maximum and Minimum Temperatures of Optics during Hot Case of Example Combination V14 and Fractal Black EOL

Altogether, the optical path stays thermally stable for all coating combinations, indicating a functional thermal insulation of the structure holding the optical path from the instrument's baffle unit. Also, an even temperature distribution of the optical elements and barrel is found, which does not affect the optical performance of the instruments negatively. Furthermore, degradations of the applied coatings on the baffle unit leading to higher temperatures on the shield, cone, and TWU window do not significantly affect the optical performance of the instrument.

Only considering these results, no coating combination holds any improvement or benefit, and no decision on one particular combination can be made.

10.5 Radiative and Conductive Heat Fluxes

Another criterion to evaluate the performance of the applied coating combinations is the radiative and conductive heat flows from the instrument to the S/C and/or the environment. Heat flows coming from the instrument to the individual parts are noted as negative values, while heat flows that are incoming to the instrument are indicated as positive values. However, the following results are only applicable for VenSpec-M, because VEM is wrapped in MLI and therefore no radiative interactions between the instrument and the S/C are possible.

No significant changes from the BOL to the EOL conditions can be spotted during the cold-case orbit. This is true for all coating combinations, as they perform similarly. Figure 10-15 shows an exemplary diagram of the heat flows for the EOL condition of V14 and Fractal Black during the cold-case orbit and Figure 10-16 during the hot-case orbit.

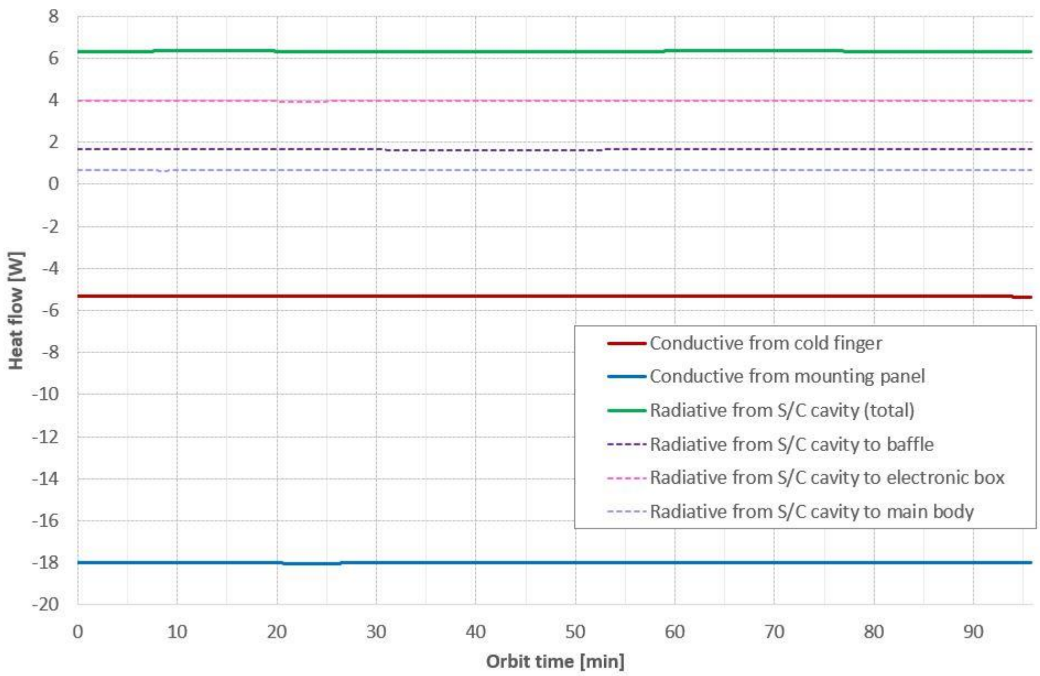

Figure 10-15: Radiative and Conductive Heat Fluxes Cold Case of Example Combination Ceranovis V14 and Acktar Fractal Black EOL

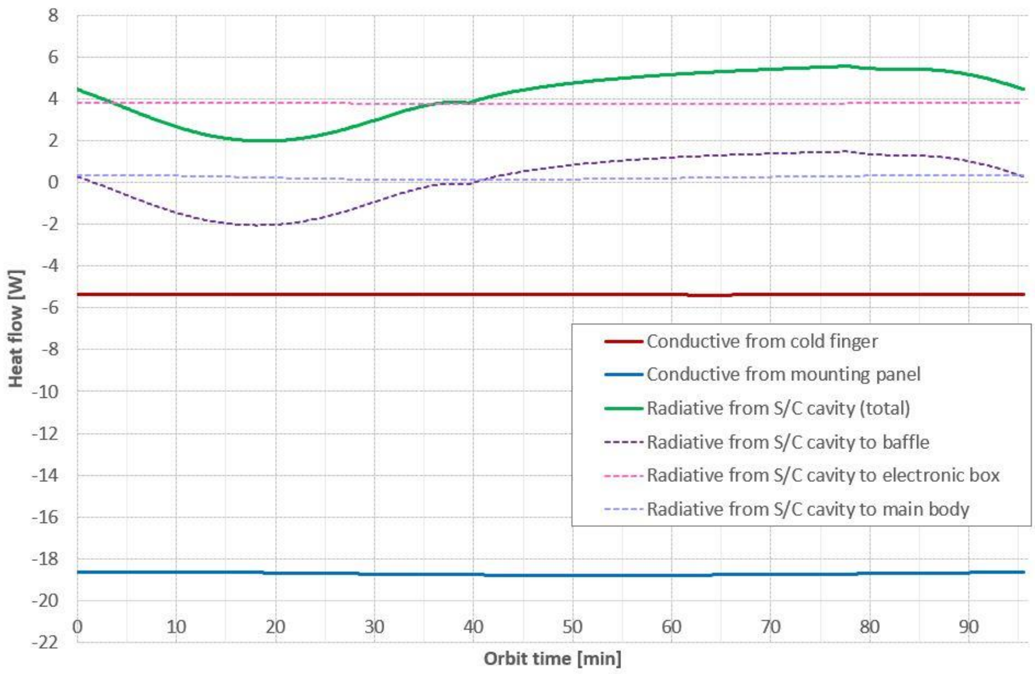

Figure 10-16: Radiative and Conductive Heat Fluxes Hot Case of Example Combination Ceranovis V14 and Acktar Fractal Black EOL

During the hot-case orbit, a change in the radiative heat flows from the S/C cavity to the baffle unit can be seen. This change is visible in the heat flows from the S/C cavity to the whole instrument, too. Due to degradation, as the baffle unit gets hotter at the beginning of the hot-case orbit, the heat flows from S/C to the baffle unit are negative. That means that the baffle unit heats the surrounding S/C cavity. This can be a concern as heat flows may reach a high value and can therefore disturb the thermal control system of the S/C itself. Employing that, Table 10-7 shows the maximum heat flows from the baffle unit to the S/C cavity at BOL and EOL conditions for each coating combination. The values determined here serve as a basis for the requirements Req-BS-007, and Req-BC-007 from Chapter 5.2.

Coating Combination	Radiative Heat Flux BOL	Radiative Heat Flux EOL	Change of Radiative Heat Flux
V14_Acktar	0.02	2.05	2.03
V14_Z307	0.01	2.05	2.04
V14_PUK	0.02	2.03	2.01
A276_Acktar	1.23	2.79	1.56
A276_Z307	1.23	2.79	1.56
A276_PUK	1.23	2.78	1.55
AZ93_Acktar	0.46	1.20	0.73
AZ93_Z307	0.46	1.20	0.74
AZ93_PUK	0.47	1.17	0.71

Table 10-7: Maximum Radiative Heat Fluxes from Baffle Unit to S/C Cavity [W]

The difference in heat flows in total and the change of the heat flow from BOL compared to EOL conditions by using different black coatings on the baffle cone is minimal compared to using different white coatings on the baffle shield.

Using V14 on the baffle shield, the heat flows at BOL conditions stay the lowest, followed by AZ-93 and A276. In the EOL condition, AZ-93 has the lowest heat flows, followed by V14, and lastly A276. However, the highest increase in the heat flow can be found using V14, followed by A276, followed by AZ-93.

Altogether AZ-93 features the lowest radiative heat flows at EOL conditions as well as the lowest change in the heat flow and very low flows in the BOL condition. V14 has very low heat flows in the BOL condition but with the most significant change. The heat flows at the EOL condition are almost twice as high compared to the AZ-93 values. A276 holds no benefits at all and, from the point of view of the radiative heat flows, is not recommended to be used on the baffle shield's exposed surfaces.

10.6 Selection of Coating Combination

The performed analysis shows good thermal insulation between the baffle unit and the optical path because temperature increases in the baffle unit do not affect the optical path. The stability of the optical path shows the optical elements staying at an equal temperature level over all coating combinations with almost identical maximum differences in temperature. Therefore, the main criterion for choosing a suitable coating combination from a thermal point of view are the maximum, minimum, and average temperatures on the baffle unit, and the temperature increases due to degradation.

Concerning the maximum temperature, AZ-93 performs best under all preselected white coatings, with the lowest temperatures on the baffle shield and cone. Concerning the minimum temperatures, V14 holds the lowest temperatures on the baffle shield and cone. That is explained by the overall better performance of V14 on BOL conditions, but with higher degradation compared to AZ-93, leading to worse performance at EOL conditions, compared to AZ-93. A276 reached the most elevated temperatures in all cases. Despite having a lower temperature increase over the mission duration, compared to V14, it may not be used as a preferred coating on the baffle shield.

The decision between V14 and AZ-93 is more complicated. Both coatings do not influence the thermal stability of the optical path, but they lead to slightly different temperatures at the baffle shield and cone. On critical and sizing mission cases at the beginning of the science phase, where the coatings are near the BOL conditions, V14 may be selected due to better performance, but AZ-93 may be preferred at EOL conditions. This is also shown by the results obtained for the radiative heat fluxes, as the heat flux from the baffle unit to the S/C cavity stays the lowest with V14 on BOL conditions and with AZ-93 at EOL conditions.

Because of V14 qualification for the ESA mission BepiColombo and the possibility to clean or even seal the samples with a qualified coating procedure, the degradation of the coating due to solar irradiation can be reduced as shown in [25]. This may favor the decision to use V14 on the baffle shield as the preferred coating.

Another result of this analysis shows no significant improvements or benefits by using one specific black coating on the baffle cone. The temperature differences in all cases are minimal and the selection does not affect the radiative heat fluxes to the S/C cavity. All black coatings are performing equally, so the decision can only be made on technical data of the pristine coating. As Fractal Black is qualified to a maximum working temperature of at least 450°C [38], Z307 to 121°C [39], and MAP PUK to 130°C [40], Fractal Black is the preferred coating for the baffle cone, offering the highest margin concerning the maximum temperatures reached on the baffle cone, which is 106.35°C.

Altogether, this analysis leads to a selection of the Ceranovis V14 and Acktar Fractal Black coating combination on the baffle unit with an alternative coating combination of AZ Technology AZ-93 and Acktar Fractal Black.

11. Conclusion and Outlook

11.1 Compliance Requirements and Constraints

Based on the requirements presented in Chapter 5 the main degradation mechanisms present during the mission were identified and quantitatively determined. The expected degradations of the preselected coatings have been determined theoretically and a thermal analysis was conducted to enable a comparison of the effects of different coating combinations on the thermal and optical performance of VEM/VenSpec-M. Due to the availability of SPICE data and detailed thermal models, these effects were studied on the VenSpec-M instrument. However, these results are also applicable to the VEM instrument due to the very similar geometry and similarly long duration of the individual mission phases.

The results showed that the preselected TCCs degraded individually due to ATOX and ESH fluxes. However, all coating combinations performed quite similarly on the thermal and optical performance of the instrument due to the good thermal decoupling of the baffle unit from the rest of the instrument. However, as a result of the final thermal analysis two coating combinations are preferred, Ceranovis V14 with Acktar Fractal Black, and AZ-Technology AZ-93 with Acktar Fractal Black. To enable a final decision on the coatings to be used they are evaluated independently in a trade study including the derived requirements and non-thermal aspects that play a major role in the selection. Figure 11-1 compares the preselected white TCCs in the form of a simple trade study.

Requirement		Ceranovis V14	Aeroglaze A276	AZ-Technology AZ-93
Req-BS-001	Change BOL/EOL reflectivity/emissivity	0.01/0.0	0.017/-0.03	0.003/0.0
Req-BS-002	Change BOL/EOL reflectivity/emissivity	0.33/0.05	0.282/0.03	0.108/0.0
Req-BS-003	Change BOL/EOL reflectivity	0.0	0.0	0.0
Req-BS-004	Max Operating Temperature	430°C	121°C	1400°C
Req-BS-005	Alpha/Epsilon BOL	0.098	0.295	0.165
Req-BS-005	Alpha/Epsilon EOL	0.443	0.635	0.287
Req-BS-006	Electrically Conductive	Yes	Yes	Yes
Req-BS-007	Heat Flux to S/C Cavity	Low	Low	Low
Other Aspects	Other Missions	BepiColumbo	Not known	ISS
	Availability	Good	Good	Difficult
	Heritage at DLR	Used before	No	No
	Potential Improvement	Cleaning/Sealing	Not known	Not known

Figure 11-1: Trade Study White TCCs

This trade study confirms the decision to focus on the preferred use of V14 and AZ-93. The Aeroglaze coating is degraded the most based on ATOX fluxes, not only in the thermo-optical properties but as well in the coating material itself, as it has an erosive effect. Furthermore, the thermo-optical properties at BOL and EOL are comparatively less suitable. An exclusion criterion is the maximum operable temperature of this coating, that is including almost no margin to the maximum temperature expected at the baffle shield, which is 116°C during the hot-case orbit of the science phase.

When comparing V14 and AZ-93, it is noticeable that V14 degrades more under ESH. However, as part of a qualification for BepiColombo, processes were developed that contain a cleaning or sealing method that can reduce degradation due to high ESH. Therefore, there is still room for improvement compared to the

AZ-93 coating. Furthermore, the availability of the V14 coating is better and it has already been used in other missions at the DLR. Also, a test of this coating on the specified radiation dose expected over the entire mission duration has already been performed. This test showed no degradation due to charged-particle radiation.

Based on the conducted trade study the Ceranovis V14 coating is a suitable TCC for usage on the baffle shield. Due to the heritage at DLR, good availability, room for improvements of the degradation due to ESH, and the overall very good thermo-optical properties this coating is finally selected. Furthermore, as shown in Figure 11-1, the V14 coating is compliant with all requirements concerning the surfaces of the baffle shield derived in Chapter 5.2.

Consequently, this selection and the results of the thermal analysis of the different coating combinations make Acktar Fractal Black the matching complement to the selected white TCC. Nevertheless, a similar trade study including the derived requirements presented in Chapter 5 and other significant non-thermal aspects is also conducted for the preselected black TCCs. This trade study is presented in Figure 11-2.

Requirement		**Acktar Fractal Black**	**Aeroglaze Z307**	**MAP PUK**
Req-BS-001	Change BOL/EOL reflectivity/emissivity	0.0/0.0	-0.02/0.01	-0.02/0.01
Req-BS-002	Change BOL/EOL reflectivity/emissivity	0.0/0.0	0.02/0.04	-0.2/0.0
Req-BS-003	Change BOL/EOL reflectivity	0.0	0.0	0.0
Req-BS-004	Max Operating Temperature	450°C	121°C	130°C
Req-BS-005	Alpha/Epsilon BOL	1.077	1.056	1.021
Req-BS-005	Alpha/Epsilon EOL	1.077	1.000	0.815
Req-BS-006	Electrically Conductive	Yes	Yes	Yes
Req-BS-007	Heat Flux to S/C Cavity	Low	Low	Low
Other Aspects	Other Missions	Solar Orbiter	JUICE	Plato
	Availability	Good	Good	Good
	Heritage at DLR	Other Acktar	Often used	Often used
	Potential Improvement	Not known	Not known	Not known

Figure 11-2: Trade Study Black TCCs

This trade study confirms the decision on Acktar Fractal Black as a suitable coating for the baffle cone. No degradation based on ATOX fluxes and ESH is expected, also the coating was already tested to the specified radiation dose expected over the mission lifetime with no degradation in thermo-optical properties. The other black TCCs experienced little degradation due to ATOX fluxes and on MAP PUK is expected to degrade the most due to ESH with a decrease in absorptance of 0.2. All coatings have been used before at DLR and are used on several missions. The main criterion for selecting the most suitable coating is the difference between the maximum operable temperature of the coatings compared to the maximum temperature at the baffle cone expected. This temperature can be as high as 113°C leaving very little margin on the Z307 and PUK coating.

Based on this study the Acktar Fractal Black coating is finally chosen as a suitable TCC to be applied on the baffle cone. In combination with the selected Ceranovis V14 coating on the baffle shield, this coating combination holds the most benefits and is found to be a combination with the highest margins on maximum temperatures, doesn’t affect the thermal and optical performance due to its degradation during the mission, has a good heritage at DLR, and is used on many other space missions. Furthermore, as shown in Figure 11-2, the Acktar Fractal

Black coating is compliant with all requirements concerning the surfaces of the baffle cone derived in Chapter 5.2.

The AR coating of the TWU window showed no significant degradation due to ATOX fluxes or ESH and is therefore compliant with the ATOX and ESH requirements Req-TW-001, and Req-TW-002. That’s due to the expected degradation in transmission happening at a wavelength laying outside the science wavelength band of VEM/VenSpec-M. This theoretically derived degradation was also confirmed from tests at ESTEC where samples of the TWU window with the NIR-II coating showed comparable or even lower degradation in transmission on wavelengths outside the science wavelength band. Furthermore, tests on samples of the windows exposed to the specified radiation dose showed also no degradation and are therefore compliant with the radiation requirements Req-TW-003, and Req-TW-005. The final thermal analysis showed also no evidence of a negative impact on the thermal or optical performance of VEM/VenSpec-M, making it compliant with requirement Req-TW-004. Therefore, the use of this type of AR-coating on the TWU window is recommended, as it can allow observations of the instrument through the TWU window even after degradation to its EOL thermo-optical properties. Due to this ability, the TWU window is expected to be compliant with the requirement stating that the TWU window shall not impede by design the instrument function in case of a failure of the opening mechanism.

11.2 Conclusions

The results of this thesis showed that besides ATOX fluxes the main degradation mechanism influencing the thermo-optical properties of the applied TCCs the most is the solar and albedo radiation at Venus. A low charged-particle radiation dose was specified for the missions, due to the lack of radiation belts at Venus. This lower dose is not negligible for external surfaces. However, they are not critical for any degradation of the applied TCCs. This has already been confirmed by some charged particle radiation tests of TCC samples and TWU windows.

The derived procedure to approximate ATOX fluxes inside baffle openings as a function of its geometry and AOA provides a to-be-proven conservative absolute ATOX flux for all surfaces of interest of both instruments’ baffle units. These ATOX fluxes have only a minor effect on the thermo-optical properties of TCCs with almost no effect on ceramic white coatings and up to no effect at all on Acktar black coatings. However, TCCs with organic constituents are heavily affected. Thermo-optical properties of these coatings degrade significantly more compared to TCCs without organic constituents. Furthermore, ATOX has a corrosive effect on these coatings resulting in a thickness reduction and mass loss. Therefore, the usage of TCCs with organic constituents in an ATOX-rich environment is not recommended.

The ESH values determined in the aerobraking, and science phase turned out to be over-conservative, due to the usage of the absorbed environmental heat fluxes including reflected sun and albedo fluxes inside the baffle unit. Also, the ESH values during the aerobraking phase were approximated including orbits on which the instruments are looking directly into the sun for a long duration. Therefore, the derived degradation based on these high ESH values is over-conservative too, leading to absolute EOL thermo-optical properties.

However, besides the conservative EOL properties of the TCCs, the effects on the thermal and optical performance of the instruments are kept low and almost similar across all preselected coating combinations, which is approving good thermal isolation of the baffle unit from the rest of the instrument.

In the end, the decision on one specific coating combination was mostly done on non-thermal aspects, such as heritage and availability. The effects on the instrument's thermal and optical performance play only a minor role due to their similarity over all coating combinations. However, a suitable coating combination, able to be compliant with the derived requirements in Chapter 5, was found, namely Ceranovis V14 on the baffle shield and Acktar Fractal Black on the baffle cone.

11.3 Outlook

An important degradation mechanism that is not considered in this thesis is the aerodynamic heat flux present during the drag pass in the aerobraking phase. These heat fluxes have to be determined for both missions along with their corresponding degradation effects on the applied TCCs in future work. As the baffle unit and the TWU window are the only surfaces directly exposed to the space environment, the degradation effects of the applied TCCs are of major concern.

Also, these heat fluxes may lead to high temperatures during the drag pass, while the surfaces cool down after leaving the atmosphere of Venus to very low temperatures during long flight paths at high altitudes. These thermal cycles may have a degradation effect on the coatings and materials as well and have to be determined. Based on these results, samples of the TCCs and TWU windows can be tested.

As presented in Chapter 6 a calculation method for approximating ATOX fluxes inside S/C cavities has been derived. This calculation method can be used on other missions, where surfaces of a cavity are susceptible to ATOX degradation. This method is also applicable for non-aerobraking phases, as long as the attitude of the S/C is specified or can be determined. Further analysis based on a Monte-Carlo simulation or other comparable simulations can be made to prove or evaluate the results of the approximation. Based on such results, tests of the selected coatings to the determined ATOX fluxes can be performed to confirm the expected degradation in thermo-optical properties. This allows values for the EOL thermo-optical properties with lower uncertainty.

Chapter 8 described the determined ESH values during the aerobraking and science phase. Also, for these derived values, testing of TCC samples in suitable facilities may be needed to confirm the theoretically derived degradation.

Based on the selected coatings, Ceranovis V14 and Acktar Fractal Black, further analysis of contamination and its effects on the degradation can be performed, to write requirements and derive procedures for contamination control. Also, procedures for handling and cleaning these types of TCCs can be derived.

X. Bibliography

[1] VDI-Gesellschaft Verfahrenstechnik und Chemieingenieurswesen, (2013) VDI-Wärmeatlas. Springer-Verlag Berlin Heidelberg, 2013, doi: 10.1007/978-3-642-19981-3

[2] Ley, W., Witmann, K., and Hallmann W., (2019) Handbuch der Raumfahrttechnik. Hanser Verlag München, 2019, doi: 10.3139/978-3-446-45429-3

[3] ITP Engines UK Ltd., (2015) EASATAN-TMS Thermal Engineering Manual. ITP Engines UK Ltd., 2014

[4] ITP Engines UK Ltd., (2022) EASATAN-TMS Thermal User Manual. ITP Engines UK Ltd., 2022

[5] Taylor, F., Svedhem, H., and Head, J., (2018) Venus: The Atmosphere, Climate, Surface, Interior and Near-Space Environment of an Earth-Like Planet. Space Science Reviews 214:35, 2018, doi: 10.1007/s11214-018-0467-8

[6] Banks, B., et al., (2004) Low Earth Orbital Oxygen Interactions with Materials. NASA/TM—2004-213223, 2004, doi: 10.2514/6.2004-5638

[7] Reddy, M., (1995) Effect of low earth orbit atomic oxygen on spacecraft material. Journal of Material Science 30, 281-307, 1995, doi: 10.1007/BF00354389

[8] Rooij, A., (2010) Corrosion in Space. Materials Technology, Materials for Space Applications, 2010, doi: 10.1002/9780470686652.eae242

[9] Ahmadjian, M., et al., (1992) Infrared Spectral Measurement of Space Shuttle Glow. Geophysical Research Letters, Vol 19, No. 10, Pages 989-992, 1992, doi: 10.1029/92GL00051

[10] Ghail, R., et al., (2021) EnVision Understanding why Earth’s closest neighbor is so different. European Space Agency, Assessment Study Report, 2021

[11] (2023) ENVISION Spacecraft System Requirements Document (SSRD), ESA-ENVIS-EST-SC-RS-002, 2023

[12] Howell, E., (2023, 26. Juni) Problems with NASA asteroid mission Psyche delay Venus probe's launch to 2031. SPACE, https://www.space.com/nasa-problems-psyche-venus-probe-veritas-launch-delay

[13] Smrekar, S., et al., (2020) VERITAS Discovering the Secrets of a Lost Habitable World. National Aeronautics and Space Administration, 2020

[14] Ryan, C., (2021) VenSpec-M Design Description. VESM-DLR-PL-DD-001-Instrument Design Description, 2021

[15] Del Togno, S., (2023) Thermal Analysis Report. VESM-DLR-PL-AN-0008, 2023

[16] (2023, 26. Juni) barbecue mode Standard. European Cooperation for Space Standardization, https://ecss.nl/item/?glossary_id=413

[17] Gauvin, M. and Freniere, E., Reducing stray light in Opto-Mechanical Systems. Lambda Research Corporation

[18] Outram, B., (2009) Black Coatings to Reduce Stray Light. OPTI 521-Optomechanical Engineering, 2009
[19] Dern, P., (2022) VenSpec-M ICD. VESM-DLR-PL-ICD-0004, 2022
[20] Banks, B., et al., (2003) Atomic Oxygen Effects on Spacecrafts Materials. NASA TM—2003-212484, 2003
[21] Voirin, T., (2022) Atomic Oxygen during aerobraking. ESA-ENVIS-EST-MIS-HO-030_Is2_0, 2022
[22] Dodge, R., (2021) Environmental Requirements Document. VERITAS_DRAFT_ERD_D-96573_Rev6_20220721b_LRR066457, 2021
[23] (2022) EnVision Environment Specification. ESA-ENVIS-EST-SYS-SP-001, 2022
[24] Finckenor, M., et al., (2003) Contamination, UV Radiation, and Atomic Oxygen Effects on ISS Thermal Control Materials. 41st Aerospace Sciences Meeting and Exhibit, 2003, doi: 10.2514/6.2003-1084
[25] Holynska, M., et al., (2019) Studies of White Ceramic Coatings for ESA's BepiColombo Mission to Mercury. Journal of Spacecraft and Rockets, Vol. 59, Np.5, 2019, doi: 10.2514/1.A34230
[26] Walter, I., (2022) Baffle shield coating ATOX sensitivity. VER-DLR-VEM-TN-0001, 2022
[27] Kenny, M., et al., (2009) Further Analysis of Thermal Control Coatings on MISSE for Aerospace Applications. National Space and Missile Materials Symposium, 2009
[28] Golden, J., (1994) Results of the Examination of LDEF Polyurethane Thermal Control Coatings. NASA Contractor Report 4617, 1994
[29] (2023, 26. Juni) AZ-93 White Thermal Control, Inorganic Paint / Coating. AZ Technology, https://www.aztechnology.com/product/1/az-93
[30] Huang, A., et al., (2008) Characterizing the Optical Performance of AZ93 with a Fluoropolymer Overcoat under Ultraviolet Exposure. Proceedings of SPIE – The International Society for Optical Engineering, 2008, doi: 10.1117/12.793727
[31] (2023, 26. Juni) Fractal Black Coating. Acktar, https://acktar.com/product/fractal-black/
[32] Salomon, Y., et al., (2009) Qualification of Acktar Black Coatings for Space Application. 2009
[33] Romoli, M., et al., (2017) METIS: the visible and UV coronagraph for solar orbiter. Proceedings Volume 10563, International Conference on Space Optics-ICSO 2014, 2017, doi: 10.1117/12.2304274
[34] Grigorevskiy, A., et al., Complex Influence of Space Environment on Optical Properties of Thermal Control Coatings.
[35] (2023, 26. Juni) Anti-Reflection (AR) Coatings. Edmund Optics, https://www.edmundoptics.eu/knowledge-center/application-notes/lasers/anti-reflection-coatings/
[36] Ianno, N. and Speckman, D., (2010) The Effect of Deposition Conditions on the Atomic Oxygen induced Degradation of MGF2 Anti-Reflective Coatings. 35th IEEE Photovoltaic Specialists Conference, 2010, doi: 10.1109/PVSC.2010.5614585

[37] Brieva, A., (2023) ATOX Testing of optical materials for EnVision. ESA-TECQEE-LAB-TR-2023-001061, 2023
[38] (2021) Acktar Black Worlds Blackest Coating. Brochure, ACM Coatings GmbH, 2021
[39] Aeroglaze Z307 Polyurethane Coating. Technical Data Sheet, Socomore
[40] Sierra, G., et al., (2022) MAP AQ and MAP AQ PUK: Water-Borne Coatings as Alternatives to High Space Legacy PU1 and PUK Coatings. MAP SPACE COATINGS website, 2022
[41] (2023, 26. Juni) Stainless Steel 316 1.4401. ThyssenKrupp, https://www.thyssenkrupp-materials.co.uk/stainless-steel-316-14401.html
[42] (2023, 26. Juni) EN AW-7075 Aluminium Datenblatt 3.4365 AlZnMgCu1,5 (AlZn5,5MgCu). Welt Stahlsorten, https://www.weltstahl.com/aluminium-7075/
[43] (2022) EOS Aluminium AlSi10Mg. EOS GmbH, Material Data Sheet, 2022
[44] (2023, 26. Juni) Titan-6AL4V | WL 3.7164 | Datenblatt. S+D Metals, https://www.sd-metals.com/de/sd-werkstoffe/titanlegierungen/ti-6al4v-wl-3-7164-datenblatt/

XI. Declaration of Independence and Confidentiality

I hereby declare that I have prepared this master's thesis independently, that I have not submitted it elsewhere for examination purposes, and that I have not used any resources other than those indicated. All knowingly used text excerpts, quotations, or contents of other authors have been explicitly marked as such.

This thesis may not be reproduced, published, or made available to third parties, either in full or in part, without the written consent of the author, the supervising lecturer, or the company.

Joshua Weber

Aachen, 11.07.2023